Titre: Title:	Seismic demands within gravity dams and appurtenant structures including reservoir and rock foundation effects
Auteur: Author:	Siamak Ohadi
Date:	2020
Type:	Mémoire ou thèse / Dissertation or Thesis
Référence: Citation:	Ohadi, S. (2020). Seismic demands within gravity dams and appurtenant structures including reservoir and rock foundation effects [Mémoire de maîtrise, Polytechnique Montréal]. PolyPublie. https://publications.polymtl.ca/4181/

URL de PolyPublie: PolyPublie URL:	https://publications.polymtl.ca/4181/
Directeurs de recherche: Advisors:	Najib Bouaanani
Programme: Program:	Génies civil, géologique et des mines

POLYTECHNIQUE MONTRÉAL

affiliée à l'Université de Montréal

Seismic demands within gravity dams and appurtenant structures including reservoir and rock foundation effects

SIAMAK OHADI

Département des génies civil, géologique et des mines

Mémoire présenté en vue de l'obtention du diplôme de *Maîtrise ès sciences appliquées*

Génie civil

Decembre 2019

POLYTECHNIQUE MONTRÉAL

affiliée à l'Université de Montréal

Ce mémoire intitule:

Seismic demands within gravity dams and appurtenant structures including reservoir and rock foundation effects

présenté par **Siamak OHADI**

en vue de l'obtention du diplôme de *Maîtrise ès sciences appliquées*

a été dûment accepté par le jury d'examen constitué de :

Samuel YNIESTA, président

Najib BOUAANANI, membre et directeur de recherche

Sayouba TINTA, membre externe

DEDICATION

To my lovely family and of course to Arezoo who is my strength whenever I am weak

ACKNOWLEDGEMENTS

By using this page, although it is not enough, I would like to express my gratitude to people who have supported and helped me throughout this intense period of learning which results are summarized in this thesis.

I would first like to particularly thank my thesis advisor, professor Najib Bouaanani, Ph.D., who kept a sense of humour when I was stressed. From the very first moment I met him, he had faith on me, encouraging and directing me through the right direction.

I would also like to acknowledge professor Yniesta, Ph.D., for accepting to be the president of this study. My sincere thanks also go to Mr. Tinta, M.Sc. A, for being a member of jury for this research study.

I would also like to thank Wenbo Duan, Sylvain Renaud, Tarik Fethi Saichi who were always ready to eagerly share their knowledge with me.

Last but not the least, my profound gratitude goes to my family and to my lovely spouse for providing me with unfailing support and continuous encouragement throughout my years of study and through the process of researching and writing this thesis. This accomplishment would not have been possible without them.

RÉSUMÉ

Ce mémoire vise à étudier les effets des fondations sur les sollicitations sismiques au sein des barrages poids et des structures connexes à l'aide d'analyses par éléments finis. À cette fin, des composantes sismiques horizontales et verticales sont appliqués aux systèmes barrage-réservoir-fondation pour évaluer les effets de l'interaction sol-structure sur les spectres de plancher des accélérations horizontale et verticale, représentant les accélérations maximales des structures annexes au barrage.

Le système barrage-réservoir-fondation est modélisé en utilisant des éléments finis solides bidimensionnels (2D), incluant des éléments spéciaux assurant l'interaction fluide-structure à l'interface barrage-réservoir, et des conditions aux limites absorbantes, i.e. amortisseurs visqueux de Lysmer-Kuhlemeyer, aux limites inférieures et latérales du domaine modélisé de la fondation du barrage. La masse de la fondation du barrage est incluse dans les modèles numériques. Par conséquent, un processus de déconvolution est effectué pour obtenir les signaux sismiques à la base de la fondation. Un programme MATLAB efficace a été programmé à cet effet. Parallèlement au traitement des données sismiques, et l'application des transformées de Fourrier (FFT, IFFT), une analyse temporelle a été effectuée à chaque itération du processus de déconvolution. Le signal sismique résultant a été modifié à l'aide de deux techniques d'ajustement. Des analyses de sensibilité ont été effectuées pour étudier les effets des dimensions de la fondation, sa flexibilité et des conditions aux limites du domaine sur la convergence et la précision des résultats, ainsi que l'efficacité des techniques employées.

Les signaux horizontaux et verticaux obtenus de la déconvolution sismique ont été utilisés pour effectuer des analyses dynamiques temporelles des systèmes barrage-réservoir-fondation, afin d'évaluer les effets de la masse de la fondation et de l'interaction sol-structure sur les spectres d'accélération de plancher au sein des barrages étudiés. Les effets de la flexibilité des fondations et du taux d'amortissement sur les sollicitations sismiques sont également étudiés.

La déconvolution et les analyses sismiques sont effectuées sur deux barrages poids. Un barrage de 121 m de haut (Pine Flat), et un plus petit barrage poids de 35 m de haut. Les accélérations horizontales et verticales du séisme de Taft (1952) sont utilisées pour illustrer les résultats.

ABSTRACT

This research aims at investigating rock foundation effects on the seismic demands with concrete gravity dams and their appurtenant structures using finite element analyses. For this purpose, horizontal and vertical seismic components are applied to dam-reservoir-foundation systems to evaluate the effects of soil-structure interaction on both horizontal and vertical acceleration floor spectra, representing maximum acceleration response experienced by dam appurtenant structures.

The dam-reservoir-foundation system is modelled using bidimensional (2D) solid finite elements, including fluid-structure interaction special elements at the dam-reservoir interface, and absorbing boundary conditions, i.e. viscous Lysmer-Kuhlemeyer dampers, at the bottom and lateral boundaries of the dam foundation domain. The mass of the dam foundation is included in the finite element models. Therefore, a deconvolution process is carried out to obtain the deconvolved earthquake signals at the base of the foundation. An efficient MATLAB code was programmed for this purpose. Along with the data processing techniques programmed, i.e. FFT, IFFT processes, a transient time-domain analysis was performed for each deconvolution iteration, and the output deconvolved signal was modified using two different adjustment techniques. Sensitivity analyses were carried out to investigate the effects of the dimensions of the foundation, as well as boundary conditions and dam foundation flexibility on the convergence and accuracy of the results, and the efficiency of the techniques used.

The obtained horizontal and vertical deconvolved signals were used as input for transient dynamic analyses of dam-reservoir-foundation systems, to evaluate the effects of massed foundation on the floor acceleration response spectra within the dams. The effects of foundation flexibility and damping ratio on the seismic demands are also investigated.

The deconvolution and seismic analyses are performed on two gravity dams. A 121-m high dam, i.e. tallest non-overflow monolith of Pine Flat dam, and a smaller 35 m gravity dam monolith. The recorded horizontal and vertical components of Taft ground motion (1952) were used for illustration purposes.

TABLE OF CONTENTS

LIST OF TABLES

LIST OF FIGURES

LIST OF SYMBOLS AND ABBREVIATIONS

Abbreviations

ABC	Absorbing boundary condition
FE	Finite elements
FEM	Finite element method
FERC	Federal Energy Regulatory Commission
FFT	Fast Fourier Transform
FRS	Floor Response Spectrum
ICOLD	International commission on large dams
IFFT	Inverse Fast Fourier Transform
LBC	Lateral boundary condition
USACE	United States Army Corps of Engineers
USBR	United States Bureau of Reclamation
USCOLD	United States Committee on Large Dams
USSD	United States Society of Dams

Symbols

a , b	Dimensionless parameters in viscous damping coefficients
$a(j)$	Real part of the input motion at the base of foundation in frequency domain
$Amp_T(j)$	Target amplitude for each frequency
$Amp_R(j)$	Output amplitude for each frequency
b	Length of the elements at the bottom of the foundation
$b(j)$	Imaginary part of the input motion at the base of foundation in frequency domain

$\beta_p(\omega)$	Modification factor for the vertical motion
$\beta_s(\omega)$	Modification factor for the horizontal motion
$C.F(j)$	Correction factor of Fourier amplitudes
C_n	Damping coefficient for the normal direction
C_S^{eq}	Equivalent shear wave velocity
c_s	Damping coefficient of the SDOF system of the appurtenant structure
C_t	Damping coefficient for the shear direction
E	Young's modulus
ξ_s	Equivalent damping ration of the SDOF system of the appurtenant structure
F_n	Normal resistance force of the dashpots on the edge of the boundary
$F_p^{Input}(t)$	Vertical nodal forces at the base of the foundation
f_s	Frequency vibration of the SDOF system of the appurtenant structure
$F_S^{Input}(t)$	Horizontal nodal forces at the base of the foundation
F_t	Tangential resistance force of the dashpots on the edge of the boundary
$\varphi_p^{Response}(\omega)$	Phase value of the Vertical response velocity in frequency domain
$\bar{\varphi}_s^{Shift}(\omega)$	Effective phase shift for the horizontal motion
$\bar{\varphi}_p^{Shift}(\omega)$	Effective phase shift for the vertical motion
$\varphi_p^{Target}(\omega)$	Phase value of the vertical target velocity in frequency domain
$\varphi_s^{Input}(\omega)$	Phase value of the horizontal input velocity in frequency domain
$\varphi_p^{Input}(\omega)$	Phase value of the vertical input velocity in frequency domain
$\varphi_s^{Response}(\omega)$	Phase value of the horizontal response velocity in frequency domain
$\varphi_s^{Target}(\omega)$	Phase value of the horizontal target velocity in frequency domain

Φ	Nodal fluid potential vector
l_o	Length of the element at the boundary
m_s , c_s , k_s	Mass, damping and stiffness of the SDOF secondary structure
μ	Poisson's ratio of the boundary material
σ	Normal stresses on the boundary of the foundation
t	Thickness of the elements at the bottom of the foundation
τ	Shear stresses on the boundary of the foundation
U	Relative displacement vector
$\ddot{u}_g$	Horizontal acceleration at the base of the dam
$\ddot{u}_p$	Horizontal acceleration of point p at crest
$\dot{u}_p^{Input}(t)$	Velocity time history ground motion of compressional waves
$\left\|\dot{u}_p^{Input}(\omega)\right\|$	Absolute value of the vertical input velocity in frequency domain
$\dot{u}_p^{Input\ (new)}(\omega)$	New vertical input motion at the base of foundation in frequency domain
$\dot{u}_p^{Input}(\omega)$	Vertical component of the input velocity in frequency domain
$\left\|\dot{u}_p^{Response}(\omega)\right\|$	Absolute value of the vertical response velocity in frequency domain
$\dot{u}_p^{Respons}\ (\omega)$	Vertical component of the response velocity in frequency domain
$\left\|\dot{u}_p^{Target}(\omega)\right\|$	Absolute value of the vertical target velocity in frequency domain
$\dot{u}_p^{Target}(\omega)$	Vertical component of the target velocity in frequency domain
$\ddot{u}_s$, $\dot{u}_s$, u_s	Relative horizontal acceleration, velocity and displacement of SDOF secondary structure
$\dot{u}_S^{Input}(t)$	Velocity time history ground motion of shear waves
$\dot{u}_s^{Input}(\omega)$	Horizontal component of the input velocity in frequency domain

$\left\|\dot{u}_s^{Input}(\omega)\right\|$	Absolute value of the horizontal input velocity in frequency domain
$\dot{u}_s^{Input\ (new)}(\omega)$	New horizontal input motion at the base of foundation in frequency domain
$\dot{u}_s^{Response}(\omega)$	Horizontal component of the response velocity in frequency domain
$\left\|\dot{u}_s^{Response}(\omega)\right\|$	Absolute value of the horizontal response velocity in frequency domain
$\dot{u}_s^{Target}(\omega)$	Horizontal component of the target velocity in frequency domain
$\left\|\dot{u}_s^{Target}(\omega)\right\|$	Absolute value of the horizontal target velocity in frequency domain
$\ddot{v}_g$	Vertical acceleration at the base of the dam
v_n	Normal particles' velocity
$\ddot{v}_p$	Vertical acceleration of point p at crest
V_p	Velocity of the primary waves (compressional waves)
$\ddot{v}_s\ ,\ \dot{v}_s\ ,\ v_s$	Relative vertical acceleration, velocity and displacement of SDOF secondary structure
V_s	Velocity of the secondary waves (shear waves)
v_t	Tangential particles' velocity

LIST OF APPENDICES

CHAPTER 1 INTRODUCTION

This chapter aims to introduce the context of this study, as well as the problem investigated. The objectives along with the methodology utilized to fulfil them are described. The contents of the thesis are presented at end of this chapter.

1.1 Context of study

Dams are a fundamental component of a society's infrastructure. Understanding their seismic behaviour is important; not only to protect human lives, but also to avoid or reduce structural damage that may lead to dam rupture or reservoir release, with major potential consequences in terms of human and economical losses. Reported earthquake-induced dam failures, e.g. Pacoima arch dam subjected to the San Fernando earthquake in 1971, although relatively rare, regularly raise concerns leading to the continuous improvement of approaches of seismic dam design and safety evaluation.

Significant research has been devoted to study the seismic safety of dam-reservoir-foundation systems including several advanced analytical or numerical approaches. However, little attention has been devoted to the seismic behaviour and safety of dam appurtenant structures. Some of the critical systems attached to the dam, e.g. electromechanical equipment, can indeed be highly sensitive to earthquakes even in regions of low to moderate seismicity due to dynamic amplifications over dam height. For example, accelerations recorded at three dam sites during the Saguenay earthquake showed amplifications of about 10 times from rock to the dam crest (Rainer and Dascal, 1991). Therefore, in many cases, appurtenant structures can be at higher seismic hazard than the dam itself. Failure of such structures could critically affect the operation, the safety and the performance of a hydroelectric facility. Thus, modern guidelines, such as ICOLD (2010) recommend that seismic input at the base of appurtenant structures account for ground motion amplification. Floor response spectra (described in detail later) can then be used to assess the seismic response of safety-critical appurtenant systems located near dam crest where ground motions can be significantly amplified from dam base. Although floor response spectra have been widely studied in the context of nuclear facilities and multi-storey buildings, studies on the amplification of seismic demands within gravity dams are still rare, especially accounting for the

effects of combined earthquake-induced interactions from the impounded reservoir and rock foundation.

1.2 Problem statement

The assessment of the seismic demands within dams and their appurtenant structures requires accounting for dynamic interactions between the dam, the reservoir and the foundation. Some previous studies focused on the effects of water modeling assumptions on such seismic demands under horizontal and vertical earthquake components (Bouaanani and Renaud 2014, Bouaanani et al. 2018). However, these studies considered a rigid dam foundation. Therefore, there is still a need to investigate the effects of soil-structure interaction, i.e. massed foundation, radiation damping and wave propagation, on the seismic demands within dams and their appurtenant structures subjected to horizontal and vertical earthquake components.

1.3 Research objectives

The main objective of this research is to investigate the seismic demands within concrete gravity dams and their appurtenant structures considering the effects of impounded reservoir, massed rock foundation, appropriate boundary conditions. The seismic demands are expressed in terms of acceleration floor response spectra. The general objective can be broken down to five specific objectives as follows:

- Evaluating two existing techniques in the literature for time-domain deconvolution analysis of the input free-field ground motion signals in terms of efficiency and accuracy.
- Programming and performing deconvolution procedures to investigate the sensitivity of the results to various factors, such as rock foundation flexibility, size and boundary conditions.
- Studying the effects of the rock foundation flexibility on the amplification of horizontal and vertical floor acceleration spectra within gravity dams impounding compressible water reservoirs.
- Studying the effects of damping ratio of the foundation on the amplification of floor response spectra on a small and a large gravity dam structure.

- Evaluating the effects of dam size effects on the floor acceleration response spectra associated with dam-reservoir-foundation systems.

1.4 Methodology

In this section, the methodology adopted to investigate rock foundation effects on seismic demands within dams and the appurtenant structures is described. First, a deconvolution process is done in order to obtain the deconvolved signals which should be applied at the base of the massed foundation. A MATLAB code is programmed based on an iterative data processing procedure using the FFT and IFFT formulations. A time-domain seismic analysis is performed through finite element modelling, so the obtained output signal at the surface of the foundation could be adjusted using two different adjustment techniques at the end of each iteration. Several analyses are carried out next to investigate the effects of size, lateral boundary conditions and flexibility of the foundation profile on the accuracy and correctness of the deconvolution technique. For this purpose, Pine Flat gravity dam (121 m high) was selected based on material properties and the geometry provided by USSD (2017) and the deconvolution process is illustrated using Taft ground motion acceleration (1952).

The seismic demands within Pine Flat gravity dam, and a smaller (35 m high) gravity dam are then evaluated by determining acceleration floor response spectra when the dams are subjected to horizontal and vertical components of Taft earthquake (1952). The models consist of the dams, along with their impounded reservoirs with compressible water, and a massed rock foundation. The horizontal and vertical acceleration floor response spectra of the dam-reservoir-foundation models are compared with the reference model consisting of the dam-reservoir system with a rigid foundation.

1.5 Organization of thesis

This thesis is organized in six chapters including this introduction Chapter, and four appendices.

A literature review related to concrete gravity dams and to their seismic behaviour, numerical modelling and analyses is presented in Chapter 2. In Chapter 3, modelling issues related to the numerical modelling of Pine Flat dam are discussed. In Chapter 4, two adjustment techniques for

seismic deconvolution analysis are described, applied to Pine Flat dam and the results are compared. The effects of the flexibility and damping of a rock massed foundation on seismic demands within two dams and their appurtenant structures are discussed in Chapter 5. The conclusions of this research are given in Chapter 6.

Appendix A presents examples of the velocity time-history and Fourier amplitude obtained using the developed deconvolution MATLAB code. A convergence study to evaluate the dimensions of the massed rock foundation is presented in Appendix B. The results of the modal analysis (e.g. frequencies and mode shapes) of the tallest non-overflow monolith of Pine Flat gravity dam are discussed in Appendix C. Appendix D compares the response spectra of horizontal and vertical convolved seismic signals to the target free-field ground motions.

CHAPTER 2 LITTERATURE REVIEW

This chapter presents a summary of the literature review related to the numerical modeling and seismic analysis of concrete gravity dams.

2.1 Earthquake impacts on concrete dams

Earthquake-induced failures or major damaging events in concrete dams have been rarely reported in the literature. For example, in 1962, 15 m high Hsingfengkiang buttress dam in China was subjected to a strong local earthquake, suspected of being caused by reservoir-triggered seismicity. The event significantly damaged the dam, and resulted in considerable horizontal and longitudinal cracking near the crest of the dam (Shen et al., 1974; ICOLD, 2008). Koyna dam, a 103 m high straight gravity dam in India, is another illustration of the vulnerability of dams to earthquakes. It was hit in 1967 by an earthquake which induced horizontal cracks on the downstream and upstream faces of the non-overflow blocks near the crest (e.g. ICOLD, 2008). Major repairs were carried out strengthen the non-overflow monoliths by adding buttresses to ensure their stability (e.g. Chopra and Chakrabarti, 1973). Sefid rud gravity buttress dam in Iran can be also mentioned as another example. In 1990, one of the most catastrophic seismic events in the region, Manjil-Rudbar earthquake, left over 35,000 people dead and the complete destruction of the city (Wieland and Fan, 2004). The 106 m high buttress dam was severely damaged, as illustrated in Figure 2.1, including horizontal cracks at lift joints, spalling of concrete along the vertical joints, as well as observed sliding between monoliths. Even though the dam was not designed to withstand such significant accelerations, its performance was quite satisfactory, and its stability was not of concern. The cracked areas were repaired using epoxy grouting along with post tensioning strands (e.g. USCOLD, 2000; ICOLD, 2001; Ahmadi et al., 1992).

Figure 2.1 Sefid Rud buttress dam - Horizontal cracks at lift joints (Wieland and Fan, 2004)

Pacoima arch dam (Figure 2.2) in the US, with a height of 111 m and a crest length of 180 m, was damaged during the San Fernando earthquake in 1971 (e.g. Serafim, 1987). The dam suffered opening of the contraction joints, as well as, movements of the abutment rock, one of the most critical potential failure modes in arch dams (Ghanaat, 2004). This earthquake had a major impact of the improvement of dam seismic design approaches.

Figure 2.2 Pacoima dam – left and right abutments (Alves, 2005)

2.2 Earthquake impacts on appurtenant structures

Various appurtenant structures and equipment are required to properly service the dam or ensure its operation. These include of spillways, outlet works, gates, valves, power plants, etc. Earthquake-induced defects to these appurtenant structures and equipment could critically affect the operation, the safety and the performance of a given hydroelectric facility. Therefore, during and after an earthquake, it is essential that the appurtenant structures remain operational. Figure 2.3 illustrates the collapse of Shih-Kang dam during Chichi earthquake in Taiwan in 1999 (Wieland, 2016).

Figure 2.3 Failure of Shih-Kang dam during Chichi earthquake in Taiwan (Wieland, 2016)

2.3 Progressive analysis methodology and failure modes

To assess the dynamic response of a hydraulic structure to earthquakes, a series of analyses with different levels of complexity can be performed. The dam seismic evaluation can begin with the simplest methods, and then progress towards more complex linear and non-linear methods as needed. Through this process, engineering judgement is required along with satisfying safety criteria and verifying the appropriateness of numerical results (USACE, 2003; Ghrib et al., 1997).

The first two phases of this progressive approach are pseudo-static and pseudo-dynamic analysis methods. The third phase is the first level in which the time history aspect of the earthquake is considered. Nonlinear dynamic analysis is the last level of the progressive method and the most powerful method of seismic analysis. The dynamic response of concrete gravity dams to earthquakes is a complex phenomenon. However, these massive plain concrete structures are mostly evaluated based on the linear-elastic finite element method of analysis. Tensile behaviour along with the cracking of the concrete should be assessed to ensure the safety and serviceability of the dam (USACE, 2007). Dam safety evaluation also involves the identification of all possible failure modes. The most probable structural modes of failure for the concrete gravity dams are as follow: Horizontal cracking within the dam at the concrete-concrete interfaces or at the foundation-dam interface is one of the common modes of failure. Cracking usually occurs at the heel of the dam, as well as near the crest when the earthquake is in the upstream direction. However, cracking occurs at the level of slope discontinuity and near the toe of the dam when the earthquake is in the downstream direction (Figure 2.4). Due to the cracked sections in the dam or dam-foundation interface, considered as weak planes, the sliding may happen. Therefore, the permanent displacements should be within acceptable limits in order to prevent the rupture of the structure or damage to appurtenant structures. Internal erosion by seepage, piping, is another main concern. It occurs around hydraulic structures and through cracks within the dam and the interface of the dam and its foundation.

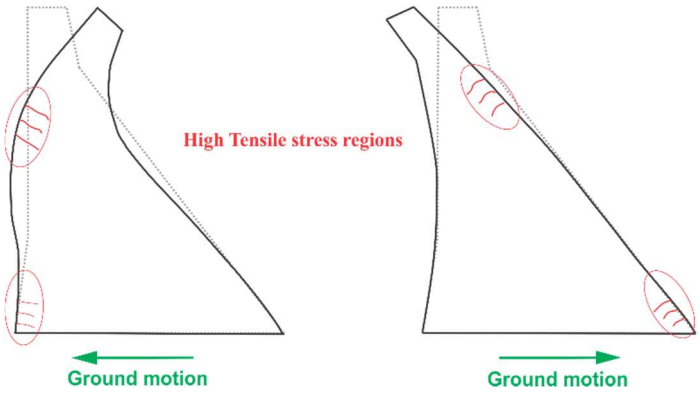

Figure 2.4 Gravity dam – High tensile stress regions (Adopted from USACE, 2007)

2.4 Seismic evaluation of concrete dams

2.4.1 Finite element techniques

The finite element method is considered the most popular numerical method for structural analysis. This numerical analysis technique is used to obtain approximate solutions for a variety of physical engineering problems, including dam engineering. Some specialised finite element codes have been developed to facilitate the 2D and even more complex 3D finite element idealizations of dam-reservoir-foundation rock systems (EAGD 84, EACD 96). Recourse to commercial software, such as ADINA (2018), is however more common. In this work, a 2D idealization is used for the numerical simulation of gravity dams under the assumption of plane stress or plane strain. The interactions of the three substructures, i.e. dams, water and rock foundation, and the associated boundary conditions are problems specific to dams that may complexify the analyses.

2.4.1.1 Fluid-Structure interaction

The dynamic response of the concrete dam may be significantly influenced by its interaction with the impounded water, water compressibility and the absorption of hydrodynamic waves at reservoir bottom. The importance of hydrodynamic effects was first demonstrated by the simplified added mass formulation of Westergaard (1933), defining hydrodynamic forces as inertia forces associated with a given volume of water attached to the dam face and moving back and force with the structure during earthquake shaking. The limitations of his assumption include 2D idealization of a rigid monolith with vertical upstream face impounding a semi-infinite reservoir (Figure 2.5).

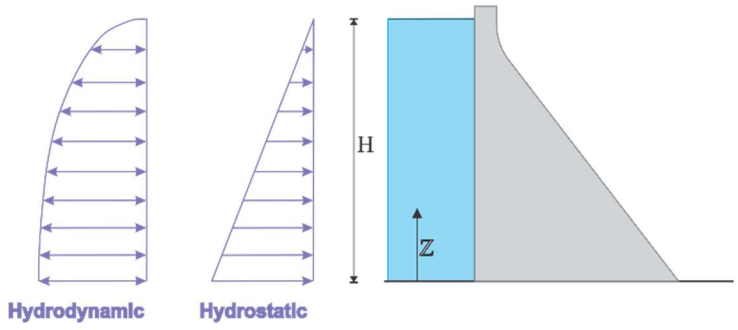

Figure 2.5 Hydrostatic and hydrodynamic forces during earthquake excitation (Zangar, 1952)

Several researchers extended Westergaard's work by including some of the complexities for their models, e.g. Zangar (1952) determined the hydrodynamic pressure for the 2D monoliths with

sloping upstream face. Several researchers developed efficient simplified and practical methods taking into account both the flexibility of the dam and the compressibility of the water in the reservoir (e.g. Fenves and Chopra, 1985; Bouaanani and Perrault, 2010; Miquel and Bouaanani, 2010).

The finite element modeling of fluid-structure interaction is more and more accessible to practicing engineers. It is a powerful technique susceptible of accounting of various complex phenomena typical of dams (e.g. fluid-structure interaction, water compressibility, etc.). Two main formulations are available to model a dam reservoir using finite element, i.e. the Lagrangian and Eulerian approaches. In the Lagrangian approach, the solid and fluid elements share the same type of state variable, i.e. displacements. A considerable advantage of this method is that the equilibrium and the compatibility are automatically satisfied between the nodes located at the fluid-solid interfaces. Therefore, no special interface elements are needed to be modeled. Although the shape functions for both elements are the same, fluid elements are characterized by a volumetric modulus of elasticity equal to that of the fluid compressibility modulus. A zero-shear resistance is associated with the fluid elements. In the Eulerian approach, however, the behavior of fluid is defined by a velocity potential, pressure or velocity, while displacement is used as a state variable for solid elements. Interface elements are required to ensure the compatibility and equilibrium conditions at the boundaries between the solid and the fluid. The Eulerian approach yields to potential-based fluid finite elements defined with a scalar variable, which reduces the number of degrees of freedom and thus computational requirements in terms of execution time and memory.

The Eulerian approach is used in this work. A symmetric potential-based method by Everstine (1981), in which the fluid variable is defined using velocity potential, Φ, is programmed in the finite element software ADINA. The Φ-U formulation assumes that the displacements at the fluid-structure interface are small, that the fluid is non-viscous and irrotational, but can be compressible or incompressible. A detailed explanation of this formulation can be found in Everstine (1981) and Bouaanani and Lu (2009).

2.4.1.2 Dam-foundation interaction

Dam-foundation interactions during earthquakes cannot always be neglected (e.g. According to United States Army Corps of Engineers, 2007). Such interactions are generally associated with added flexibility and damping, e.g. radiating or material damping in the foundation. A flexible rock

foundation elongates the vibration periods of the dam and the additional damping reduces the structural response. Two main general methods are available to model the dam and the rock foundation, i.e. the “direct method” and “substructure method”. Simplified idealizations are often used to reduce the complexities associated with soil-structure interaction. Rock foundation models suitable for concrete hydraulic structures can be distinguished into (USACE, 2007):

1- Massless foundation model: a massless finite element model could be an acceptable simplifying approach when the supporting the studied concrete dam is constructed on a qualified rock foundation. The dimensions of the foundation compared to the structure are not needed to be large and the input seismic load can be applied at the base of foundation model.

2- Viscoelastic foundation model: if the elastic modulus of the rock site is considerably lower than the massive concrete, the simplified massless foundation model is no longer valid, since it excludes the inertia and damping effects of the foundation. Assuming similar rocks cover a large area through foundation depth, this idealization may be realized by means of frequency-dependent “impedance functions” consisting of real and imaginary components. The stiffness and inertia of the foundation is represented by the real part and the damping is defined as the imaginary part, e.g. Fenves and Chopra (1984), Løkke and Chopra (2014).

3- Coupled finite element soil-structure interaction model: in such models, finite elements are used to simulate and couple the seismic response of the different substructures.

4- Lumped-parameter model: frequency-independent springs, masses and dampers attached to the dam are used to model and replace the response of the rock foundation.

Concrete gravity, arch-gravity and arch dams, including impounded water and the foundation rock, may be analyzed in a complete system in time domain using standard finite element method with massless foundation rock, or separately in frequency domain (substructures method). The substructures method in frequency domain can be used if homogeneous material properties are considered for the foundation. The size of the massless foundation for the arch-dam model is affected by the modulus ratio of the foundation to the concrete. If the ratio is higher than one, the dimensions of the foundation could be equal to the dam height in all directions. However, in case which $\frac{1}{2} < E_f / E_c < \frac{1}{4}$, twice the dam height is at least necessary for the size of the foundation in all directions. Boundary conditions for the foundation could be considered fixed at the bottom,

since the rigid bedrock is beneath the soil. However, for each side, considering horizontal excitation, only vertical translation degree of freedom is fixed, while for vertical excitation, horizontal translations are blocked (USACE, 2003).

2.4.1.3 Deconvolution

The difficulties and uncertainties associated with soil-structure interaction problems have led to the adoption of oversimplified massless foundation models. In such cases, only the stiffness of the rock foundation contributes to the seismic response, while inertia forces and damping are neglected. In a massless rock foundation, the free-field recorded ground motions can be applied at the base of the foundation model, as seismic signals do not change as they propagate in this case. In a more realistic case of a massed rock foundation, free-field recorded ground motions can no longer be applied directly at the base of the foundation and a deconvolution process has to be applied (Remier, 1973).

Deconvolution analysis could be done using computer programs such as SHAKE (1972), designed for the seismic analysis of horizontally layered rock foundations, characterised by a shear modulus, a density and a viscous damping, and generally assumed as uniform and extending horizontally to infinity. Léger and Boughoufalah (1989) investigated the seismic response of concrete gravity dams including the interaction of the dam with a massed rock foundation, and subjected to various earthquake input mechanisms. In particular, they compared the effects of a standard rigid base model, a massless foundation and deconvolved input models. Bayraktar et al. (2005) also assessed free-field input mechanisms for dam-reservoir foundation systems. Clough et al. (1985) studied the effects of dynamic interaction in arch dams. In all these publications, the ground motions at the surface were obtained using the SHAKE program. The nonlinear seismic analysis of semi-unbounded dam-reservoir-foundation systems was investigated recently by Løkke and Chopra (2017) using direct finite element method. A massed rock foundation was assumed. Spatially variable seismic excitations were used to evaluate the nonlinear behavior of gravity dams by Huang and Zerva (2014). The massed foundation was considered in their study and the specified free-field spatially varying earthquake ground motions were applied at the surface of the foundation. Khazaei Poul and Aspasia Zerva (2018a), used both frequency- and time-domain approaches for the deconvolution process, to evaluate the nonlinear response of concrete gravity dams including the

effects of massed rock foundation. It is shown that time-domain approach provides more accurate results than the frequency approach, and more conservative results were when a massless rock foundation was included in the analysis.

The deconvolution used in this study was originally proposed by Reimer (1973) based on Fourier analysis. An iterative procedure initiates by applying the target ground motions at the bottom of the foundation. The transient wave propagation problem is then solved through finite element modelling at the point of interest, generally located at the surface of the rock foundation. Next, using Fourier analysis, a comparison is made in the frequency domain between the acceleration response obtained at the top and the target ground motion acceleration. Fast Fourier transform (FFT) and Inverse Fast Fourier Transform (IFFT) algorithms are used in order of transfer the signals from time domain to the frequency domain and vise versa. There are different types of correction factors, i.e. phase-amplitude and spectrum density procedures. For example, a correction factor proposed by Reimer (1973) can be defined by dividing Fourier amplitudes of both signals. Employing the correction factor, the ground motion acceleration at the base of the foundation is modified and then transferred to the time domain. This modified signal is applied at the base of the foundation and the finite element analysis of the wave propagation is repeated. At this iteration, another comparison should be made between the obtained ground motion at the top of the foundation and the target free-field recorded ground motion to ensure a satisfactory modified input signal. This iterative procedure is repeated until the output signal at the top matches the recorded free-field ground motion. A modified adjustment technique for the high frequency ground motion records using response spectrum density was presented by Sooch and Bagchi (2014).

2.5 Appurtenant structures

Damage to secondary structures could result in significant threats to the safety, functionality, or even worse, the failure of the supported structure. Therefore, it is essential to ensure the structural integrity of such critical components under seismic loads. Two methods can be generally used to evaluate seismic demands on appurtenant structures: ‘floor response spectra’ or ‘Combined primary-secondary system’ (Chen and Soong, 1988). Floor response spectra have been widely used and are selected in this work (Singh and Sharma, 1985; Chen and Soong, 1988). They define the maximum dynamic response of a secondary structure, assuming its mass can be neglected with respect of the primary structure, i.e. the dam, to which it is attached. In this case, the primary and

the secondary systems can be studied individually, first the response behaviour of the dam structure at the support point of the appurtenant structure is determined while the effect of the secondary system is neglected. Then, the floor response spectrum is used to obtain the seismic behaviour of the secondary system. In the case of a 2D finite element model, horizontal and vertical earthquake components of the chosen ground motion can be applied at the base of the structure. Then, the absolute acceleration at the point of interest, P, representing the attachment of the secondary structure to the primary one, is determined by adding the acceleration of the point at crest relative to the base of the primary structure to the ground excitations. Floor seismic demands of the appurtenant structure, simplified as SDOF systems, is defined by knowing the natural frequency and the damping ratio of the attached structure. The motion equation of the SDOF system of the secondary structure is written as:

$$m_s\ddot{u}_s + c_s\dot{u}_s + k_s u_s = -m_s(\ddot{u}_p + \ddot{u}_g) \tag{2.1}$$

$$m_s\ddot{v}_s + c_s\dot{v}_s + k_s v_s = -m_s(\ddot{v}_p + \ddot{v}_g) \tag{2.2}$$

where $\ddot{u}_s, \dot{u}_s$ and u_s represent respectively the relative horizontal displacement, velocity and acceleration and $\ddot{v}_s$. $\dot{v}_s$ and v_s represent respectively the relative vertical displacement, velocity and acceleration of the point P to its base. The floor acceleration demand at point P is then defined as the maximum absolute acceleration response of the secondary system for a frequency vibration $f_s = \frac{1}{2\pi}\sqrt{\frac{k_s}{m_s}}$ and damping coefficient c_s or equivalent damping ratio $\xi_s = \frac{c_s}{4\pi m_s f_s}$.

The floor spectra of the maximum accelerations of the secondary systems as a function of frequencies and for a given damping ratio ξ_s can then be obtained for a given point P. Figure 2.6 illustrates the computation of floor acceleration spectra at point P located at dam crest, representing the attachment of the SDOF appurtenant structure foundation, while the dam is subjected to the horizontal and vertical components of a given earthquake.

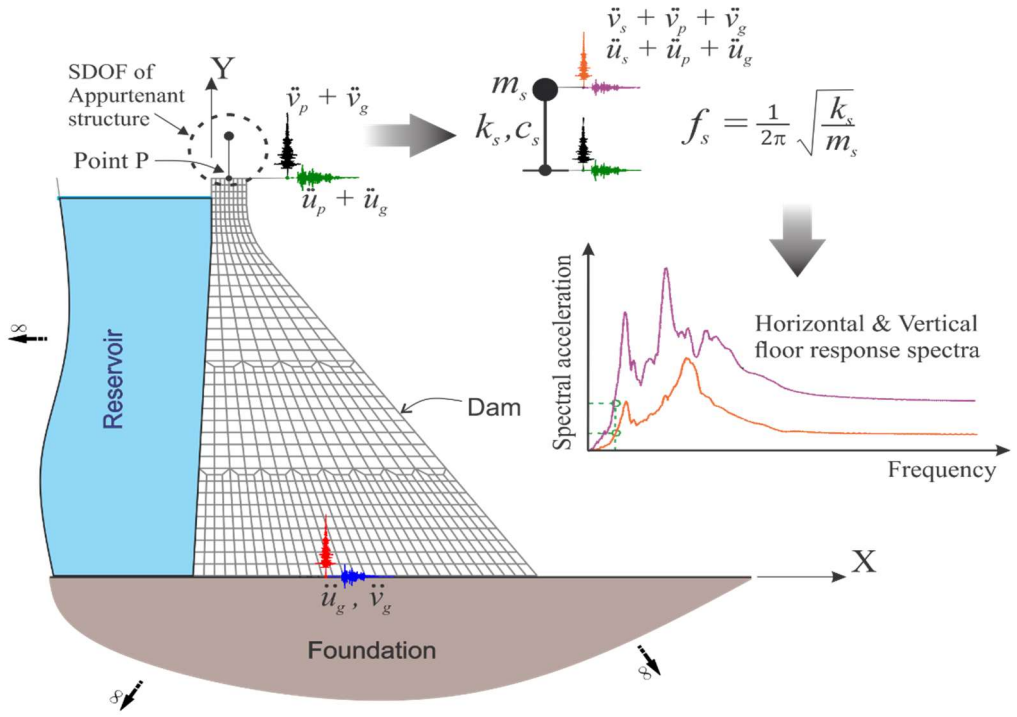

Figure 2.6 Illustration of floor response spectra calculation at point P

CHAPTER 3 DAM-RESERVOIR-FOUNDATION SYSTEM MODELLING ASSUMPTIONS AND APPROACHES

This chapter presents the assumptions and numerical approaches adopted for modeling a two-dimensional dam-reservoir-foundation system. A description of the main parameters for seismic analysis of such systems are given in detail. The dynamic interactions between the substructures (i.e. dam, reservoir, and rock foundation), the modeling of massed rock foundation and its effect on recorded free-field ground motion acceleration are also discussed. The tallest non-overflow monolith of Pine Flat gravity dam (e.g. Hall, 1986; USBR, 2018), located on King's River in California, is used next to illustrate the assumptions and the finite element modelling methodology adopted.

3.1 Finite element model and types of analyses

3.1.1 Geometry of the model

The height and the thickness of the tallest non-overflow monolith (no. 16) of Pine Flat dam are 400 ft and 50 ft, respectively, while its length at the crest is 1,840 ft. Figure 3.1 shows the geometry of the middle plane of the tallest monolith as well as some main features.

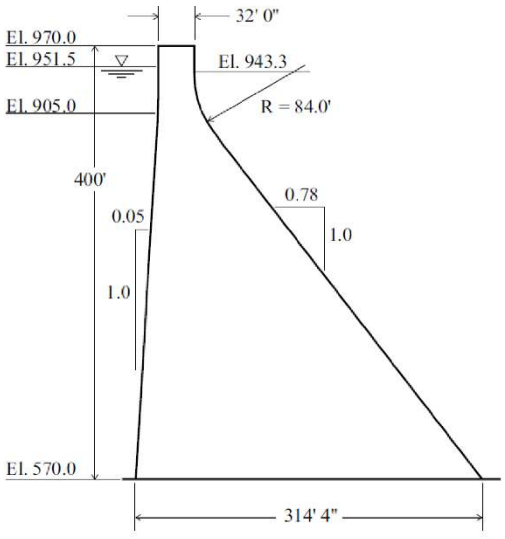

Parameters	Value
Maximum height above excavation	400 ft
Width at the crest	32 ft
Maximum width at the base	314 ft 4 in
Elevation of the crest	970.0 ft
Elevation of the base	570.0 ft
Normal water level	951.5 ft
Downstream slope	0.78H / 1V
Upstream slope	0.05H / 1V

Figure 3.1 Cross section and main features of the non-overflow monolith (no. 16) of Pine Flat dam (adopted from USBR 2018)

The material properties used for the numerical modeling of the concrete dam, rock foundation and the impounded water are summarized in Table 3.1 (USSD, 2017) with units in Imperial and International Systems for convenient reference. Two sets of rock foundation properties were provided by USSD (2017), but only one set is considered herein. The dam and the foundation materials are assumed linear elastic, homogeneous and isotropic in all the analyses. A numerical model of the dam-reservoir-foundation system is shown in Figure 3.2. In this figure the length of the reservoir is 2.5 times of the height of the dam and the depth of the foundation is chosen equal to the dam height for illustration purposes. The modeling of the three sub-structures is explained in the following sections.

Table 3.1 Material properties used for the dam-reservoir-foundation model

Material	Parameters	Imperial system		International system	
		Properties	**Units**	**Properties**	**Units**
Concrete	Modulus of elasticity	3250000	lb/in^2	22.407961203	GPa
	Density	155	lb/ft^3	2482.86	kg/m^3
	Poisson's ratio	0.20	-	0.20	-
Rock foundation	Modulus of elasticity	3250000	lb/in^2	22.407961203	GPa
	Density	155	lb/ft^3	2482.86	kg/m^3
	Poisson's ratio	0.20	-	0.20	-
Water	Density	62.5	lb/ft^3	1000	kg/m^3
	Bulk modulus			2,069,731,086.336	N/m^2
	Wave velocity	4720	ft/sec	1,438.656	m/sec

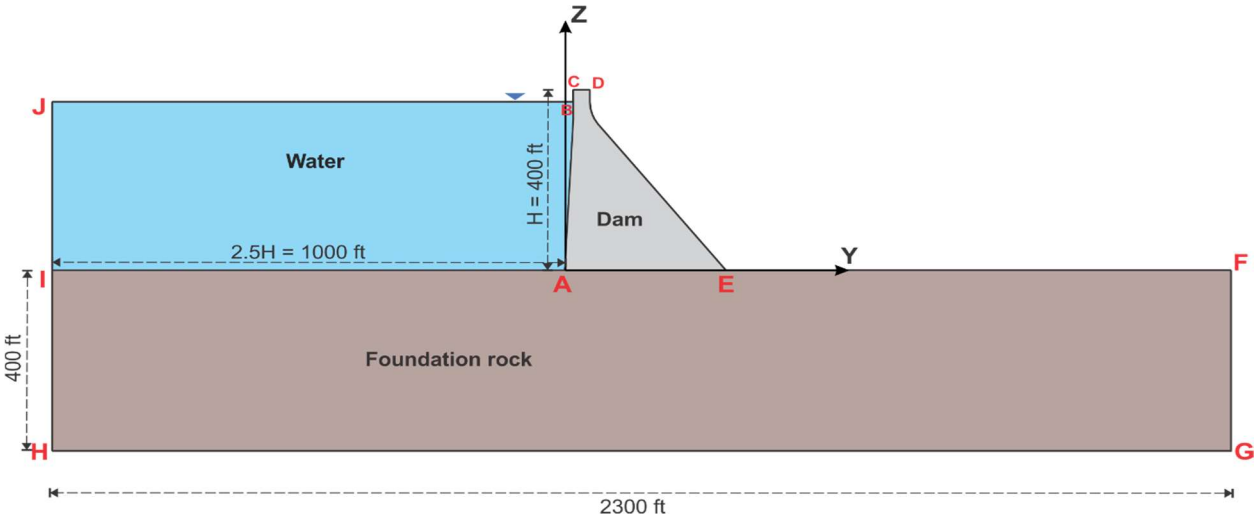

Figure 3.2 Cross section of the numerical model of the whole system using H as the depth of the foundation (adopted from USSD 2017)

3.1.2 Modelling of the dam monolith

The selected monolith of Pine Flat dam is modelled using 2D solid 4-node plane strain elements. The finite element commercial software ADINA was used for this purpose. Each node has two translational degrees of freedom. The meshing of the dam is denser at crest and at the base as illustrated in Figure 3.3. The appropriateness of the mesh density was verified based on a detailed convergence study using modal analyses as described in appendix C. To ensure maximum accuracy, 4-node transition elements were enforced (through programming) in some locations (as illustrated in Figure 3.3) to avoid recourse to Constant Strain Triangles (CSTs) which are otherwise automatically created by the software.

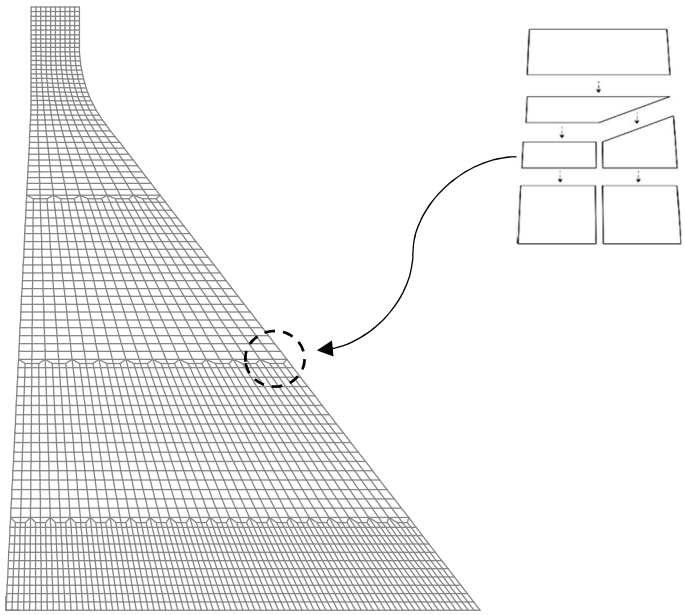

Figure 3.3 Two-dimensional mesh of the monolith 16 of Pine Flat dam and the trasition pattern

3.1.3 Modelling of the impounded reservoir

The reservoir is modelled using 2D 4-node potential-based fluid elements. The meshing of the reservoir is more refined closer to the dam face as shown in Figure 3.4. Water is assumed to be non-viscous, irrotational and compressible with a density of ρ_r = 1000 kg/m^3 and a bulk modulus of μ_r= 2.069 GPa, corresponding to wave propagation velocity of 1438 m/sec.

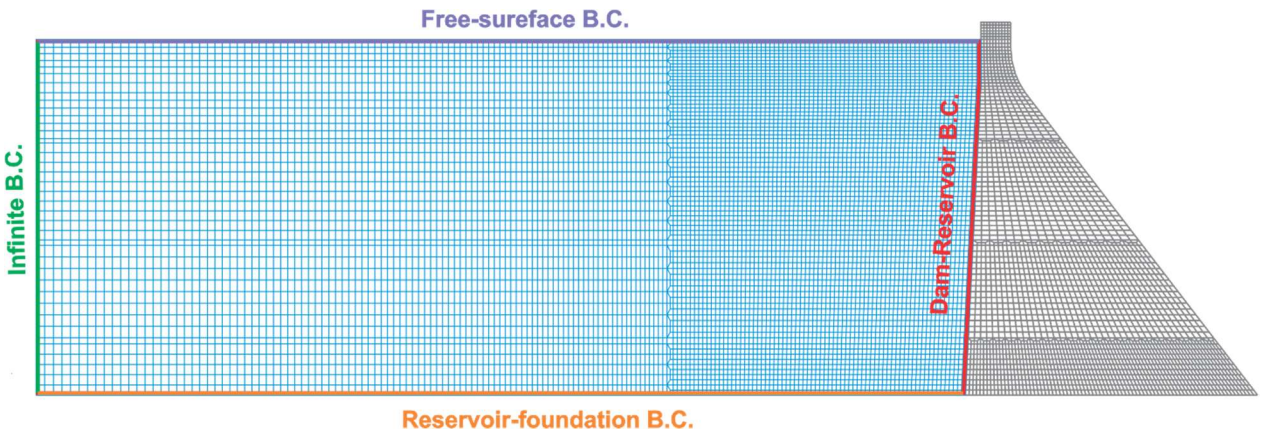

Figure 3.4 Numerical simulation of the dam-reservoir system and the reservoir boundary conditions

The Eulerian approach and the Φ-U formulation are programmed in ADINA to simulate the fluid-structure interaction (Bouaanani and Lu, 2009; ADINA, 2018). In the present case, such interactions occur at dam face (i.e. dam-reservoir interface) and reservoir bottom (i.e. reservoir-foundation interface). The Φ-U formulation connects velocity potentials or hydrodynamic pressure to the displacements of the dam or foundation nodes at the interfaces.

Choosing appropriate boundary conditions is an important step in the numerical modeling of dam-reservoir systems. The velocity potential in the reservoir should satisfy a free surface boundary condition, with or without gravity waves, a radiation boundary condition simulated herein by infinite elements at the upstream end of the reservoir, and a boundary condition at reservoir bottom accounting for the interaction between the reservoir and the foundation. Neglecting the effects of gravity waves at reservoir surface is common and justified. A null fluid potential is then imposed at the free surface of the reservoir. The infinite elements at the upstream end of the reservoir (Olson and Bathe, 1985) are to be positioned at a reservoir truncation length far enough from dam face to prevent or reduce reflection of earthquake-induced outgoing waves. Although wave absorption at reservoir bottom (i.e. due to sedimentation) can be modelled using simplified techniques (e.g. Fenves and Chopra 1984; Bouaanani and Lu 2009), it is neglected in this work.

3.1.4 Modelling of the rock foundation and the deconvolution method

The rock foundation is modelled using the same type of 2D solid plane strain finite elements used to model the dam monolith. The meshing of the rock foundation is optimized to find a compromise between required calculation time and accuracy. The dam monolith is assumed to be fully attached

to its foundation (i.e. sliding is not allowed). In order to investigate the effects of lateral boundary conditions (LBCs) on the accuracy of the output convolved signals, several types of such conditions are defined, including fixed, sliding and absorbing boundaries. Using a fixed boundary condition leads to the artificial reflection of the outgoing waves at the boundaries which may result in overestimation and unrealistic seismic response of the structure. Absorbing boundary conditions, e.g. viscous dampers, could simulate an infinite condition at a physical truncation boundary of the dam rock foundation model. Table 3.2 categorizes the different models chosen for deconvolution analyses including and excluding the dam and the reservoir. Two different depths are considered to investigate the effects of the foundation depth on the accuracy of the convolved signals obtained at the surface of the foundation.

Table 3.2 Models to be studied in deconvolution sensitivity analyses of Pine Flat dam-reservoir - foundation system

Foundation depth (H*)	Lateral Boundary conditions	Dam	Impounded water
1H	Fixed	Excluded	Excluded
1H	Sliding	Excluded	Excluded
1H	Absorbing	Excluded	Excluded
1H	Fixed	Included	Excluded
1H	Sliding	Included	Excluded
1H	Absorbing	Included	Excluded
1H	Fixed	Included	Included
1H	Sliding	Included	Included
1H	Absorbing	Included	Included
3H	Fixed	Excluded	Excluded
3H	Sliding	Excluded	Excluded
3H	Absorbing	Excluded	Excluded
3H	Fixed	Included	Excluded
3H	Sliding	Included	Excluded
3H	Absorbing	Included	Excluded
3H	Fixed	Included	Included
3H	Sliding	Included	Included
3H	Absorbing	Included	Included

* H is the height of the dam monolith.

First proposed by Lysmer and Kuhlemeyer in 1969, viscous boundary tractions represent a system of dashpots located at the artificial truncated boundaries which could damp out the reflection of the outgoing propagating waves. Being independent of wave frequency, the suggested ABC can even serve non-harmonic waves as it is the case for seismic ground motions. Although this model is formulated based on approximative local scheme, which the solution at any time step depends only on the current node and the current time step, its convenience has made it much more attractive for numerical implementation. In a 2D dam foundation model, the dashpots attached to the normal and tangential DOFs of each node of the foundation boundary correspond to a pair of stresses expressed as:

$$\sigma = a\rho_{\mathrm{f}}V_p v_n \tag{3.1}$$

$$\tau = b\ \rho_{\mathrm{f}}\ V_s\ v_t \tag{3.2}$$

where σ and τ are the normal and shear stresses on the boundary, respectively; v_n and v_t represent normal and tangential particle velocities of the boundary, respectively; ρ_{f} is the mass of the rock foundation; V_p and V_s represent the velocities of the primary and secondary waves traveling through the media, respectively; a and b are dimensionless parameters. Maximum wave absorption is achieved when choosing a and b equal to 1. If the rotation of the boundary is small, the normal and tangential resistant forces provided by the dashpots are given by:

$$F_n = -a\ \rho_{\mathrm{f}}\ V_p\ v_n\ l_o \tag{3.3}$$

$$F_t = -b\ \rho_{\mathrm{f}}\ V_s\ v_t\ l_o \tag{3.4}$$

where l_o is the length of the finite element of the foundation boundary to which the dashpot is attached. In a 2D finite element model, a unit thickness is considered. The viscous damping coefficients, shown in Figure 3.5, and corresponding to the normal and tangential dashpots can be expressed as:

$$C_n = a\ \rho_{\mathrm{f}}\ V_p\ l_o \tag{3.5}$$

$$C_t = b\ \rho_{\mathrm{f}}\ V_s\ l_o \tag{3.6}$$

in which the compressional and shear wave velocities are obtained as:

$$V_p = \sqrt{\frac{E_{\mathrm{f}}\,(1-\upsilon_{\mathrm{f}})}{\rho_{\mathrm{f}}(1+\upsilon_{\mathrm{f}})(1-2\upsilon_{\mathrm{f}})}} \tag{3.7}$$

$$V_s = \sqrt{\frac{E_f}{2\rho_f(1+\upsilon_f)}} \tag{3.8}$$

where E_f and υ_f denote the Young's modulus and Poisson's ratio of the rock foundation, respectively.

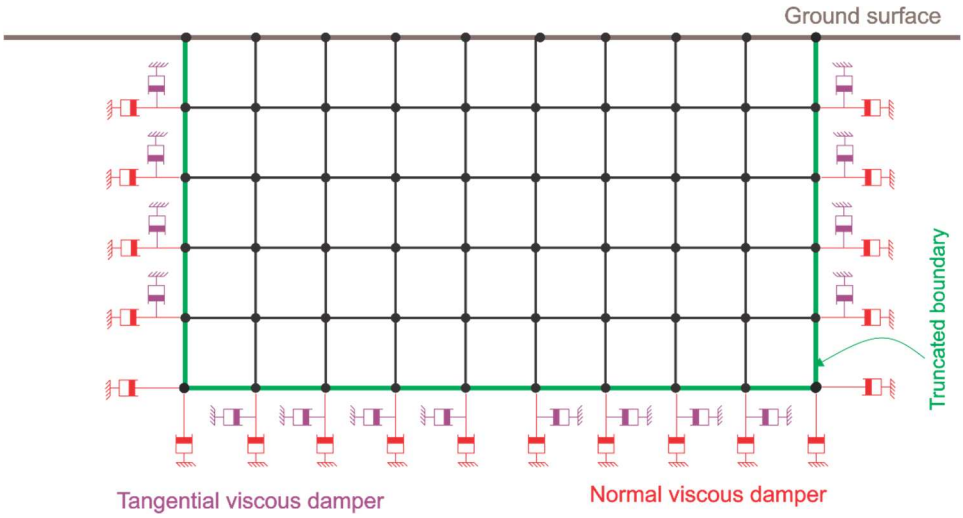

Figure 3.5 Viscous boundary illustration in numerical simulation of a finite domain

A viscous damping ratio is also associated with the rock foundation and varied to account for damping effects. For the purpose of direct integration method, corresponding coefficients of Rayleigh damping are determined based on a frequency-domain analysis. Figure 3.6 shows the numerical finite element modelling of the dam including the flexible massed foundation.

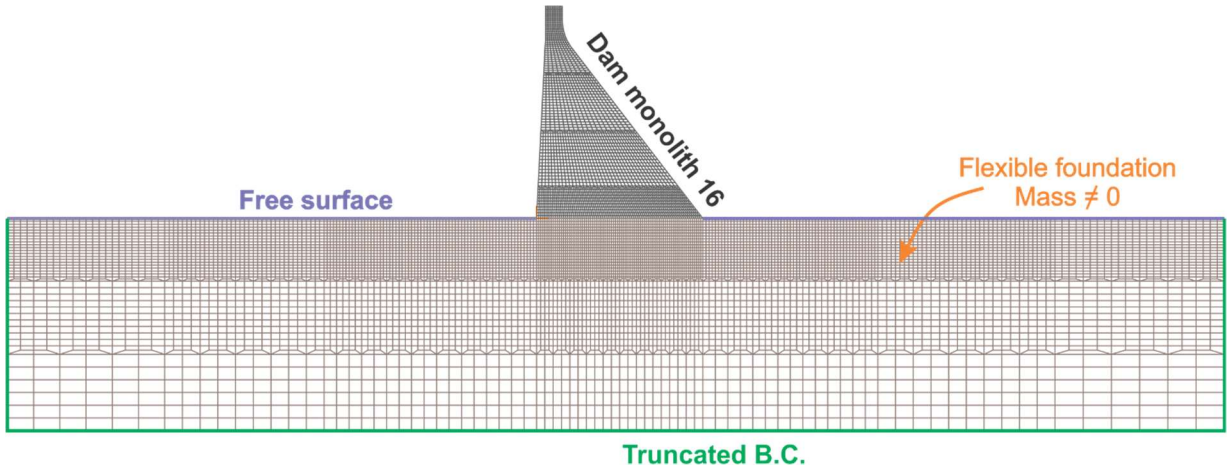

Figure 3.6 Numerical finite element dam-foundation model

The mass of the dam foundation is considered in the analysis, and thus related inertia forces. Therefore, seismic signals change through the foundation when propagating vertically towards the surface. A deconvolution process has then to be performed to define the deconvolved signals at the base of the foundation which correspond to a given target free-field ground acceleration at the surface, as illustrated in Figure 3.7. Using deconvolution analysis, the amplitude and frequency content of the earthquake ground motion are adjusted to get the desired output signal at the dam-foundation interface.

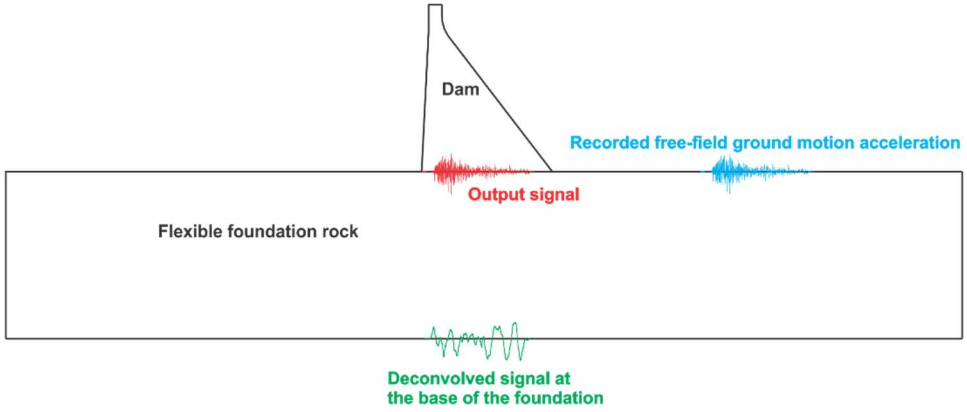

Figure 3.7 Illustration of deconvolved signal causing an output signal which matches the recorded free-field ground motion

As discussed in Chapter 2, the deconvolution process is based on Fourier analysis (Remier, 1973) and finite element time-domain analysis. This iterative procedure is initiated by applying the free field ground motion at the base of the dam foundation. Performing a numerical finite element analysis using ADINA, the acceleration at the top of the foundation (here the point at the middle of the dam-foundation interface) is determined. The ground motion acceleration obtained at the surface of the foundation is then compared to the recorded free field acceleration, after both signals are transformed from time domain to the frequency domain using Fourier transform (Cooley and Tukey, 1965). Figure 3.8 illustrates the transformation of the recorded free field horizontal component of Taft ground motion from time domain to the frequency domain using Fast Fourier Transform (FFT).

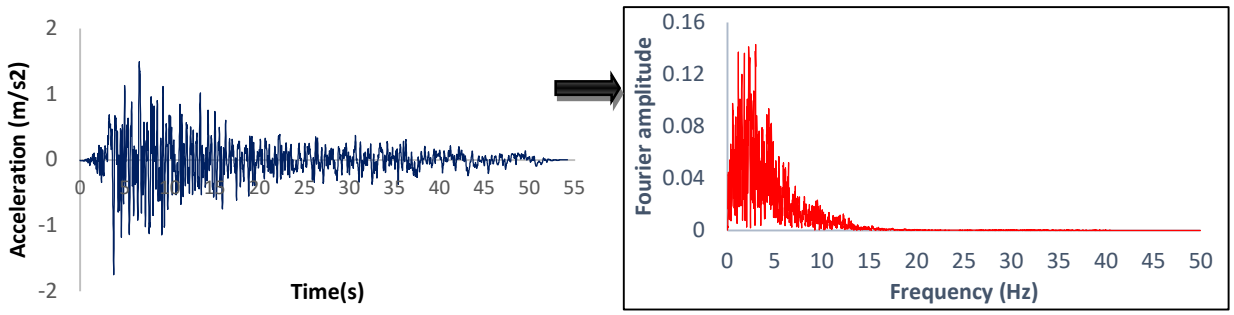

Figure 3.8 Fourier spectrum of the recorded free-field horizontal component of Taft ground motion acceleration

Converting the signals from time domain to the frequency domain, and again converting back from frequency domain to the time domain is done using the FFT and inverse fast Fourier transform (IFFT) algorithms, respectively. A program was written in MATLAB (2017) for this purpose. Having input, output and free field signals, a correction factor is calculated based on adjustment techniques described in the next Chapter 4. A new signal is generated and applied at the base of the dam foundation in the next iteration. Using IFFT, the modified signal in frequency domain is converted back to the time domain and used in finite element analysis to reproduce another signal at the dam-foundation interface. This process is repeated until the output signal at the top of the foundation (here the dam-foundation interface) closely matches the recorded free field ground motion acceleration. A criteria can be established to determine the number of sufficient iterations. In the present case, the acceleration response spectra of the target and modified signals are compared and an error is computed at each iteration. Iterations are stopped when an error less of 10% over the entire range of the response spectra is obtained (Sooch and Bagchi, 2014). The last modified signal applied at the base of the foundation and satisfying the convergence criteria is referred to as the deconvolved signal and is used to evaluate the seismic behaviour of the dam-foundation systems.

Figure 3.9 illustrates the acceleration response spectra of the horizontal and vertical components of the free-field ground motion compared to the ones of the convolved signals at the top of the dam foundation.

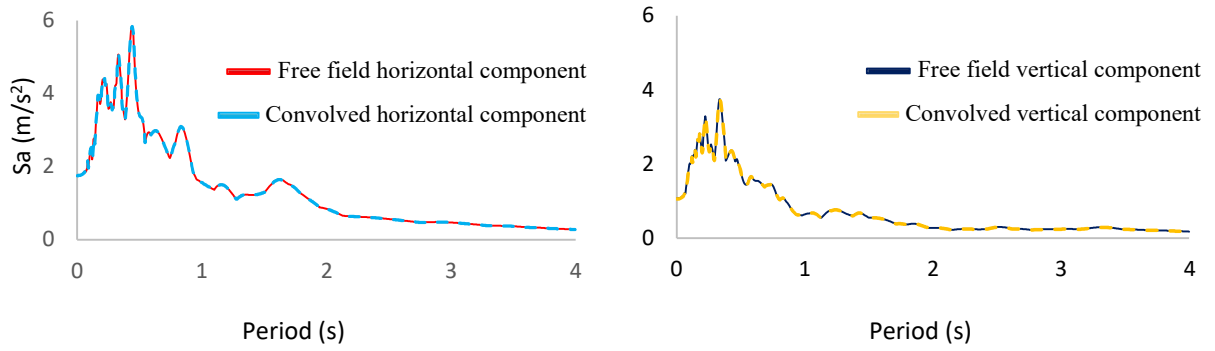

Figure 3.9 Comparing the acceleration response spectra of the Taft free-field ground motion to the ones of convolved signals

(a) horizontal component, and (b) vertical component.

The previous approaches are applied to construct coupled dam-reservoir-foundation systems as the one illustrated in Figure 3.10.

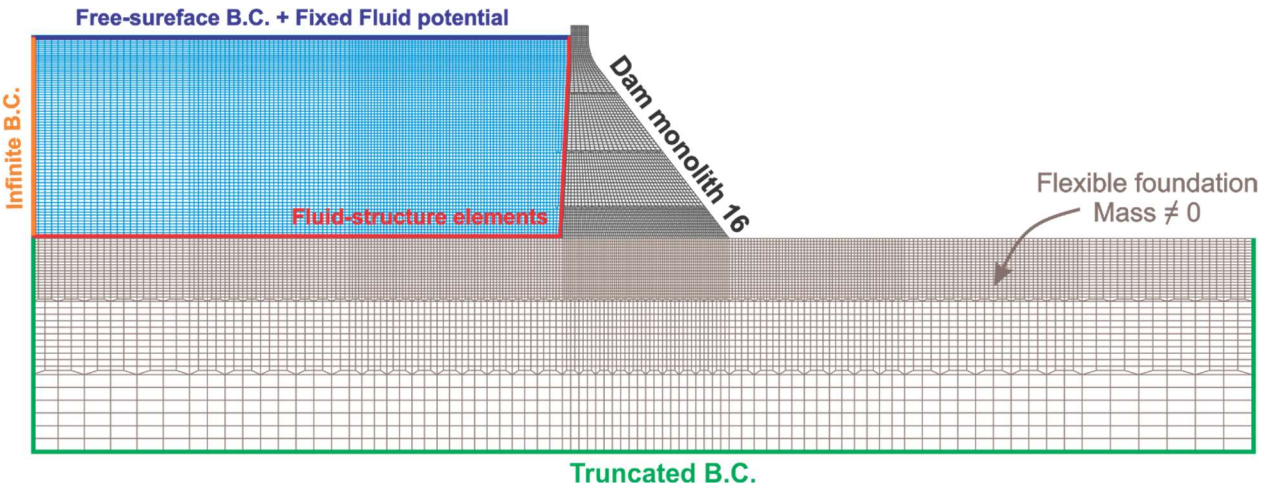

Figure 3.10 Numerical two-dimensional simulation of the dam-reservoir-foundation model

3.2 Seismic loads

Horizontal and vertical components of Taft ground motion are used to conduct the sensitivity analyses of the deconvolution process for Pine Flat dam. Recorded on July 21st, 1952, the Taft ground motion accelerations are applied in upstream-downstream and vertical directions

simultaneously to the foundation, dam-foundation and dam-reservoir foundation models, listed in Table 3.2, to investigate the accuracy and the efficiency of the deconvolution analysis for each of the models. Horizontal and vertical components of Taft earthquake are shown in Figure 3.11 (a). The maximum values of accelerations are 0.18g and 0.11g respectively for the horizontal and the vertical ground motions. The recording time step and the total duration of this earthquake are 0.01 and 54.15 seconds, respectively.

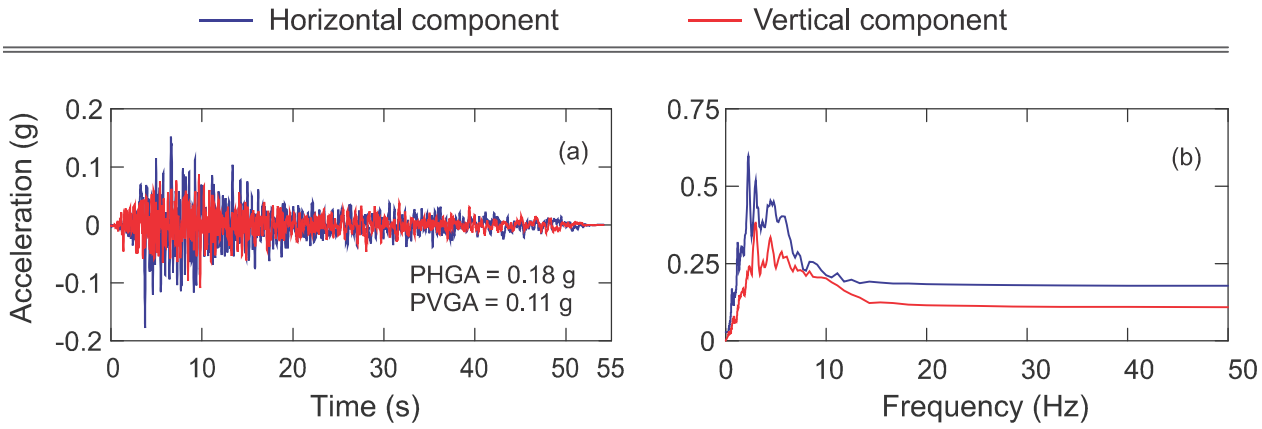

Figure 3.11 Taft earthquake (1952)

(a) horizontal and vertical accelerograms; (b) acceleration response spectra determined for 5% damping

CHAPTER 4 DECONVOLUTION SENSITIVITY ANALYSIS

Considering dam-foundation interaction in dynamic analyses of dam-reservoir-foundation systems introduces flexibility along with additional damping, which may affect the seismic response of the dam and appurtenant structures. The massless foundation assumption is utilized extensively in the literature and in the practice due to its simplicity. Considering only the stiffness of the foundation, the dam-foundation dynamic interaction is then reduced to a series of spring acting at the base of the dam, while inertia forces and damping of the foundation are ignored. This simplification also affects how earthquake input loads are applied. The absence of the foundation mass leads to an infinite wave velocity causing ground motion signals to propagate within the foundation instantaneously, without any changes. Therefore, recorded free-field ground motions can be applied effortlessly at the base of the foundation. A massed foundation is considered as a more realistic way of accounting for dam-foundation dynamic interaction. In this case, the seismic signals change within the foundation rising toward the dam. Therefore, the free-field recorded ground motions cannot be applied directly at the base of the foundation. A deconvolution process is then needed in order to obtain the signal at the base which produces the recorded free-field ground motion signal at the top (here dam-foundation interface). The appropriate deconvolved motion can be derived by utilizing either frequency domain analysis (Clough et al., 1985; Léger and Boughoufalah, 1989; Bayraktar et al., 2005) or data processing technique (Reimer, 1973; Khazaei poul and Zerva, 2018b; Robbe, 2017) along with time domain analysis. Data processing method, based on the mathematical model of the system, is utilized to deconvolve the seismic motions by adjusting the Fourier transform of the surface and base ground motions as suggested by Reimer (1973).

This chapter compares two adjustment techniques used in the literature for the deconvolution process in terms of accuracy and efficiency. A series of sensitive analyses are performed to investigate the effects of dimensions, flexibility and boundary conditions of the foundation, as well as, excluding or including the static weight of the system along with the presence of the dam and the reservoir during the process. Pine Flat dam subjected to horizontal and vertical components of Taft ground motion is used as an example for this purpose.

4.1 Deconvolution adjustment techniques

4.1.1 Phase-amplitude modification procedure

The phase-amplitude modification procedure suggested by Khazaei poul and Zerva (2018b) is suitable to deconvolve both horizontal and vertical components of a ground motion in linear viscoelastic media. The recorded free-field ground motion, termed as Target surface ground motion, consists of the horizontal component, which is assumed to consist mainly of shear waves (S-waves), and the vertical component, which mostly contains compressional waves (P-waves). The step-by-step procedure is as follows:

1- To calculate damping ratio and the equivalent properties of the soil layers, sensitivity analyses should be performed prior to the deconvolution process.

2- The deconvolution process initiates by building the finite element model of the foundation rock. An appropriate boundary condition (e.g. absorbing boundary condition, infinite elements, perfectly matched layers) muse be applied at the truncated boundaries. So, the reflection of the outgoing waves back into the model is prevented. In this research study the absorbing boundary is defined based on viscous boundary scheme developed by Lysmer and Kuhlemeyer (1969), described in Chapter 3.

3- The selected target time-history ground motion accelerations cannot be applied directly to the quiet boundary. Instead, first the accelerations is integrated to obtain velocities and then the effective horizontal and vertical time history nodal forces are calculated using equations (4.1 a,b) and are applied on nodes at the base of the soil profile.

$$F_S^{Input} = 2\,\rho\,b\,t\,C_S^{eq}\dot{u}_S^{Input}(t) \tag{4.1-a}$$

$$F_p^{Input} = 2\,\rho\,b\,t\,C_p^{eq}\dot{u}_p^{Input}(t) \tag{4.1-b}$$

where $\dot{u}_s^{Input}(t)$ and $\dot{u}_p^{Input}(t)$ represent respectively the velocity time history ground motion of S-waves and P-waves at depth. C_s^{eq} and C_p^{eq} are the equivalent shear and compressional wave velocities. ρ is the density of the soil. b and t are the length and the thickness of the elements at the bottom of the foundation. The factor of 2 is used to compensate the half of the energy which propagates downwards (Mejia and Dawson, 2006). The input velocity time histories are assumed to be half of the target value for the first

iteration. This division, here by two, will increase the convergence speed of the deconvolution method (Ju, 2013).

4- A time-domain analysis is then carried out using the effective nodal forces stated at step 2 in order to obtain the dynamic response ground motion at the top of the foundation.

5- Target, input and response ground motions (i.e. the velocity time histories) are transformed to frequency domain using Fast Fourier Transform (FFT) as expressed in equations 4.2 to 4.4 in terms of their amplitude and phase.

$$\dot{u}_s^{Target}(\omega) = \left|\dot{u}_s^{Target}(\omega)\right| \exp\left[i\varphi_s^{Target}(\omega)\right] \quad (4.2\text{-a})$$

$$\dot{u}_p^{Target}(\omega) = \left|\dot{u}_p^{Target}(\omega)\right| \exp\left[i\varphi_p^{Target}(\omega)\right] \quad (4.2\text{-b})$$

$$\dot{u}_s^{Input}(\omega) = \left|\dot{u}_s^{Input}(\omega)\right| \exp\left[i\varphi_s^{Input}(\omega)\right] \quad (4.3\text{-a})$$

$$\dot{u}_p^{Input}(\omega) = \left|\dot{u}_p^{Input}(\omega)\right| \exp\left[i\varphi_p^{Input}(\omega)\right] \quad (4.3\text{-b})$$

$$\dot{u}_s^{Response}(\omega) = \left|\dot{u}_s^{Response}(\omega)\right| \exp\left[i\varphi_s^{Response}(\omega)\right] \quad (4.4\text{-a})$$

$$\dot{u}_p^{Response}(\omega) = \left|\dot{u}_p^{Response}(\omega)\right| \exp\left[i\varphi_p^{Response}(\omega)\right] \quad (4.4\text{-b})$$

6- The new modified input ground motion is generated based on the following expressions:

$$\dot{u}_s^{Input\ (new)}(\omega) = \beta_s(\omega).\left|\dot{u}_s^{Input}(\omega)\right| \exp\left[i(\varphi_s^{Target}(\omega) - \bar{\varphi}_s^{Shift}(\omega))\right] \quad (4.5\text{-a})$$

$$\dot{u}_p^{Input\ (new)}(\omega) = \beta_p(\omega).\left|\dot{u}_p^{Input}(\omega)\right| \exp\left[i(\varphi_p^{Target}(\omega) - \bar{\varphi}_p^{Shift}(\omega))\right] \quad (4.5\text{-b})$$

where

$$\beta_s(\omega) = \left|\dot{u}_s^{Target}(\omega)\right| \ / \ \left|\dot{u}_s^{Response}(\omega)\right| \quad \text{Modifying factor}$$

$$\beta_p(\omega) = \left|\dot{u}_p^{Target}(\omega)\right| \ / \ \left|\dot{u}_p^{Resonse}(\omega)\right| \quad \text{Modifying factor}$$

$$\bar{\varphi}_s^{Shift}(\omega) = \varphi_s^{Response}(\omega) - \varphi_s^{Input}(\omega) \quad \text{Effective phase shift}$$

$$\bar{\varphi}_p^{Shift}(\omega) = \varphi_p^{Response}(\omega) - \varphi_p^{Input}(\omega) \quad \text{Effective phase shift}$$

7- The new input motion, then, transferred back from the frequency domain to the time domain using the inverse Fourier Transform (IFFT) to compute the new time history nodal forces and to perform a new analysis in the next iteration.

8- After each iteration a comparison must be made between the convolved ground motion (Response motion) and the target ground motion to see if the results are satisfying.

4.1.2 Amplitude modification procedure

The adjustment technique in this section is based on Fourier analysis proposed by Reimer (1973). The iterative deconvolution procedure is as follows:

1- The finite element model of the dam-foundation system is created by means of any FE commercial software. According to Bayraktar et al. (2010) the size of the foundation should be large enough, three times the height of the dam, to accommodate the local displacement near the dam. Boundary condition is defined based on tied degrees of freedom for the lateral sides, so it makes the soil column act one-dimensionally. Therefore, the boundary nodes of lateral sides at the same level are constrained to have the same displacement (Sooch and Bagchi, 2014). In this research, three different lateral boundary conditions are implemented to the model, while the base of the foundation model is considered fixed.

2- Target ground motion time history acceleration, considered as the input acceleration in the first iteration, is applied at the bottom of the foundation.

3- The wave propagation analysis is performed and the output time history acceleration at the point of interest on the foundation surface, i.e. the middle point at the dam-foundation interface, is determined.

4- Similar to the previous procedure, the reproduced acceleration time history at the top, the input and the free-field acceleration, all are converted to frequency domain using Fast Fourier Transform.

5- The correction factor to adjust the deconvolved signal is calculated differently compared to the phase-amplitude technique. The deconvolved signal is adjusted by using the ratio of the Fourier amplitudes of the free field and the output acceleration signals in the specific iteration for each frequency as expressed below:

$$C.F(j) = \frac{Amp_T(j)}{Amp_R(j)} \tag{4.6}$$

The new modified input motion in frequency domain is generated as:

$$a(j)_{modified} = a(j) * CF(j) \quad \text{and} \quad b(j)_{modified} = b(j) * CF(j) \qquad (4.7)$$

Where a(j) is the real part of the input motion at the base of the foundation and the b(j) is the imaginary part of the same signal in frequency domain.

6- The new modified input motion is then transferred back to the time domain using IFFT and is utilized to carry out a new wave propagation analysis in the next iteration.

7- A comparison should be made after each iteration between the convolved ground motion at the top and the selected target ground motion to see if the results are satisfying.

Table 4.1 Highlights and differences of the phase-amplitude vs amplitude modifications

Adjustment method / Parameters to compare	Phase-Amplitude modification	Amplitude modification
Primary step	Obtaining soil equivalent properties and damping ratio	---
FEM model	foundation with 4-node plain strain finite elements	Dam-foundation model using 4-node plain strain finite elements Depth of the foundation is 3 times the height of the dam
Boundary condition	Absorbing boundary condition (e.g. viscous boundary, infinite elements, PML or …)	Tied degrees of freedom at lateral sides
Signals used	Ground motion velocity used to calculate effective nodal forces at the base of the foundation	Time history ground motion acceleration
Modification factors	Fourier magnitude modifying factor $\beta(\omega) = \lvert \dot{u}^{Target}(\omega) \rvert \ / \ \lvert \dot{u}^{Response}(\omega) \rvert$ Effective phase shift $\bar{\varphi}^{Shift}(\omega) = \varphi^{Response}(\omega) - \varphi^{Input}(\omega)$	Amplitude modifying factor $C.F(j) = \frac{Amp_T(j)}{Amp_R(j)}$
Modified input	$\dot{u}^{Input\ (new)}(\omega) = \beta(\omega).\lvert \dot{u}^{Input}(\omega) \rvert \ exp\ [i(\varphi^{Target}(\omega) - \bar{\varphi}^{Shift}(\omega))]$	$a(j)_{modified} = a(j) * CF(j)$ $b(j)_{modified} = b(j) * CF(j)$

4.2 Deconvolution models

As an example of the deconvolution-convolution process, a single layer foundation is selected according to USSD benchmark workshop (2017) on Pine Flat dam. The foundation rock has a depth equal to the height of the dam, which is 121.92m (400 ft). The shear and compressional wave velocities are assumed to be constant for the whole foundation depth. The density of the soil and its Poisson's ratio are defined as 2482.86 kg/m3 (155 lb/ft^3) and 0.2, respectively. The horizontal and vertical components of Taft earthquake (1952) were selected as the target surface ground motions. It is also assumed that the horizontal ground motion consists mainly of shear waves, and the vertical ground motion of mostly of compressional waves. The soil domain was modeled in ADINA using plane strain 2D solid finite elements as described in the previous chapter.

For the deconvolution procedure based on the phase-amplitude modification technique, viscous Lysmer-Kuhlemeyer dampers are implemented into the bottom boundary of the rock foundation. The effective nodal time-history forces are calculated based on time-history velocity and are applied at the nodes at the base of the foundation. However, for the second adjustment technique based on amplitude modification, the boundary condition at the base of the foundation is defined differently. The ground motion accelerations are applied directly at the base and the lower edge of the foundation is defined as fixed.

First, the effects of several conditions at the lateral boundaries are investigated for the foundation medium including and excluding its self-weight. Fixed boundaries, sliders, as well as viscous dampers at lateral sides are chosen to evaluate how the convolved signal could be affected by the least realistic yet easiest, to the most real one but complicated to apply. The dam and the reservoir are respectively added to the foundation to verify their influence on the accuracy of the obtained convolved signals. On the other hand, another study is carried out on the depth of the foundation. Based on a study by Bayraktar et al. (2010), in order to accommodate local displacements, the size of the foundation should be three times the height of the dam. To consider the effect of dam-foundation interaction, it is recommended that the depth of the finite foundation should be at least twice the height of the dam (Khazaei Poul et al., 2018b). Penner et al. (2017) also created a numerical model of Ruskin dam in which the foundation extends three time the height of the dam in each direction. Therefore, the depth of the foundation for the second study is chosen as 3H, where H represents the height of the dam monolith, to meet the requirements of local displacement

accommodation as well as dam-foundation interaction. Figure 4.1 illustrates the numerical simulation of the foundation models for the phase-amplitude modification technique. In this figure, the viscous dampers are shown schematically at the base of the model. Dampers are applied to the bottom end of the foundation in both normal and tangential directions. The damping coefficients depend on density, shear and compressional wave velocities. Three different cases are considered to define the condition at the foundation lateral boundaries (i.e. fixed, sliding and absorbing), as illustrated in Figure 4.2.

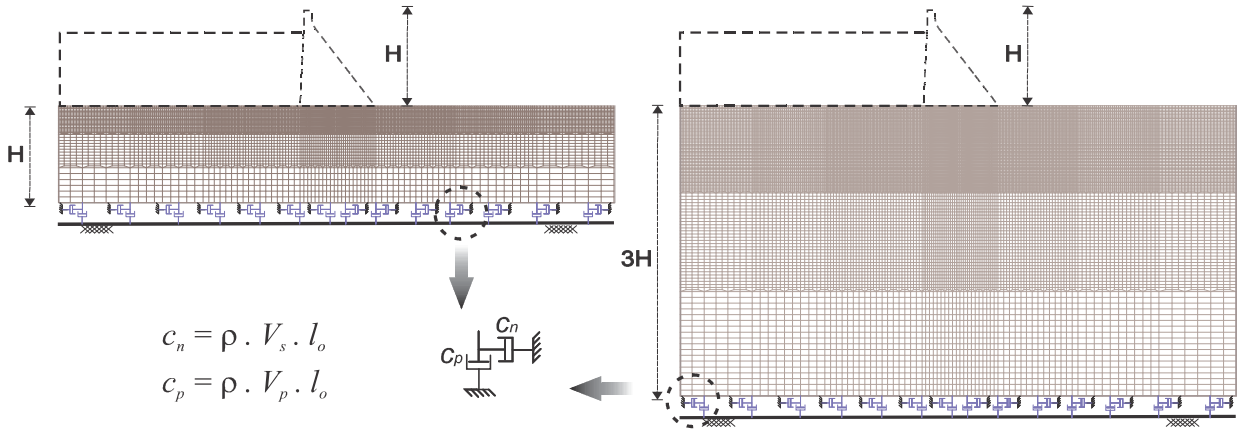

(a) (b)

Figure 4.1 Numerical simulation of the foundation models used for phase-amplitude method; (a) foundation model with 1H depth, (b) foundation model with 3H depth

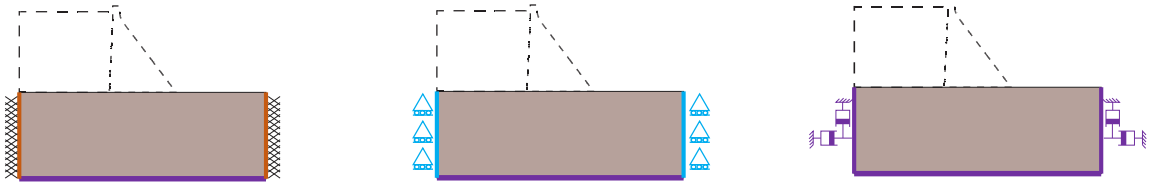

(a) (b) (c)

Figure 4.2 Lateral boundary conditions defined for the purpose of deconvolution sensitivity analyses:

(a) fixed lateral boundary condition, (b) sliding lateral boundary condition, (c) absorbing lateral boundary condition

4.2.1 Results for phase-amplitude modification procedure

A MATLAB (2017) code of the phase-amplitude modification method described earlier was programmed and used to carry out the deconvolution analysis. The goal is to determine the required input force time-histories such that the output acceleration time histories at the surface of the foundation match the target free-field ground motion. The program starts with the construction of the finite element model of the studied system through commands sent to ADINA (2018). Four different systems are considered. First, a flat box model (USBR, 2013), consisting of the rock foundation medium excluding the dam, the reservoir and any self-weight. A second system including the flat box model considering the self-weight of the foundation rock along with the deconvolution process. In the third model, the dam is added in order to verify the effects of the dam on the accuracy of the convolved signal at the dam-foundation interface. Finally, the reservoir is also included into the finite element model to give an insight of how it affects the deconvolution process. The effects of lateral boundary conditions are investigated for each of the described models. Fixed, sliding and absorbing boundary conditions are implemented to the nodes at the sides of the rock foundation.

The selected time-history ground motion accelerations are read by the program and converted to velocity time-histories; and the effective nodal time histories are calculated and applied at the nodes at the base of the foundation. Next, the time-domain time history analysis is performed. By obtaining the response signal on the surface of the foundation at the point of interest, the modification process is carried out to determine the modified input signal which is used for the next iteration. In this chapter, the comparison is made using time-history ground motion accelerations, while another comparison using response spectra is presented in appendix D. Figure 4.3 compares the horizontal and vertical components of the free-field ground motion accelerations and their related convolved signals obtained at the top surface of the foundation. As shown in Figure 4.3 (a) and (b), corresponding to the foundation model excluding the self-weight, a perfect agreement is achieved between the recorded free-field ground motion, here termed as “target motion”, and the convolved signals obtained at the top of the flat box respectively for the horizontal and vertical components, when the lateral boundaries are simulated using sliding and absorbing conditions However, in case of a fixed lateral boundary condition, discrepancies are observed at the beginning and the end of the horizontal convolved signal.

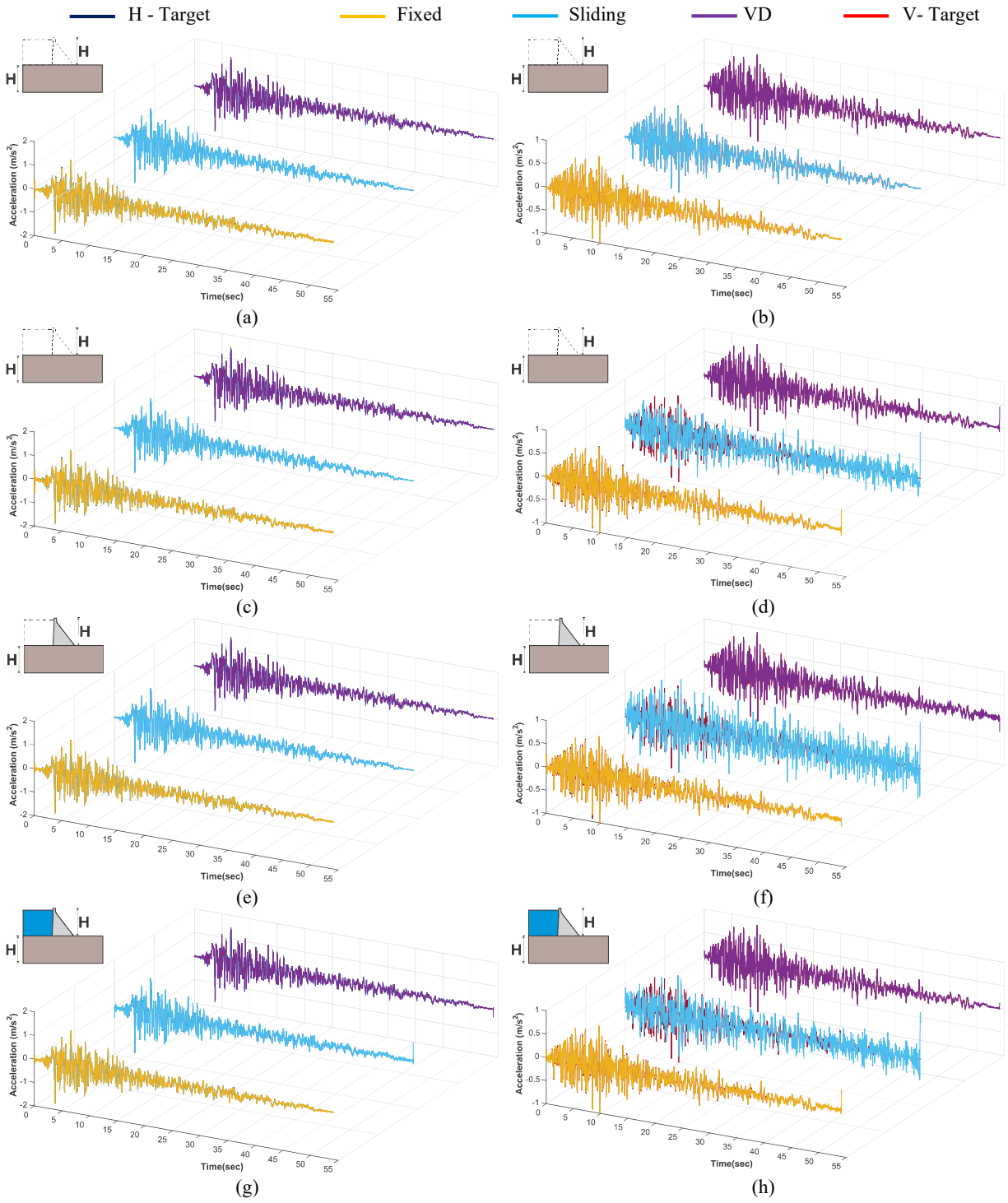

Figure 4.3 Comparing horizontal (left) and vertical (right) components of free-field acceleration vs convolved signal for the model with 1H depth including fixed, sliding and absorbing lateral B.C.

(a) and (b) Foundation only excluding its self-weight; (c) and (d) Foundation only including self-weight; (e) and (f) dam-foundation including static weight; (g) and (h) dam-reservoir-foundation including static weight

Figure 4.3 (c) illustrates a perfect match between the horizontal component of the target motion and the horizontal convolved signals for the models with sliders and viscous dampers at the lateral boundaries of the foundation model including self-weight. However, for the fixed lateral boundary condition, despite a very good match throughout the signal, there are discrepancies at the beginning and at the end of the horizontal convolved signal compared to the horizontal component of the target ground motion. Comparing vertical components in Figure 4.3 (d), the difference between target and vertical convolved signals is quite noticeable for the model with sliders. Seismic signals corresponding to the other two boundary conditions, however, show an ideal agreement throughout the whole time duration except at the beginning and at the end. Figure 4.3 (e) and (f) show respectively the comparison between the horizontal and vertical signals including the effect of the dam. As can be seen, while the horizontal convolved signals are not affected, less accurate results are obtained for the vertical components of the convolved signals. A good match is achieved for horizontal deconvolved components from the models with lateral sliders and viscous dampers. However, the discrepancies exist at the beginning and at the end of the vertical convolved signals of the same models. By including the reservoir, Figure 4.3 (g) and (h) illustrate the same trend as for the dam-foundation system. In this case, the best results for both horizontal and vertical components are obtained for the model including the lateral viscous dampers. Yet, a small discrepancy exists at both sides of the convolved signals.

Figure 4.4 compares the results from the models which foundation depth extends to three times the height of the dam. As shown in Figure 4.4 (a) and (b), a perfect match is obtained between target motions and convolved signals for both horizontal and vertical components of the models with sliding and absorbing lateral boundary conditions. As the depth of the model increases, the accuracy of the convolved signal in the model with fixed lateral boundary conditions decreases only for the horizontal component. Its vertical component still matches flawlessly. The comparison of the horizontal and vertical signals of the foundation only model including the static weight is illustrated in Figure 4.4 (c) and (d). A clean agreement is achieved for the models with sliding and absorbing lateral boundaries. However, for the horizontal convolved signal of the model with fixed B.C. a huge disagreement is obtained at the beginning of the signals. The vertical convolved signal for the same mode, nevertheless, perfectly matches the target motion.

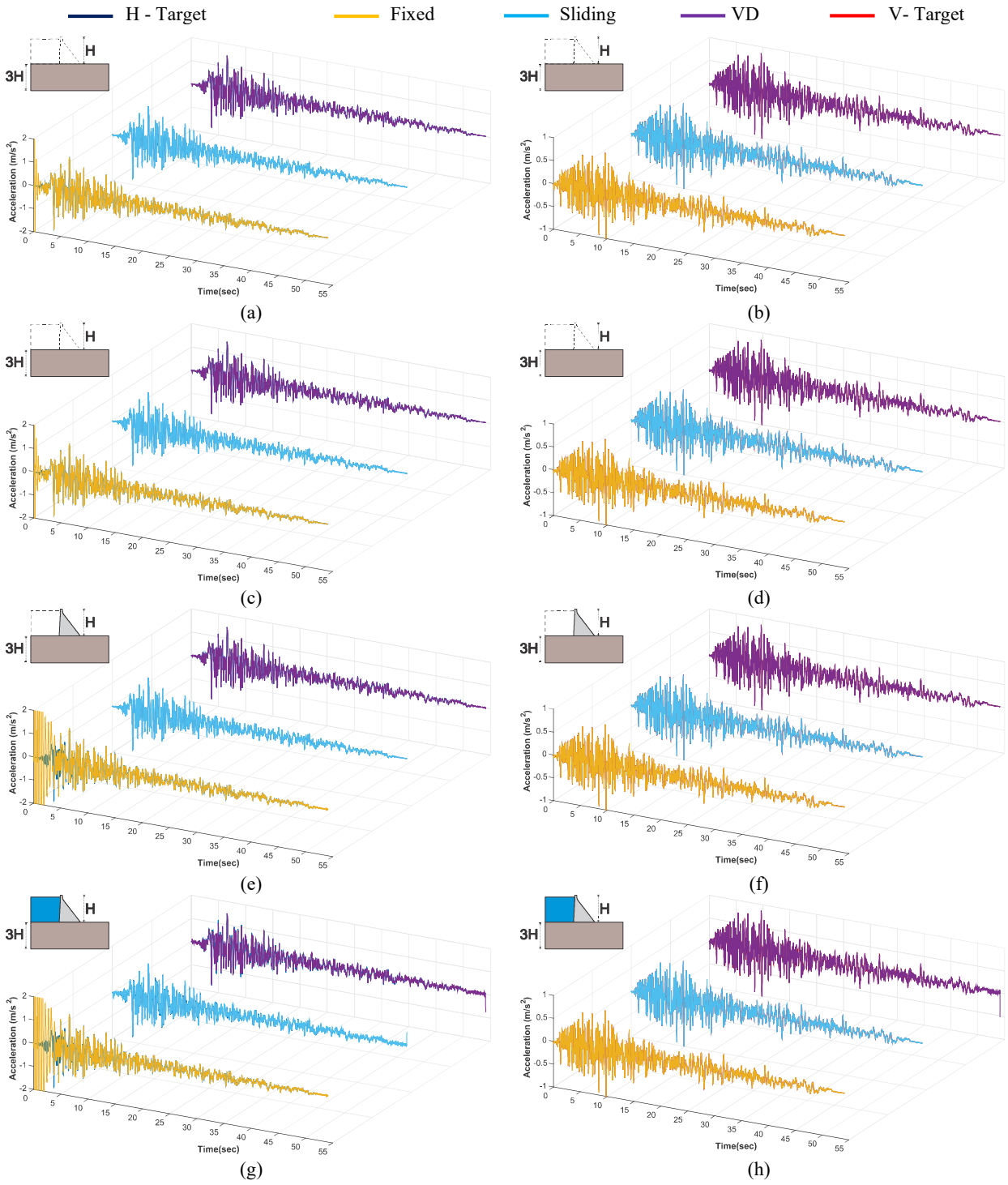

Figure 4.4 Comparing horizontal (left) and vertical (right) components of free-field acceleration vs convolved signal for the model with 3H depth including fixed, sliding and absorbing lateral B.C.

(a) and (b) Foundation only excluding its self-weight; (c) and (d) Foundation only including self-weight; (e) and (f) dam-foundation including static weight; (g) and (h) dam-reservoir-foundation including static weight

By joining the dam to the model, Figure 4.4 (e) and (f), the horizontal results related to the fixed lateral boundaries considerably lose their agreement and accuracy at the beginning, although they are matched elsewhere throughout the signal. Still for this model, the results obtained for the vertical deconvolved signals are in excellent agreement with the vertical target motion. The results for the dam-foundation model with 3H depth including the reservoir are shown in Figure 4.4 (g) and (h). As illustrated in Figure 4.4 (g), the horizontal convolved signals from the model with fixed lateral boundary conditions do not match the free-field signal at the beginning of the signal. The difference between the two signals is important. Horizontal convolved signals for models with both sliding and absorbing boundary conditions are also less accurate at the beginning and at the end of the signals. However, a very good agreement is achieved throughout these signals to the end. For the vertical components, all the models show a good agreement between the convolved and the target signals, although some slight discrepancies can still be observed at the end of the signals from the model with absorbing boundary conditions.

Figure 4.5 compares the convolved results obtained from the models with 1H depth with the ones from the models with 3H depth to show any improvement or deterioration of the convolved signals by increasing the depth of the model. As can be seen from Figure 4.5 (a) and (b), the accuracy of the horizontal convolved signals for the flat box models with fixed lateral boundaries and excluding the weight of the dam degrade with increased depth of the foundation. For the models with sliders and viscous dampers at the lateral sides of the rock foundation, the results are not affected. For the vertical components, however, the accuracy of the convolved signals is very satisfactory in both cases. In the case of the foundation model including self-weight, Figure 4.5 (c) and (d), the same trend exists for the horizontal convolved signals model with fixed lateral boundary condition. By increasing the depth of the foundation, the horizontal convolved signal is getting worse. However, much better results are obtained for the vertical convolved signals especially for the model with sliding lateral boundary conditions. No discrepancies are now observed at the beginning and at the end of vertical convolved signals. When the foundation depth is increased, more accurate vertical convolved signals are obtained for all the dam-foundation and dam-reservoir-foundation models with fixed, sliding and absorbing lateral boundary conditions. The accuracy of the horizontal convolved signals for the models with absorbing and sliding boundary conditions is also improved.

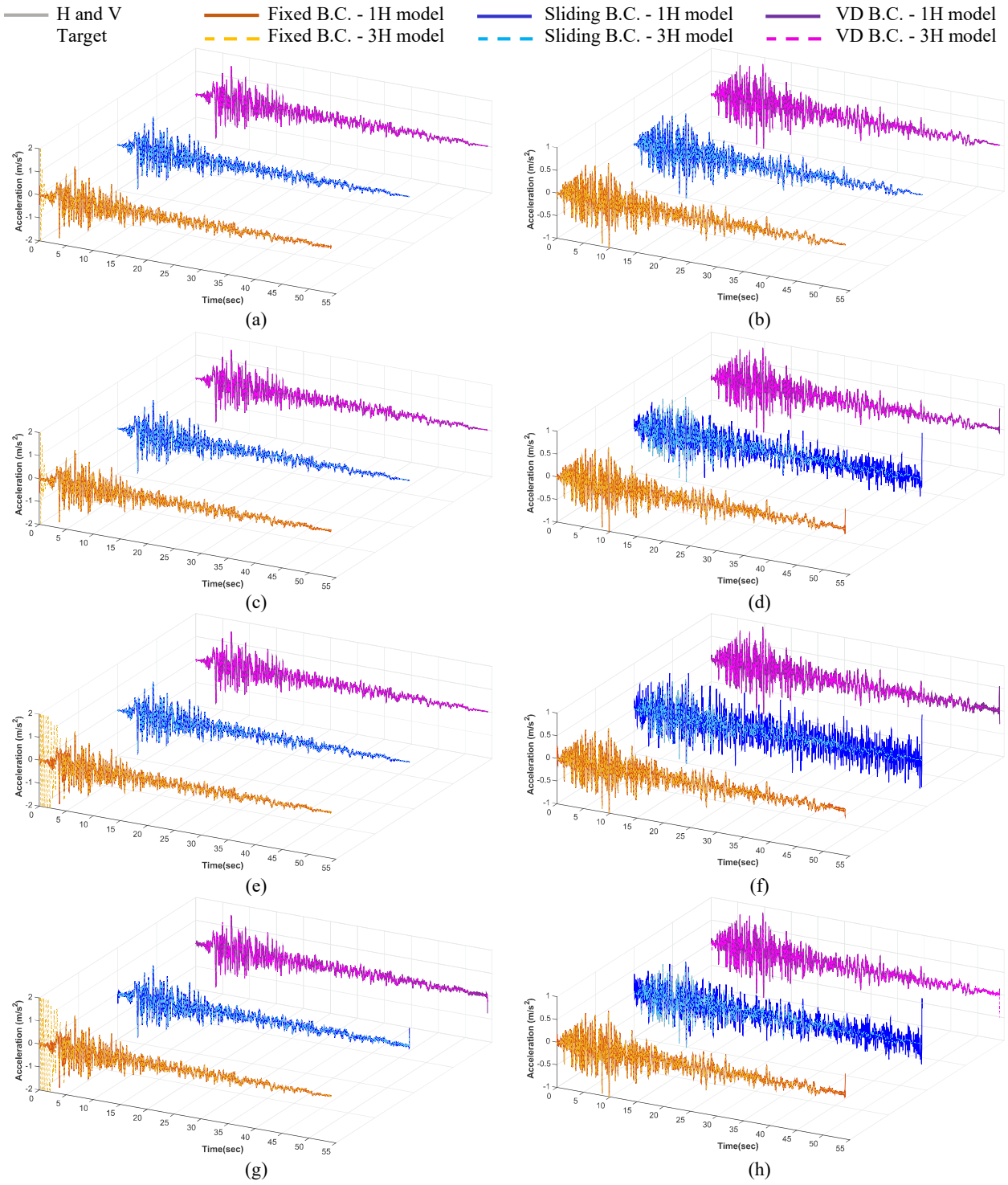

Figure 4.5 Comparing horizontal (left) and vertical (right) components of free-field acceleration vs convolved signal for the models with 1H and 3H depth including fixed, sliding and absorbing lateral B.C.

(a) and (b) Foundation only excluding its self-weight; (c) and (d) Foundation only including self-weight; (e) and (f) dam-foundation including static weight; (g) and (h) dam-reservoir-foundation including static weight

However, significantly less accurate convolved signals are obtained for the dam-foundation and dam-reservoir-foundation models with fixed lateral boundary conditions.

Another deconvolution analysis is carried out by attributing a very small value of the modulus of elasticity to the foundation rock in order to verify the effects that flexibility might have on the accuracy of the obtained convolved signal on the top surface of the foundation compared to the target ground motions. For this purpose, a small value of 4.48 GPa (i.e. one fifth of that used in the former models) was used as an elastic modulus of the rock foundation. The process is only performed for the flat box model of the foundation with 3H depth excluding the self-weight. As shown in Figure 4.6, a very good agreement is obtained for both horizontal and vertical earthquake components throughout the entire duration of the signal, except for a slight noise at the end of the convolved signals.

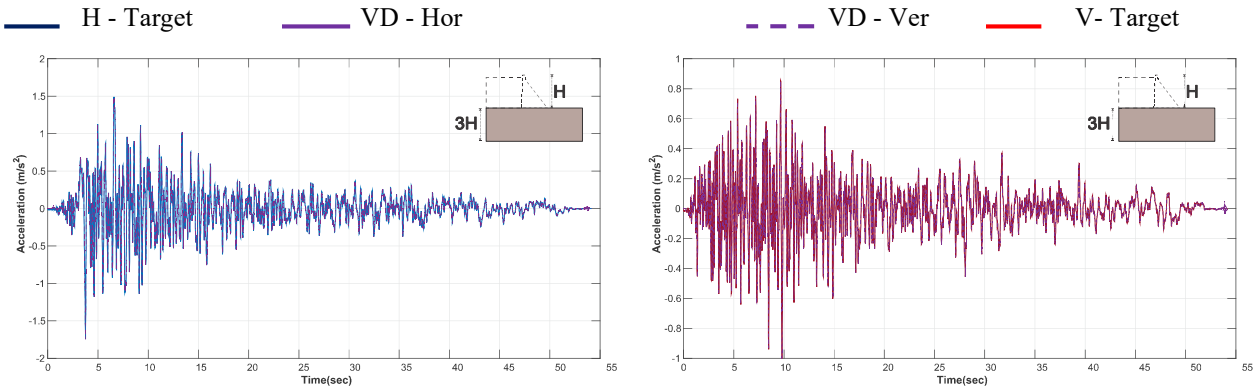

Figure 4.6 Comparing convoled signals versus target ground motion accelerations of the foundation only model with 3H depth having a very small value of Young's modulus
(a) Horizontal components; (b) Vertical components

4.2.2 Results for amplitude modification method

According to this approach, the seismic loads are applied as ground motion accelerations at the base of the dam foundation. The rock foundation model has fixed boundary conditions at the bottom edge and a depth of 3H, where H is the height of the dam. This method is evaluated only for the flat box model excluding the dam and the reservoir. Figure 4.7 shows the results obtained to verify the accuracy of the output signals compared to the target free-field ground motions when three types of lateral boundary conditions are applied (i.e. fixed, sliding and absorbing boundary

conditions). It is found that the horizontal and vertical convolved signals of the model with absorbing boundary conditions exhibit a better agreement than the other two models. A comparison of the acceleration response spectra of the target motions and their corresponding convolved signals is also presented in Appendix D.

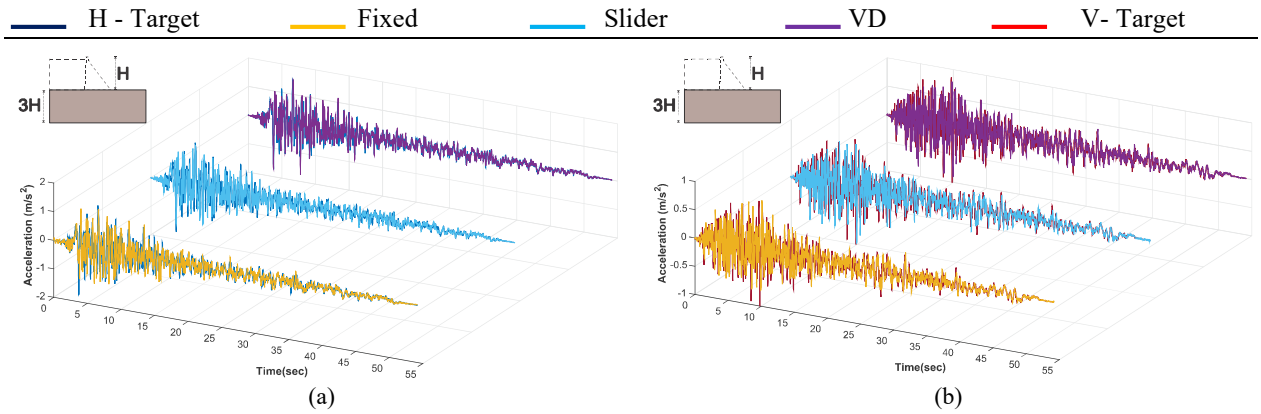

Figure 4.7 Comparing convolved signals versus free-field ground motion acceleration for the foundation-only model with 3H depth using amplitude modification approach

(a) horizontal components, (b) vertical components

4.3 Conclusions

The purpose of this chapter was to determine the input time-history signal such that the output time history acceleration at the top of the foundation matches the free-field ground motion acceleration. Two adjustment techniques reported in the literature were investigated to carry out deconvolution analysis for both horizontal and vertical seismic components in linear viscoelastic media and compared in terms of accuracy and efficiency. A series of sensitive analyses are performed to investigate the effects of dimensions, flexibility, boundary conditions of the foundation, as well as excluding or including the presence of the dam and the reservoir. The main conclusions can be summarized as follows:

1- The results show that the phase-amplitude procedure can accurately estimate the deconvolved ground motion. An excellent match is observed between the convolved and target motion for both horizontal and vertical components in flat box models. The amplitude FFT adjustment technique, however, is easier to apply but may induce inaccurate deconvolved signals.

2- Absorbing lateral boundary condition, compared to fixed and sliding lateral boundary conditions, exhibits much better agreement between the target and the convolved signals for both horizontal and vertical components using either of adjustment techniques.

3- By increasing the depth of the foundation to three times the height of the dam, the error in deconvolution results for the horizontal component increases considerably for the model with the fixed boundary condition. However, results for the models with sliding and absorbing lateral boundary conditions improves slightly. Improved accuracy is obtained for the vertical earthquake components of the model with sliding lateral boundary conditions.

4- The best results for the deconvolution process are obtained for the flat box model excluding foundation static weight. By adding the static weight, dam and the reservoir structure to the model, the accuracy of the deconvolution is affected mainly at the beginning and the end of the convolved signals.

5- The phase-amplitude method exhibits a very low sensitivity to the flexibility of the foundation. It yields excellent results for the foundation with very low elastic modulus.

6- Generally, the convergence of the deconvolution process for the flat box models using either of the lateral boundary conditions is achieved at the third or fourth iteration.

CHAPTER 5 ROCK FOUNDATION EFFECTS ON SEISMIC DEMANDS WITHIN DAMS AND APPURTENANT STRUCTURES

The effects of the soil-structure interaction on seismic demands within the dam are investigated in this chapter in terms of floor response spectra. The phase-amplitude deconvolution technique, described and verified in the preceding chapter, is utilized to perform deconvolution analyses to obtain the seismic signals to be applied at the base of the dam-reservoir-foundation models.

5.1 Size of the rock foundation model

Since the infinite domain of the foundation is truncated, a convergence study is required to determine the required size of the foundation sufficient for propagating waves to radiate out through the boundaries, i.e. no wave reflection back into the foundation domain. For this purpose, different upstream lengths are considered for the foundation model and the convergence of the dynamic response for the dam-foundation model is verified by means of the horizontal and the vertical floor acceleration response spectra at a point located at the middle of the dam crest.

The length of the foundation towards upstream is varied. The results of the convergence study are illustrated in what follows for upstream truncation lengths of 5H, 50H and 70H of the reservoir and the rock foundation, where H denotes the height of the dam monolith. The rock foundation is truncated at 3H downstream (i.e. from dam toe). The depth of the foundation is 3H as illustrated in Figure 5.1. The convergence of the horizontal and vertical floor response spectra is presented for Pine Flat dam-foundation model subjected only to the horizontal earthquake component of Taft ground motion, and then to both horizontal and vertical components of the same earthquake. The ground motions were first deconvolved for each truncation length.

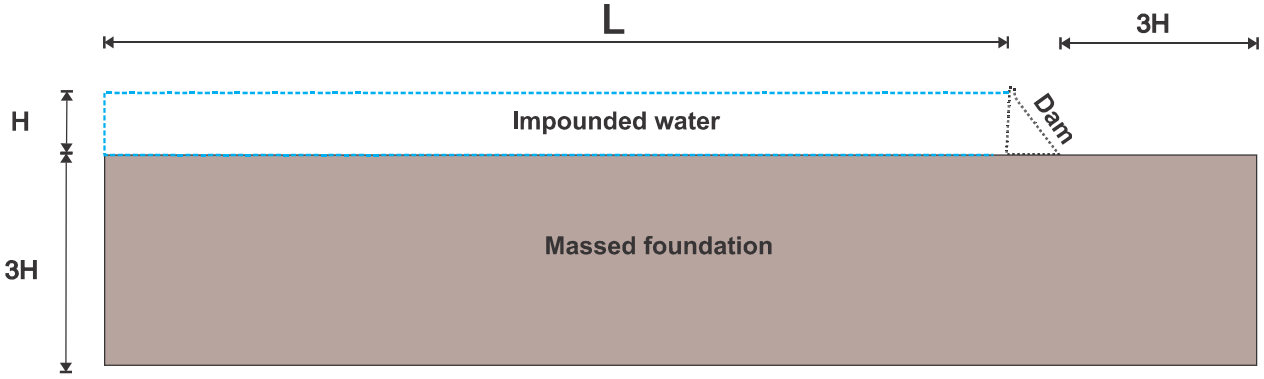

Figure 5.1 Dimensions of the reservoir and rock foundation domains

The convergence study is illustrated next for a model where the dam and the rock foundation are assumed to have the same modulus of elasticity. Viscous damping ratios of 5% and 7% are considered for the dam and foundation, respectively. Figure 5.2 shows the acceleration floor response spectra obtained at a point at the middle of the dam crest. Each floor spectral acceleration is divided by the horizontal peak ground motion acceleration (HPGA) of the ground motion to evaluate seismic amplifications from the dam base to the crest. It is seen from Figure 5.2 that the acceleration floor response spectra converge for an upstream truncation length of 50H of the reservoir and the rock foundation. This truncation length is used in the rest of this chapter.

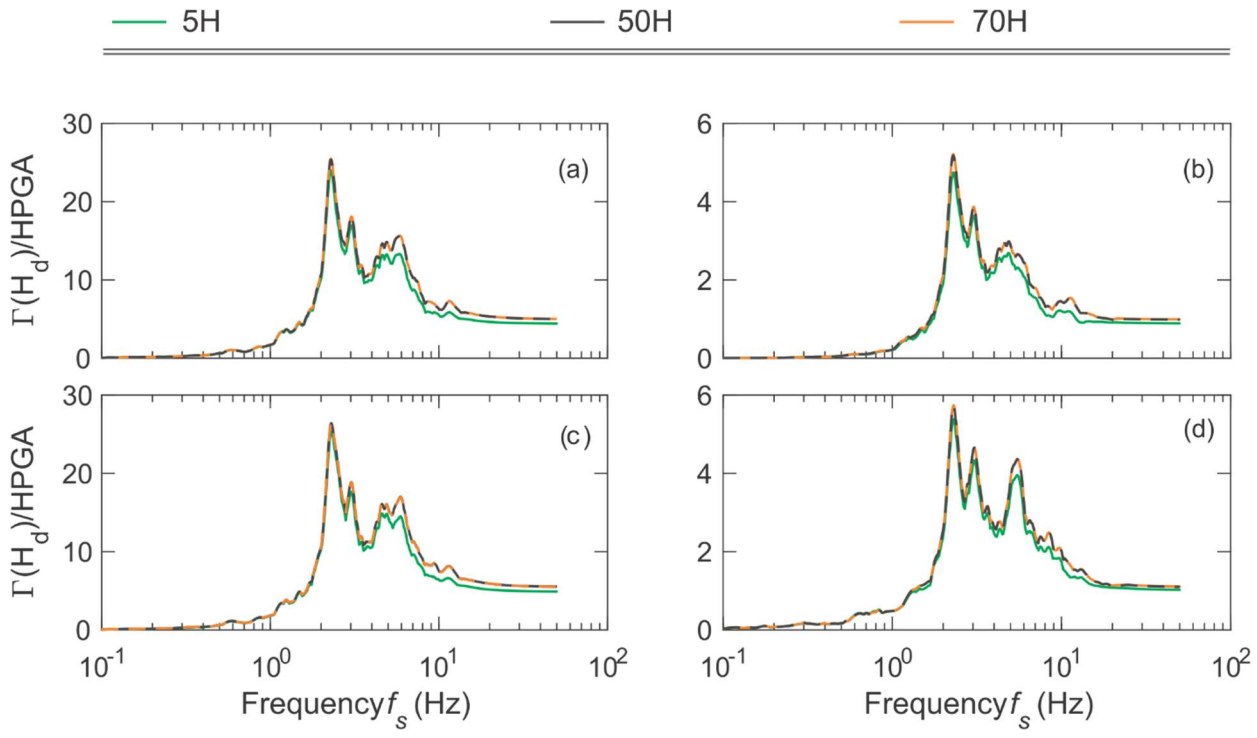

Figure 5.2 Verification of the convergence of the horizontal and vertical floor response spectra of the Pine Flat dam-massed foundation model subjected to deconvolved Taft ground motion

(a) and (b) horizontal earthquake input only; (c) and (d) horizontal and vertical earthquake input; (a) and (c) horizontal acceleration floor response spectra; (b) and (d) vertical acceleration floor response spectra

5.2 Calibration of Rayleigh damping

Absorbing boundary conditions are assigned at the lateral and bottom boundaries of the rock foundation as discussed in the previous chapter. The effective nodal forces are calculated and applied at the nodes located at the bottom of the foundation domain. The accuracy of the deconvolution process can be affected by the proper choice of natural frequencies used to calculate Rayleigh damping coefficients of the rock foundation. The case of a rock foundation with a relatively low ratio of elastic modulus to the elastic modulus of the dam, i.e. E_f/E_d =0.2, is illustrated in this section to highlight the effects of proper selection of Rayleigh damping on the accuracy of the convolved signal compared to the target free-field ground motion.

The dynamic properties of the flat box foundation model with 50H upstream truncation length are determined first, i.e. vibration frequencies, mode shapes and modal participation factors. The modes associated with significant contributions to the dynamic response of the foundation model are identified. An example of a 5%-damped frequency response curve at the point of interest (i.e. point at the middle of the dam-foundation interface) is shown in Figure 5.3 (a). A total of 500 modes were included in the analysis. The percentages of the mass participating along the Y direction are also given in Figure 5.3 (b). Table 5.1 contains the frequencies and modal mass participations (in %) corresponding to the modes contributing most to the dynamic response of the system, i.e. the fundamental, 46th and 129th vibration modes.

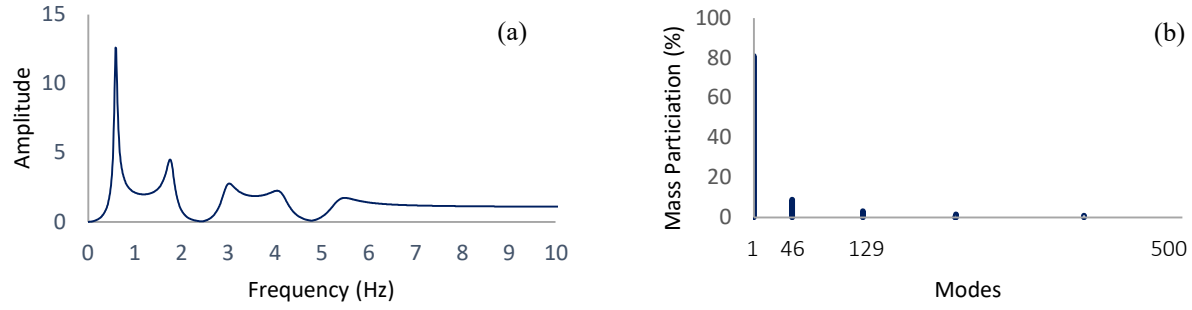

Figure 5.3 Modal properties of the dam-rock foundation

(a) Frequency response curve of the rock foundation model: (b) Percentage of the modal mass participation along Y direction considering 500 first modes

Table 5.1 Frequency and modal participation of significant modes in dynamic response of the foundation model with 50H upstream length

Mode	Frequency (Hz)	Modal participation (Y) %	Modal participation (Z) %
1	0.593	81.029	0
46	1.779	8.97668	0
129	2.965	3.21516	0

The Rayleigh damping coefficients are determined based on different sets of frequencies of the first, second and third significant modes identified previously in order to compare the effects on the convolved earthquake signals. The first set of frequencies correspond to the fundamental and second vibration modes, the second set to the fundamental and 49th vibration modes, and the third set to the fundamental and 129th vibration modes. The horizontal component of the Taft ground motion acceleration is used to illustrate the results. Figure 5.4 compares the acceleration time-history and the response spectra of the deconvolved horizontal component of Taft ground motion obtained using the different Rayleigh damping coefficients.

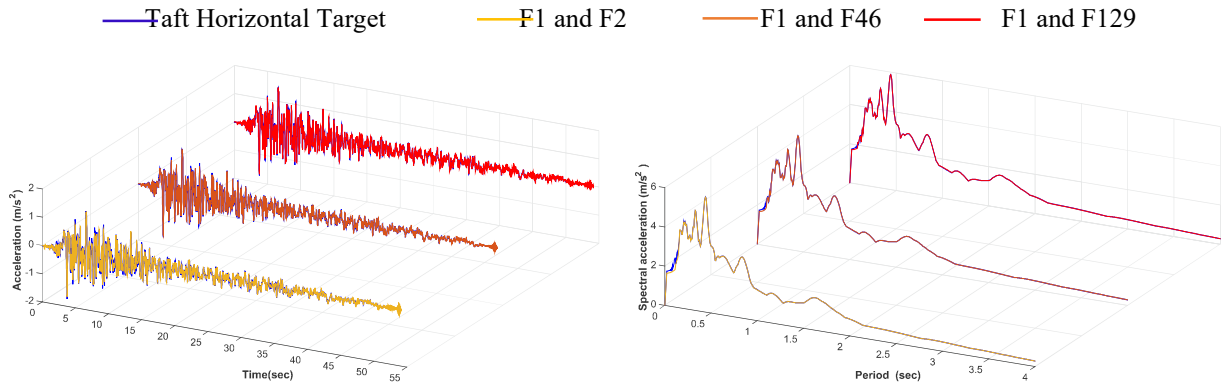

(a) (b)

Figure 5.4 Effect of Rayleigh damping on the accuracy of the horizontal convolved signals

(a) comparison between acceleration time histories; (b) comparison between response spectra of the related signals determined for 5% damping

As can be seen, the accuracy of the convolved signal at the surface of the foundation is significantly improved when the Rayleigh damping coefficients are obtained using the second and third sets of frequencies, i.e. fundamental and 49th or 129th vibration modes.

5.3 Effects of foundation flexibility and damping on dam-reservoir systems

The objective of this section is to study the horizontal and vertical floor acceleration response spectra obtained at a point at the middle of the crest of Pine Flat dam subjected to only the horizontal component of Taft ground motion, or to both horizontal and vertical components of the same record. The response of the gravity dam including impounded water effects is determined first. Water compressibility is modelled, while wave absorption at reservoir bottom is ignored. The acceleration floor response spectra are obtained from an implicit direct integration time-history dynamic analysis with a time step equal to 0.005 s. The base of the dam is considered rigid and the loads are applied as ground motion accelerations at the base. Three values of elastic modulus are considered for the rock foundation, corresponding to ratios of 2, 1 and 0.5 with respect to the elastic modulus of the dam concrete. Two viscous damping ratios are selected as 2% and 7%. Figure 5.5 shows the amplification of the horizontal and vertical acceleration floor response spectra when the dam-water system is subjected to loading cases described earlier. The horizontal and vertical acceleration floor response spectra are compared in Figures 5.5 (a) and (b). It is concluded that the vertical component of the considered Taft earthquake does not significantly affect the horizontal floor acceleration at the crest of the dam. However, the vertical floor response spectrum at crest is amplified considerably, especially at higher frequencies, when the dam-reservoir system is subjected to the horizontal and vertical components simultaneously.

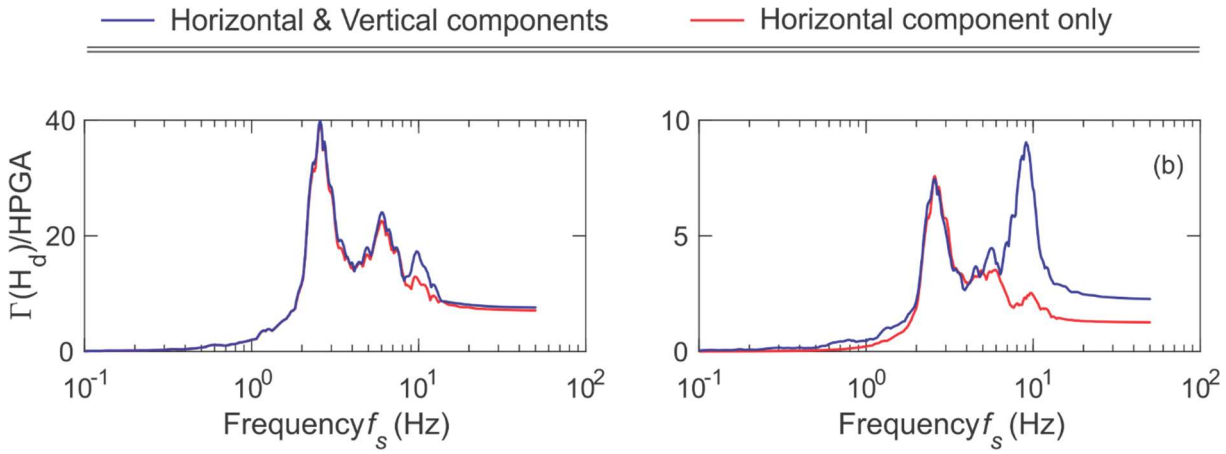

Figure 5.5 Horizontal and vertical floor response spectra at the crest of Pine Flat dam-reservoir model subjected to only horizontal or both horizontal and vertical components of Taft ground motion accelerations

(a) Horizontal acceleration floor response spectra; (b) Vertical acceleration floor response spectra

Figure 5.6 shows the floor acceleration response spectra at dam crest when the rock foundation is included in the analysis, considering viscous damping coefficients of 5% and 7% for the dam and rock foundation, respectively. It is observed that the amplifications of horizontal and vertical floor response spectra at dam crest are higher as rock foundation is stiffer. It is also seen from Figure 5.6 (b) that higher vertical accelerations are obtained at dam crest subjected to only horizontal earthquake when dam-foundation effects are included. Such effects also lead to shifting of the resonant peaks of the floor response spectra.

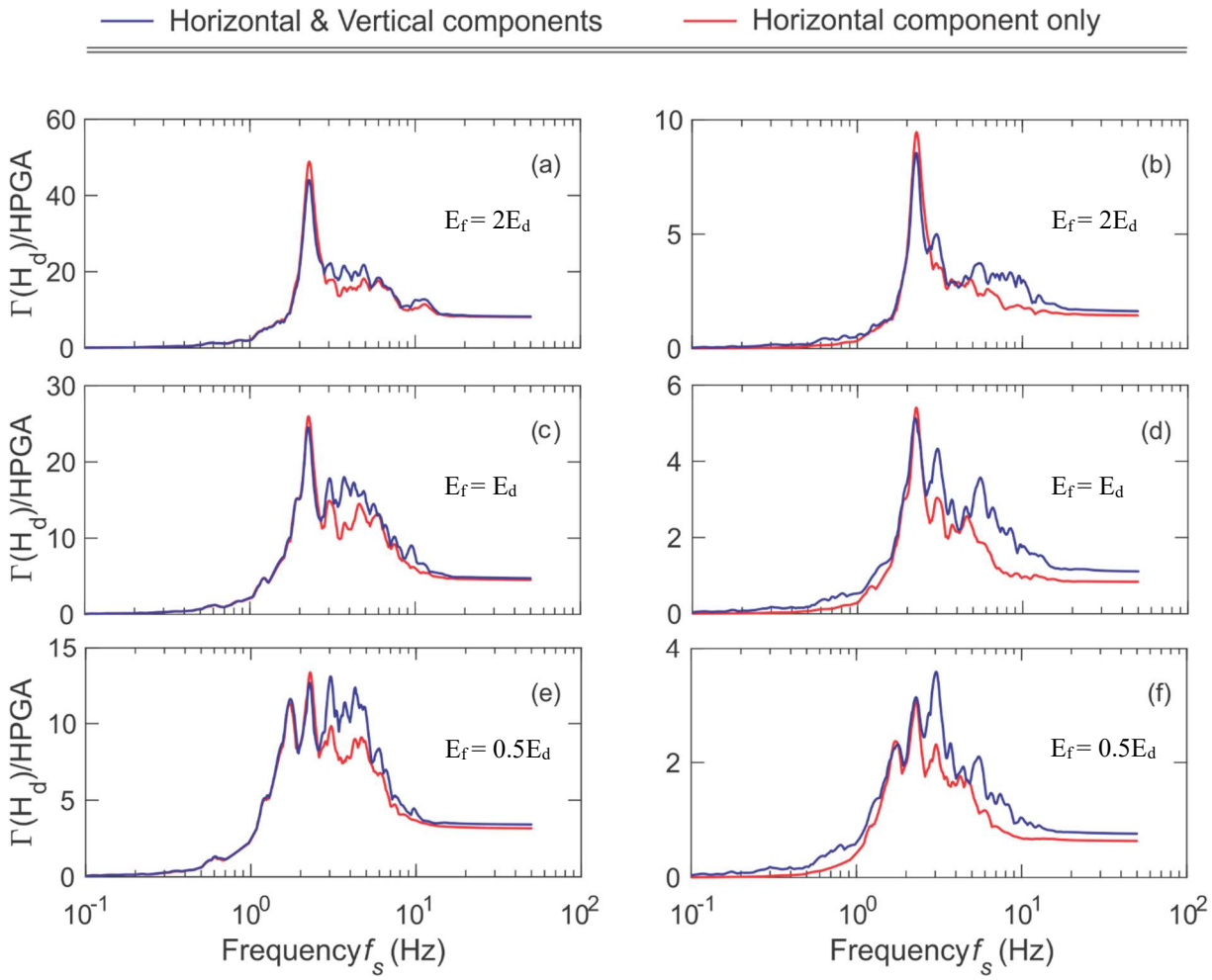

Figure 5.6 Horizontal and vertical floor response spectra at the crest of Pine Flat dam-reservoir-foundation model with 7% damping ratio subjected to only horizontal and both horizontal and vertical components of Taft ground motion earthquake

(a) and (b) elastic modulus of the foundation is twice as the elastic modulus of the dam; (c) and (d) elastic modulus of the foundation is equal to that of the dam; (d) and (e) elastic modulus of the foundation is half of the one related to dam; (a), (c) and (e): Horizontal acceleration floor response spectra; (b), (d) and (f): vertical acceleration floor response spectra.

Figure 5.7 illustrates the amplification of the horizontal and vertical floor spectral accelerations when a 2% damping ratio is considered for the rock foundation. Similar trends as previously are observed.

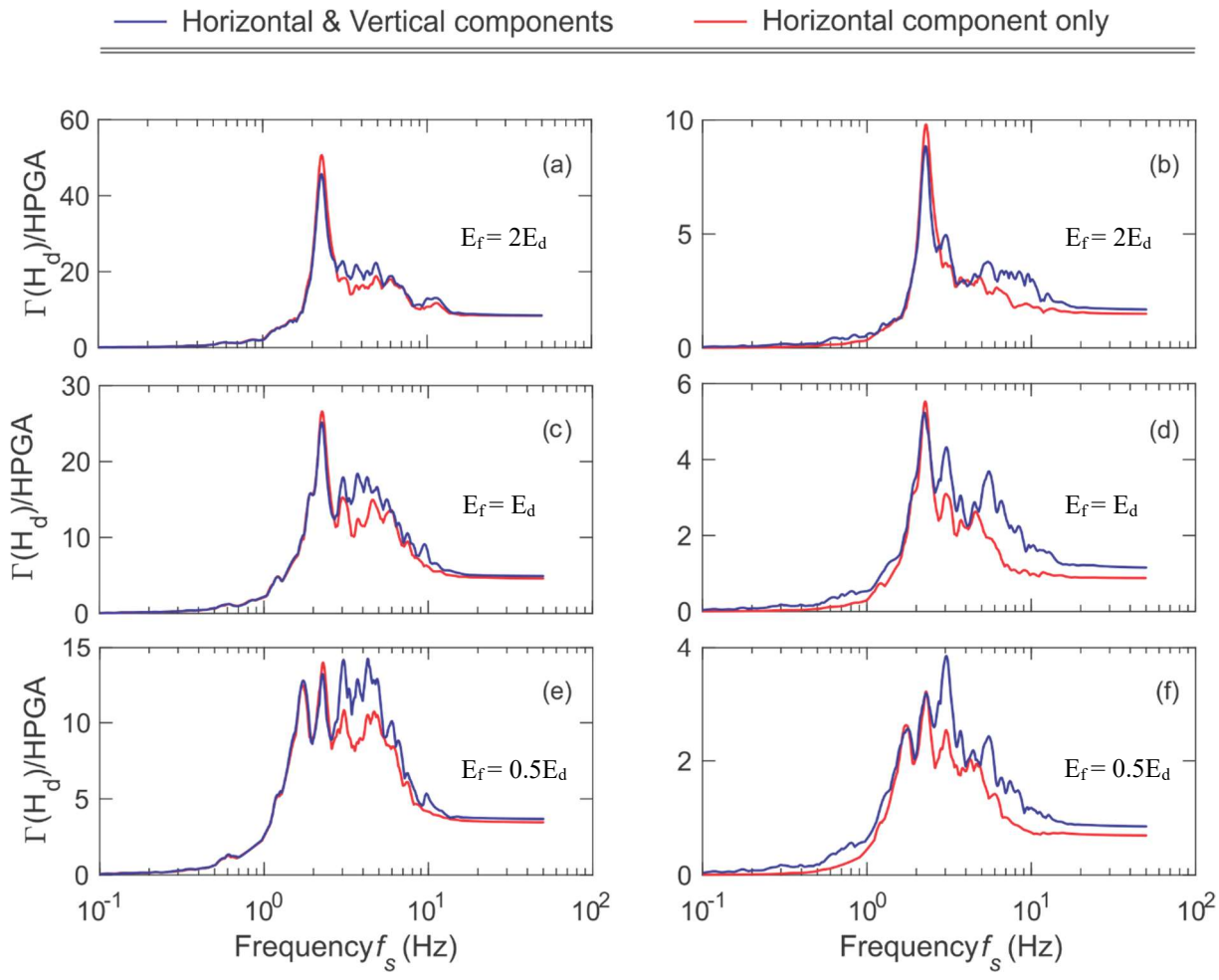

Figure 5.7 Horizontal and vertical floor response spectra at the crest of Pine Flat dam-reservoir-foundation model with 2% damping ratio subjected to horizontal only and horizontal and vertical components of Taft ground motion earthquake

(a) and (b) elastic modulus of the foundation is twice as the elastic modulus of the dam; (c) and (d) elastic modulus of the foundation is equal to that of the dam; (d) and (e) elastic modulus of the foundation is half of the one related to dam; (a), (c) and (e): Horizontal acceleration floor response spectra; (b), (d) and (f): vertical acceleration floor response spectra.

Another comparison between horizontal and vertical acceleration floor response spectra is shown in Figures 5.8 and 5.9 to highlight the influence of damping on the results. Figure 5.8 compares the results for the horizontal and vertical floor acceleration response spectra when the dam-reservoir-foundation model is subjected only to the horizontal component of the Taft ground motion. The results under both horizontal and vertical components of the same record are presented in Figure 5.9.

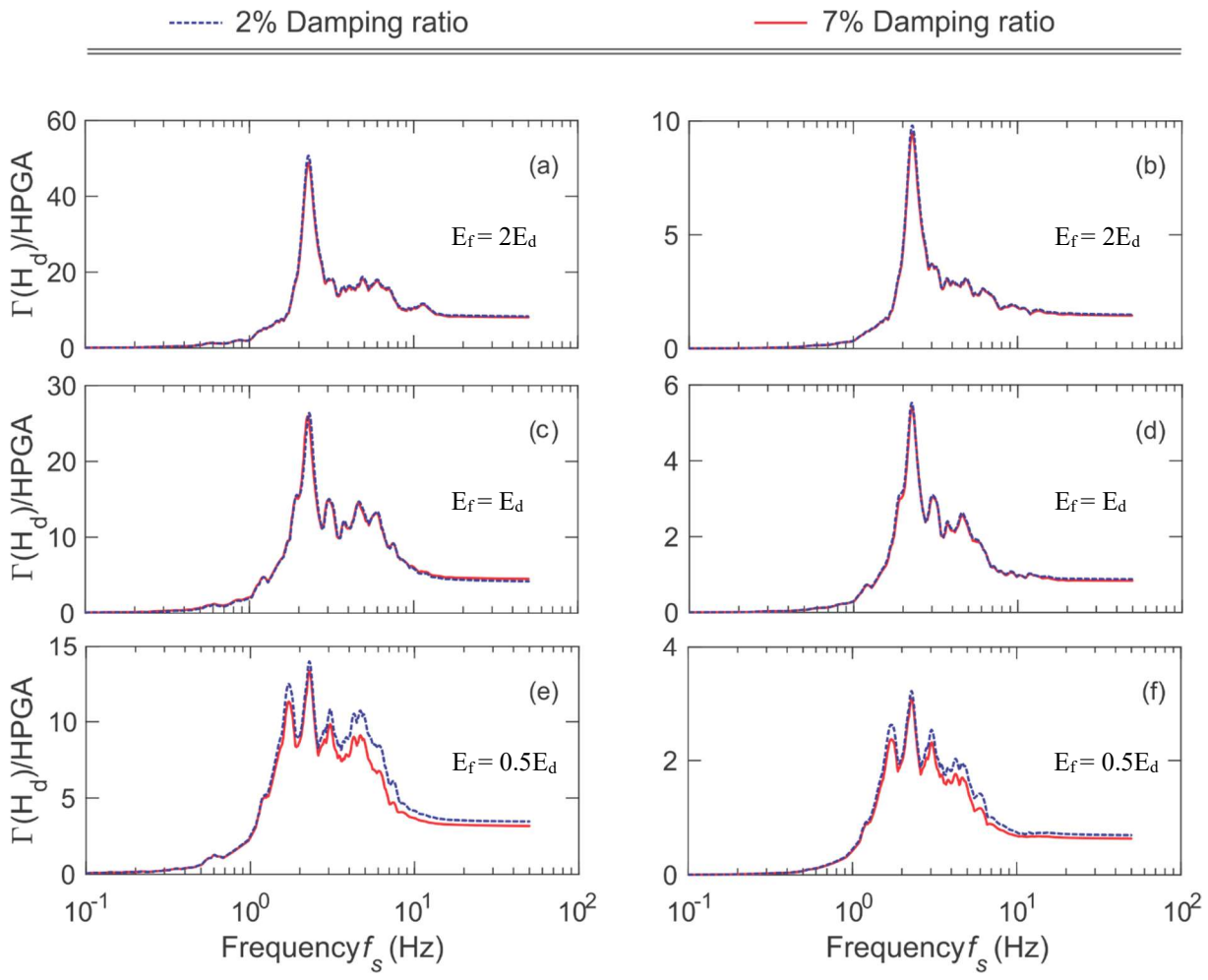

Figure 5.8 Horizontal and vertical floor response spectra at the crest of Pine Flat dam-reservoir-foundation model subjected to horizontal component of Taft ground motion earthquake

(a) and (b) elastic modulus of the foundation is twice as the elastic modulus of the dam; (c) and (d) elastic modulus of the foundation is the same as that of the dam; (e) and (f) elastic modulus of the foundation is half of the one related to dam; (a), (c) and (e) : Horizontal acceleration floor response spectra; (b), (d) and (f) : vertical acceleration floor response spectra.

These results show that horizontal and vertical floor acceleration response spectra are not significantly influenced by the damping ratio associated with a rock foundation when its flexibility is equal or higher than that of the dam. The opposite is observed when the flexibility of the rock foundation is lower than that of the dam. The results also show that horizonal and vertical floor spectral amplifications are higher when the damping ratio decreases from 7% to 2%.

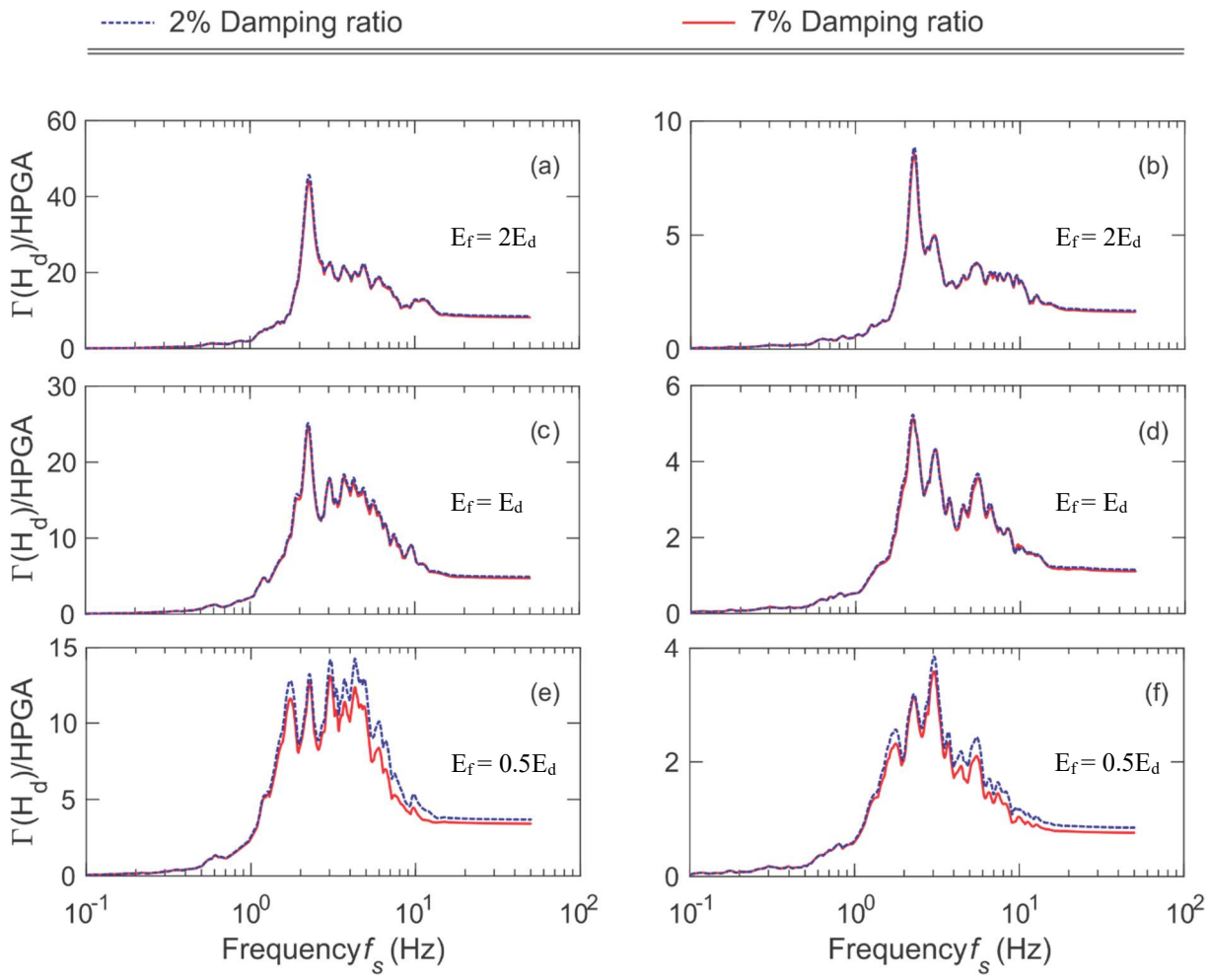

Figure 5.9 Horizontal and vertical floor response spectra at the crest of Pine Flat dam-reservoir-foundation model subjected to horizontal and vertical components of Taft ground motion earthquake simultaneously

(a) and (b) elastic modulus of the foundation is twice as the elastic modulus of the dam; (c) and (d) elastic modulus of the foundation is equal to that of the dam; (e) and (f) elastic modulus of the foundation is half of the one related to dam; (a), (c) and (e): Horizontal acceleration floor response spectra; (b), (d) and (f): vertical acceleration floor response spectra.

5.4 The effects of dam-size

In this section, the effects of dam size on the seismic demands related to a dam-reservoir-foundation system are investigated. For this purpose, a gravity dam, denoted hereafter as D35, is considered. The geometry of this small gravity dam is compared to that of Pine Flat dam in Figure 5.10. The dam has a height of 35 m, 27.5 m width at the base, and 5 m width at the crest. The level of impounded water is at 32 m. The dam, the reservoir and the rock foundation are modelled following the same methodology described in Chapter 3. The mechanical properties adopted for the D35 dam-reservoir-foundation system are summarized in Table 5.2.

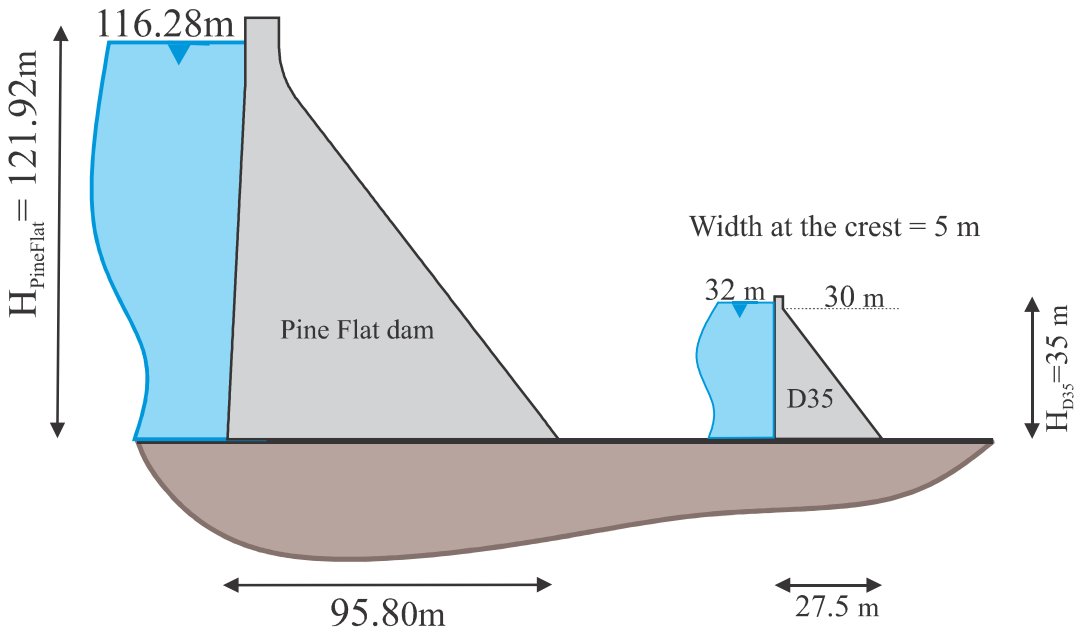

Figure 5.10 Geometry of the small & large gravity dams

Three elastic moduli are defined for the foundation with respect to the modulus of elasticity of the dam. The ratios are 2, 1 and 0.5, given respectively values of 50, 25 and 12.5 GPa for the elastic modulus of the foundation.

Table 5.2 Material properties for the synthetized small gravity dam

Material	**Parameters**	**Small dam (D35)**	**Units (SI)**
Concrete	Modulus of elasticity	25	GPa
	Density	2400	Kg/m^3
	Poisson's ratio	0.20	-
Foundation rock	Modulus of elasticity	E_f^*	GPa
	Density	2400	Kg/m^3
	Poisson's ratio	0.20	-
Water	Density	1000	Kg/m^3
	Bulk modulus	2.07 E9	N/m^2
	Wave velocity	1440	m/sec

Figure 5.11 illustrates the 2D finite element meshing of the D35 dam. Three transition layers are created, and the meshing is more refined at the crest and at the base of the dam.

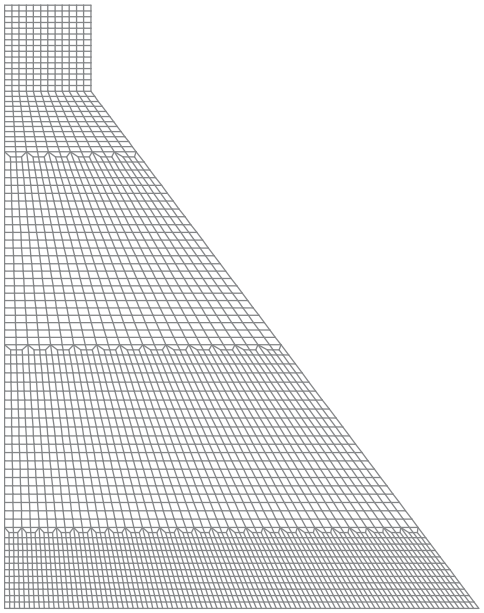

Figure 5.11 2D meshing of the D35 gravity dam

The dam is subjected to the horizontal and vertical components of Taft earthquake described previously. The same deconvolution technique used for Pine Flat is applied. The same boundary conditions discussed previously are also considered. Figure 5.12 compares the horizontal and vertical floor acceleration response spectra at the middle of the crest of the D35 dam subjected to only horizontal Taft ground motion, and both horizontal and vertical ground motions. The results

show that the amplification on the horizontal floor spectral accelerations is practically not affected. However, the vertical floor response accelerations are amplified considerably when the system is subjected to the both horizontal and vertical earthquake input. When the effects of rock foundation are included, the amplifications of the horizontal and vertical acceleration floor response spectra at the crest of the dam decrease as shown in Figure 5.13.

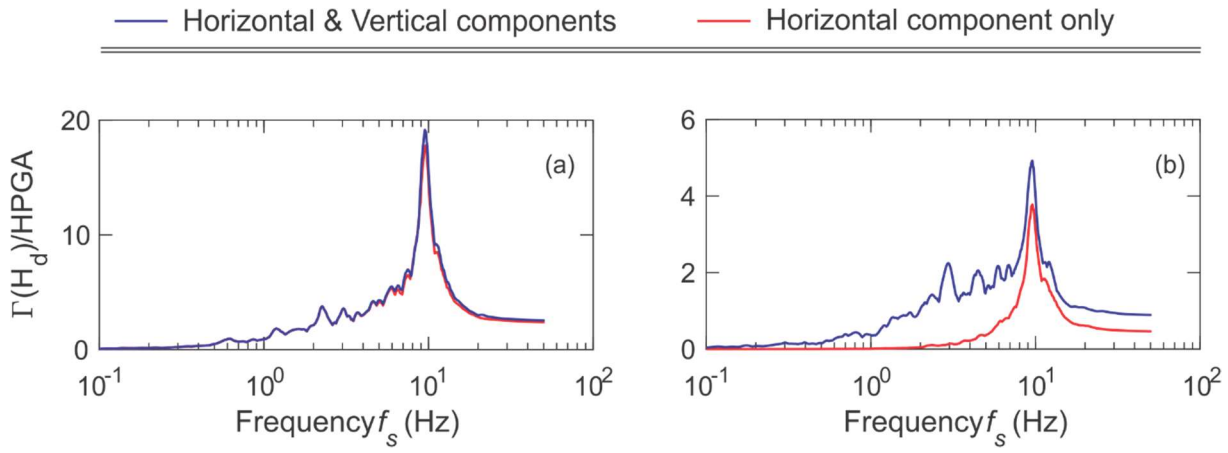

Figure 5.12 Horizontal and vertical floor response spectra at the crest of D35 dam-reservoir model including compressible water subjected to only horizontal and both horizontal and vertical components of Taft ground motion

(a) horizontal floor acceleration response spectra; (b) vertical floor acceleration response spectra

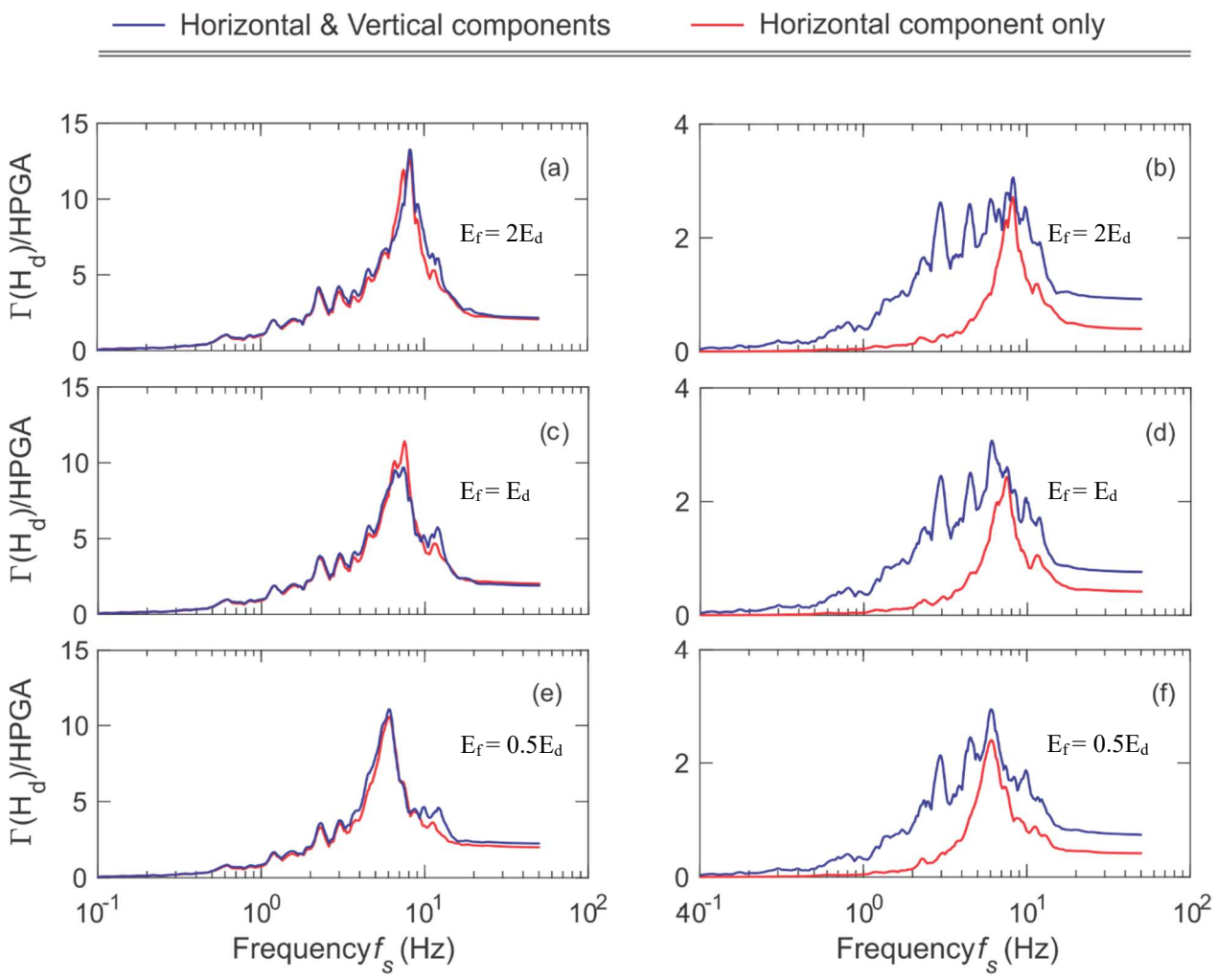

Figure 5.13 Horizontal and vertical floor response spectra at the center of the crest of D35 dam-reservoir-foundation model with 7% damping ratio subjected to horizontal only and horizontal and vertical components of Taft ground motion earthquake

(a) and (b) elastic modulus of the foundation is twice as the elastic modulus of the dam; (c) and (d) elastic modulus of the foundation is equal to that of the dam; (d) and (e) elastic modulus of the foundation is half of the one related to dam; (a), (c) and (e): horizontal acceleration FRS; (b), (d) and (f): vertical acceleration FRS

CHAPTER 6 CONCLUSION

The purpose of this research was to investigate the effects of rock foundation on seismic demands within dams and appurtenant structures. Due to potential amplifications of ground motions over the height of a dam, the supported equipment and secondary structures can be at higher seismic hazard than the dam itself. The finite element method is used in this work to investigate the seismic response of dam-reservoir-foundation systems, expressed in terms of floor acceleration response spectra, when subjected to horizontal and vertical ground motion components. Several 2D finite element models of dam-reservoir-foundation systems including fluid-structure interaction, as well as absorbing boundary conditions for the rock foundation domain were constructed. A deconvolution process was carried out to account for the mass of the rock foundation. For this purpose, an efficient MATLAB code was developed and applied to obtain the deconvolved earthquake signals at the base of the foundation. Two different adjustment techniques were applied to modify the output seismic signals obtained from transient time-domain analysis at the end of each deconvolution iteration. The effects of the dimensions of the rock foundation, the boundary conditions and dam foundation flexibility on the convergence, accuracy and efficiency of the techniques were investigated. The deconvolved seismic signals were utilized to evaluate the effects of massed foundation on dynamic behavior of dam-reservoir-foundation systems, in terms of floor acceleration response spectra within the dams. The effects of foundation flexibility and damping ratio on the seismic demands were also investigated. Two dams were considered for illustration purposes: Pine Flat dam and a smaller 35 m gravity dam.

The following main conclusions can be drawn from this study:

1- The phase-amplitude FFT adjustment technique for the deconvolution process provided an excellent agreement between the convolved and the free field ground motion acceleration. However, this procedure requires the application of absorbing boundary conditions and the determination of nodal forces at the base of the soil domain. Although the adjustment technique based on only FFT amplitude is simpler and can be more efficient, it may induce inaccurate deconvolved signals.

2- Absorbing lateral boundary conditions of the rock foundation domain, simulated using viscous Lysmer-Kuhlemeyer dampers, exhibit much better performance compared to fixed and sliding boundary conditions.

3- Increasing the depth of modelled rock foundation could lead to less accurate deconvolution results if the foundation If the rock is highly flexible.

4- Inadequate evaluation of equivalent Rayleigh damping for the purpose of transient direct integration analyses used in the deconvolution process may lead to inaccurate results.

5- The convergence for the deconvolution process for the flat box models using either of lateral boundary conditions was achieved within three or four iterations.

6- The presence of the massed flexible foundation can significantly influence the seismic demands within gravity dams. For example, some results show that the amplification of floor acceleration response spectra at the dam crest could be reduced by up to 70% when rock foundation effects are included.

7- Increasing the viscous damping ratio of the rock foundation slightly reduces the amplification of both horizontal and vertical floor acceleration spectra for the foundations with higher flexibility ratios. However, this damping effect increases with decreasing rock foundation flexibility.

8- A stiffer rock foundation generally induced higher acceleration seismic demands with the gravity dams studied.

6.1 Research Perspectives

The analyses performed in this research considered the linear behavior of the dam and the foundation. However, the material nonlinearity for the dam and the foundation, cracking, joint opening and sliding between dam-foundation interface should be considered for further research. Accounting for the nonlinear behaviour of the soil in such analyses should also be considered. Moreover, absorption of the compressional waves, due to the sedimentation at the bottom of the reservoir, should also be considered at reservoir-foundation interface. Finally, three-dimensional simulation of dam-reservoir-foundation system, i.e. 3D effects of the reservoir, input seismic loads, should be investigated as well.

REFERENCES

ADINA (2018). Theory and Modeling Guide. ADINA 9.4.

Ahmadi, M. T., Khoshrang, G., Mokhtarzadeh, A., and Jalalzadeh, A. (1992). *Behavior of a large concrete dam due to an actual maximum credible earthquake.* Paper presented at the Proceedings of the World Conference on Earthquake Engineering, Madrid, Spain, (Vol. 7, pp. 3995-4000).

Alves, S. W. (2005). *Nonlinear analysis of Pacoima dam with spatially nonuniform ground motion*: ProQuest.

Bayraktar, A., Hançer, E., and Akköse, M. (2005). Influence of base-rock characteristics on the stochastic dynamic response of dam-reservoir-foundation systems. *Engineering Structures, 27*(10), 1498-1508.

Bayraktar, A., Türker, T., Akköse, M. and Ates¸ S. (2010). The effect of reservoir length on seismic performance of gravity dams to near-and far-fault ground motions, Natural Hazards, vol. 52(2), 257–275.

Bouaanani, N. and Lu, F. Y. (2009). Assessment of potential-based fluid finite elements for seismic analysis of dam–reservoir systems. *Computers Structures, 87*(3), 206-224.

Bouaanani, N. and Perrault, C. (2010). Practical formulas for frequency domain analysis of earthquake-induced dam-reservoir Interaction. *Journal of Engineering Mechanics*, *136*(1), 107-119. doi:10.1061/(asce)em.1943-7889.0000064

Bouaanani, N. and Renaud, S. (2014). Effects of fluid–structure interaction modeling assumptions on seismic floor acceleration demands within gravity dams. *Engineering Structures, 67* 1-18.

Bouaanani, N., Renaud, S., Tinta, S. and Saichi, T. (2018). *Seismic spectra for safety evaluation of critical dam appurtenant systems and equipment*. 16th European Conference on Earthquake Engineering, Thessaloniki, Greece.

Chen, Y. and Soong, T. (1988). State-of-the-art review: Seismic response of secondary systems. *Engineering Structures*, 10(4), 218–228.

Chopra, A. K. and Chakrabarti, P. (1973). The Koyna earthquake and the damage to Koyna dam. *Bulletin of the Seismological Society of America, 63*(2), 381–397.

Clough, R. W., Chang, K., Chen, H.-Q., and Ghanaat, Y. (1985). *Dynamic interaction effects in arch dams*. Report No. UCB/EERC-85/11, Earthquake Engineering Research Center, University of California, Berkeley.

Cooley, J. W. and Tukey, J. W. (1965). An algorithm for the machine calculation of complex Fourier series. *Mathematics of computation, 19*(90), 297-301.

Everstine, G. C. (1981). A symmetric potential formulation for fluid-structure interaction. *Journal of Sound and Vibration, 79*(1), 157–160.

Fenves, G. and Chopra, A. K. (1984). *EAGD-84, A Computer Program for Earthquake Analysis of Concrete Gravity Dams Tech.*, Rep. UCB/EERC-84/11, Earthquake Engineering Research Center, University of California, Berkeley.

Fenves, G. L. and Chopra, A. K. (1984). *Earthquake analysis and response of concrete gravity dams*. Technical report UCB/EERC-84/10, University of California, Berkeley.

Fenves, G. L. and Chopra, A. K. (1985). Simplified earthquake analysis of concrete gravity dams: Separate hydrodynamic and foundation interaction effects. *Journal of Engineering Mechanics*, ASCE, 111(6), 715–735.

Ghanaat, Y. (2004). *Failure modes approach to safety evaluation of dams*. Paper presented at the Proceedings of the 13th world conference on earthquake engineering, Vancouver, B.C., Canada.

Ghrib, B., Leger, P., Tinawi, R., Lupien, R. and Veilleux, M. (1997). Seismic safety evaluation of gravity dams. *International Journal on Hydropower and Dams, 4*(2), 126-137.

Hall, J. F. (1986). Study of the earthquake response of Pine Flat dam. *Earthquake engineering & structural dynamics*, *14*(2), 281-295.

Huang, J. J. and Zerva, A. (2014). Earthquake performance assessment of concrete gravity dams subjected to spatially varying seismic ground motions. *Structure and Infrastructure Engineering, 10*(8), 1011-1026. doi:10.1080/15732479.2013.782323

ICOLD (2001). *Design features of dams to resist seismic ground motion-Guidelines and case studies*. Bulletin 120, International Commission on Large Dams.

ICOLD (2008). *Reservoirs and Seismicity: State of Knowledge*. Bulletin 137, XX pp. 33.

ICOLD (2010). *Selecting seismic parameters for large dams*. Bulletin 72.

Ju, S. H. (2013). A deconvolution scheme for determination of seismic loads in finite element analyses. Bulletin of the Seismological Society of America, 103(1): 258–67.

Khazaei Poul M. and Zerva A. (2018a). Nonlinear dynamic response of concrete gravity dams considering the deconvolution process. *Soil Dynamics and Earthquake Engineering*, 109, 324–338

Khazaei Poul M. and Zerva A. (2018b). Efficient time-domain deconvolution of seismic ground motions using the equivalent-linear method. *Soil Dynamics and Earthquake Engineering*, Volume 112, 138-151.

Léger, P. and Boughoufalah, M. (1989). Earthquake input mechanisms for time-domain analysis of dam-foundation systems. *Engineering Structures, 11*(1), 37-46.

Løkke, A. and Chopra, A. K. (2014). Response spectrum analysis of concrete gravity dams including dam-water-foundation interaction. *Journal of Structural Engineering, 141*(8), doi:10.1061/(asce)st.1943-541x.0001172

Løkke, A. and Chopra, A. K. (2017). Direct finite element method for nonlinear analysis of semi-unbounded dam–water–foundation rock systems. *Earthquake Engineering and Structural Dynamics, 46*(8), 1267-1285.

Lysmer, J. and Kuhlemeyer R. L. (1969). Finite element model for infinite media. *Journal of Engineering Mechanic*. Div,95, pp. 859-877.

MATLAB and Statistics Toolbox Release 2017b, The MathWorks, Inc., Natick, Massachusetts, United States.

Mejia, L. H. and Dawson, E. M. (2006). *Earthquake deconvolution for FLAC*. Proceedings of fourth International FLAC Symposium on Numerical Modeling in Geomechanics, Madrid, Spain.

Miquel, B. and Bouaanani, N. (2010). Simplified evaluation of the vibration period and seismic response of gravity dam-water systems. *Engineering Structures, 32*(8), 2488-2502. doi:10.1016/j.engstruct.2010.04.025.

Olson, L. G. and Bathe, K. -J. (1985). An infinite element for analysis of transient fluid-structure interactions. *Engineering Computations, 2*(4), 319-329.

Penner, O., Bergman, B., Razavi-Darbar, S., Queen, D. and Léger, P. (2017). *Nonlinear Time Domain Analysis of Ruskin Dam in LS-DYNA Including Reservoir-Foundation-Structure*

Interaction. In Proceedings of the United States Society on Dams 2017 Annual Meeting and Conference, Anaheim.

Rainer, J. H. and Dascal, O. (1991). *Behaviour of instrumented Hydro-Québec Dams during the Saguenay Earthquake*. Proceedings of Canadian dam safety conference, Whistler, BC, Canada, 189–202.

Reimer, R. B. (1973). *Deconvolution of seismic response for linear systems*. UCB/EERC-73/10, Earthquake Engineering Research Center, University of California, Berkeley.

Robbe, E. (2017). *Seismic Back Analysis of Monticello Arch Dam – Blind Prediction Workshop and Additional Analyses*. USSD annual conference, Anaheim.

Schnabel, P., Lysmer, J. and Seed, H. B. (1972). *SHAKE: A computer program for earthquake response of horizontally layered sites*. UCB/EERC-72/12, Earthquake Engineering Research Center, University of California, Berkeley.

Serafim, J. L. (1987). *A Note on the Earthquake Performance of Arch Dams*. Paper presented at the Proceedings of China-US Workshop on Earthquake Behavior of Arch Dams, Beijing, China.

Shen, C., Chen, H., Chang, C., Huang, L., Zi, T., Yang, C., Wang, T. and Lo, H. (1974). Earthquake induced by reservoir impounding and their effect on Hsinfengkiang dam. *Scientia Sinica, 17*(2), 239-272.

Singh, M. P. and Sharma, A. M. (1985). Seismic floor spectra by mode acceleration approach. *Journal of Engineering Mechanics*, 111(11), 1402–1419.

Sooch, G. S. and Bagchi, A. (2014). A new iterative procedure for deconvolution of seismic ground motion in dam-reservoir-foundation systems. *Journal of Applied Mathematics* 287605 (287610). doi:10.1155/2014/287605

Tan, H. and Chopra, A. K. (1996). *EACD-3D-96: A Computer Program for Three-dimensional Earthquake Analysis of Concrete Dams.* Report No. UCB/SEMM-96/06, University of California, Berkeley.

USACE (2003). *Time-history dynamic analysis of concrete hydraulic structures*. Technical report EM 1110 2 6051, Engineering and Design, United States Army Corps of Engineers, Washington.

USACE (2007). *Earthquake Design and Evaluation of Concrete Hydraulic Structures*. Technical report EM 1110-2-6053, Engineering and Design, United States Army Corps of Engineers, Washington.

US Bureau of Reclamation (2013). State-of-practice for the Nonlinear Analysis of Concrete Dams.

USBR, (2018). *Evaluation of Numerical Models and Input Parameters in the Analysis of Concrete Dams*, Report DSO-19-13, A Summary Report of the USSD Workshop, Miami.

USCOLD (2000). *Observed Performance of Dam During Earthquakes*. Technical report, Volume ii, U.S. Committee on Large Dams, Denver.

Westergaard, H. M. (1933). Water pressures on dams during earthquakes. *Journal of ASCE Transactions, 98*, 418–472.

Wieland, M. (2016). ICOLD's revised seismic design and performance criteria for large storage dams, *INCOLD Journal*, vol. 5, no. 2, pp. 42–48.

Wieland, M. and Fan, B.H. (2004). *The activities of the international commission on large dams (ICOLD) in the earthquake safety of large dams*. Paper presented at the Proceedings of the 13th World Conference on Earthquake Engineering, Vancouver, B.C., Canada.

Zangar, C. N. (1952). *Hydrodynamic pressures on dams due to horizontal earthquake effects*. Engineering Monographs No.11, U.S. Department of Interior, Bureau of Reclamation.

APPENDIX A EVALUATION OF MATLAB CODE

A MATLAB code is programmed in order to carry out the deconvolution analysis using data processing technique. In order to ensure the correctness of the results, commands and functions used in MATLAB, a comparison is made to SeismoSignal, an earthquake software which is used for signal processing of strong-motion data. The program is able to read accelerograms and derive the velocity, displacement, as well as Fourier spectra.

In the phase-amplitude modification technique, the very first step is to calculate the time history velocity of the ground motion acceleration. Here, as an example, horizontal component of Taft time history ground motion acceleration is selected for comparison purposes. Figure A.1 shows a comparison between the results obtained by the two software for the horizontal component of the ground motion velocity.

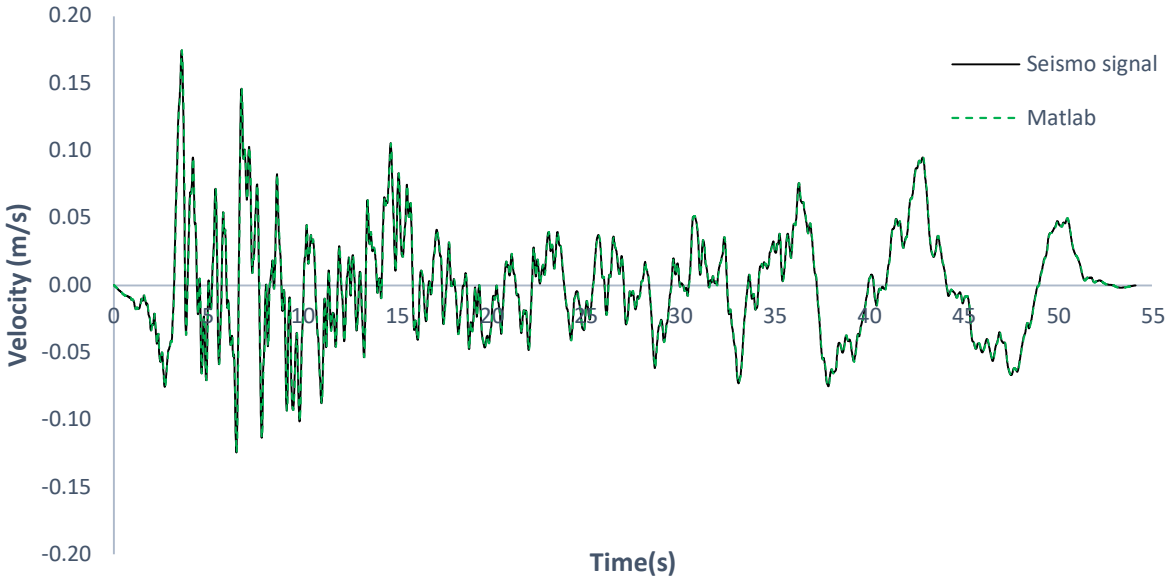

Figure A.1 Comparing the horizontal velocity time history of Taft ground motion obtained by MATLAB and SeismoSignal

In addition, another comparison is made for the Fourier spectra of the horizontal component of Taft earthquake. The results for the normalized one-sided Fourier spectra is shown in figure A.2. as it's illustrated, the amplitudes through the frequencies are perfectly matched.

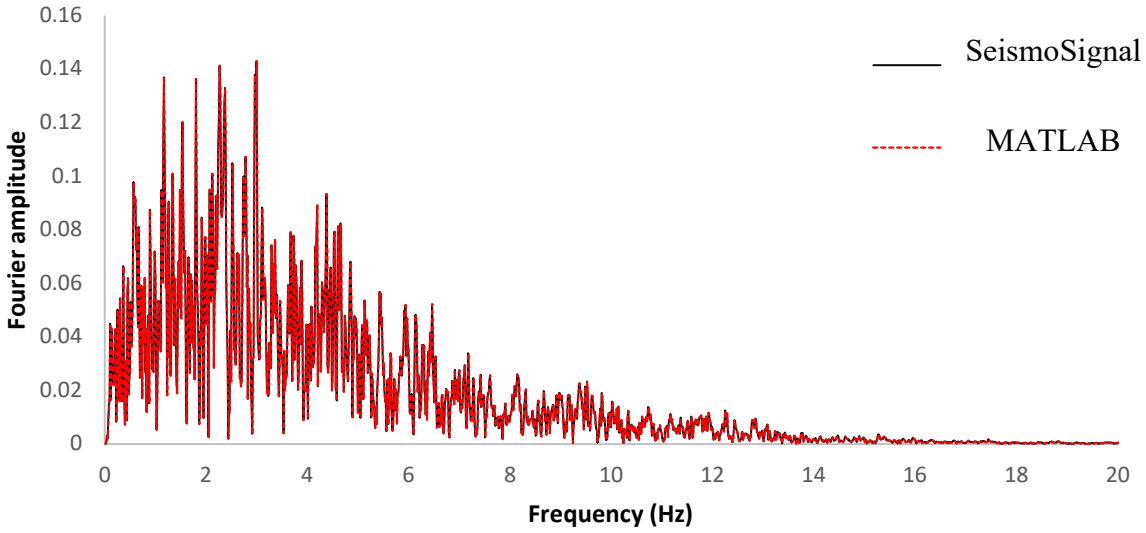

Figure A.2 Verification of the Fourier amplitude of the horizontal component of Taft ground motion acceleration obtained by MATLAB and SeismoSignal

APPENDIX B MASSED FOUNDATION CONVERGENCE ANALYSIS

A convergence study is done on the dimensions of the foundation rock. In case of static analysis, the size of foundation model is selected so that the results containing the static displacements and stresses induced in the dam have no changes by any expansion of the foundation size. In the seismic analysis however, this size should be selected so that the static results, as well as the natural frequencies and mode shapes, which control the seismic response of the dam, are calculated accurately. However, in case of flexible massed foundation, the natural frequencies of the dam-foundation model reduce with no convergence as the size of the foundation increases. Figure B.1 illustrate the dimensions of the foundation rock and the selected sizes to make the comparison. Figure B.2 compares the natural frequencies of the selected models with the original dimensions which is a = 2.5 H and b = H, where H is the height of the dam.

a=2.5H , b=2H

a=3H , b=3H

a=4H , b=4H

a=5H , b=5H

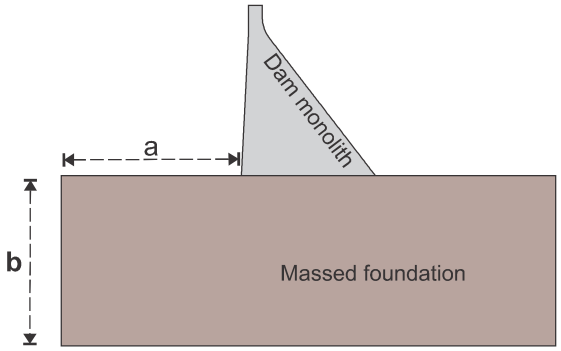

Figure B.1 Dimensions selected for the convergence study of the foundation rock

As it is illustrated in figure B.2 no convergence is occurred in natural frequencies, as well as floor response spectrum at the top of the foundation, by increasing the size of the foundation, when only the free-field ground motion accelerations are applied to the model.

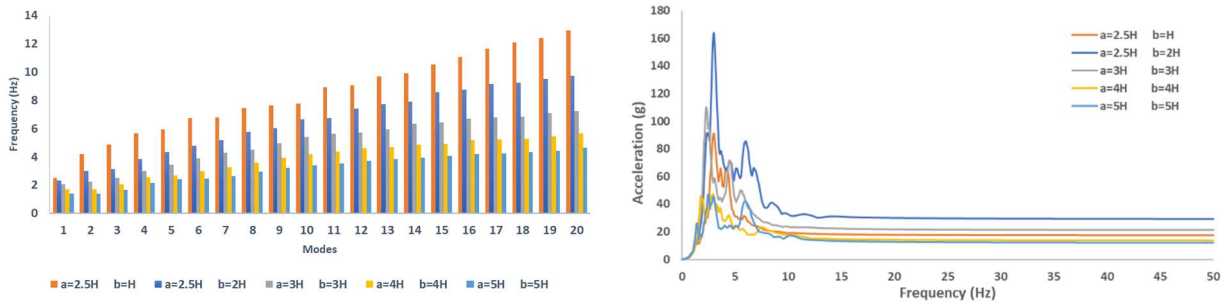

(a) (b)

Figure B.2 Comparing: (a) natural frequencies; (b) floor response spectra

APPENDIX C COMPARING 2D AND 3D MODELING OF PINE FLAT DAM IN TERMS OF NATURAL FREQUENCIES AND MODE SHAPES

Prior to the dynamic analysis, a frequency analysis should be carried out in order to obtain the natural frequencies and shape modes of the FE models. Considering the same material properties proposed by USSD, the first 20 natural frequencies are obtained for both 2D and 3D models of the tallest non-overflow monolith of the Pine-Flat dam. Although this step seems to be a very simple and basic step of the dynamic analysis, special attention should be given to it because the accuracy of the results mostly depends on the values gain from this step. Apart from the mathematical model behind this free-motion frequency analysis, choosing a correct meshing in terms of both the size and the order of elements is a very delicate process. The size of the elements should be such that a balance is established between the preciseness of the results and the computation time. Plus, refinement is necessary at the crest, as well as, at the base of the dam depending on the type of analysis. The selected monolith of the dam is modelled in both 2D and 3D. for the two-dimension model, meshing is done utilizing 2D-solid plane strain elements with 3 types of refinements, each with 4 nodes (linear) and with 9 nodes (parabolic). In case of three-dimension model, 3D-solid elements are created based on correspondent 2D model, each with 8 nodes and 20 nodes in order to better compare and judge the results. Figure C.1 shows the meshing of both 2D and 3D models, from coarse elements on the left to the most refined one on the right. To avoid unfavourable Constant Strain Triangle (CST) elements, which are created by the software along the height of the dam to adjust different divisions on the top to the ones on the bottom, several transition level with geometry ratio of 1 to 2 are created, so we can still have a better refinement with 4-noded rectangular elements to ensure more accurate results within the dam. Figure C.2 illustrates how this transition elements works. Although the seismic behaviour of the concrete gravity dam, as a short vibration period structure, is preliminary related to the fundamental mode of vibration, higher vibration modes has still its little influence. Since in modal analysis, the accumulative masses of the modes participating in the total dynamic response of the system should be at least 90% of the total mass of the structure in every direction that the ground motion is applied, a verification is done on the convergence of the higher modes (here the first 20 modes). As it is numerically illustrated in Tables C.1 and C.2, respectively the values of first twenty modes of vibration of the models in two dimensions and three dimensions, the few lower modes are converged as the size of meshing becomes finer and finer. However, for the higher modes this

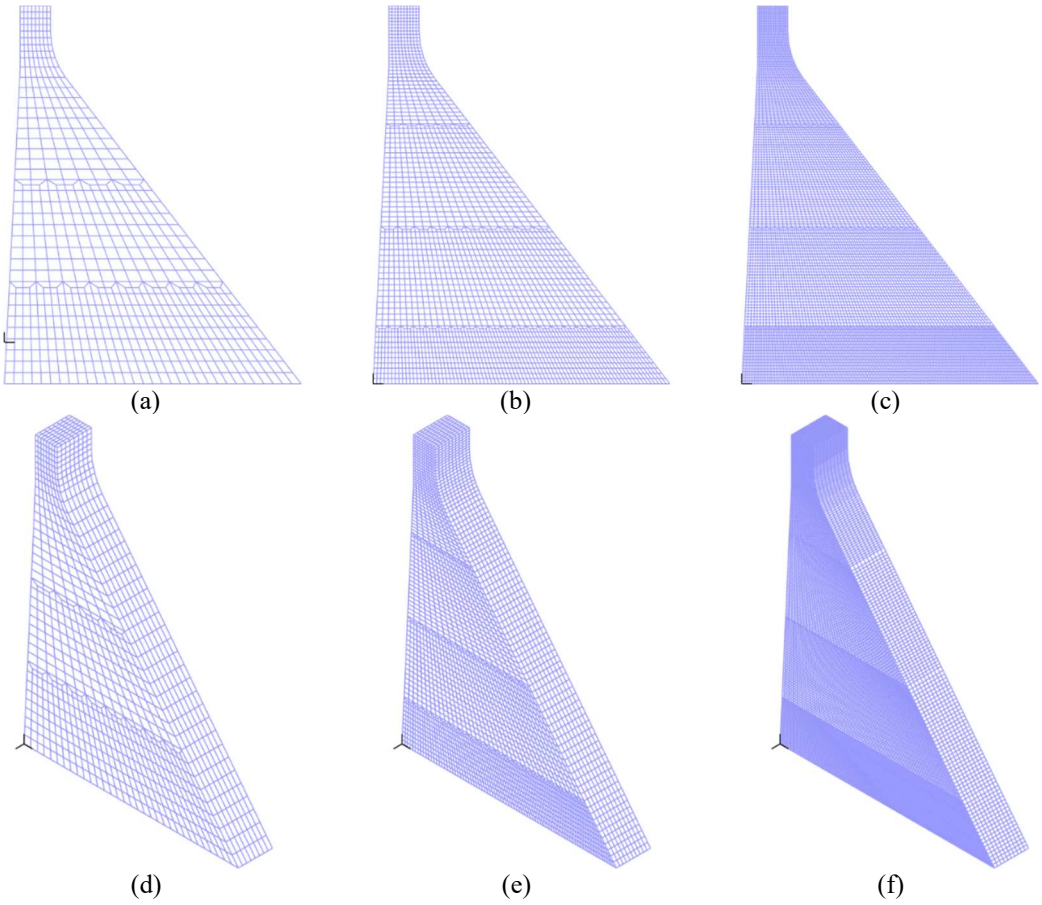

Figure C.1 Mesh refinement for 2D and 3D models of Pine Flat dam:
(a) and (d) coarse meshing; (b) and (e) less refined meshing; (c) and (f) refined meshing

convergence is still needed when the linear elements are utilized. In case of using higher order elements with parabolic interpolation function, the convergence is achieved even with the large size of meshing. The convergence criterion is usually satisfying when the difference of the frequency of the same mode with different meshing divided to the accurate value is less than 0.01 percent which is the case for all meshing with parabolic elements even with large size.

Figure C.2 Transition patterns: (a) 3D model; (b) 2D model

Table C.1 First twenty natural frequencies of the 2D model with different refinements

2D model											
Modes	Large				Medium size				Refined		
	4Nodes	Error	9Nodes	Error	4Nodes	Error	9Nodes	Error	4Nodes	Error	9Nodes
1	3.242	0.0031	3.232	0.0000	3.235	0.0008	3.232	0.00000	3.233	0.0002	3.232
2	6.675	0.0088	6.617	0.0000	6.631	0.0021	6.617	0.00001	6.620	0.0005	6.617
3	8.918	0.0009	8.910	0.0000	8.912	0.0003	8.910	0.00000	8.910	0.0001	8.910
4	11.476	0.0101	11.363	0.0001	11.390	0.0025	11.362	0.00001	11.369	0.0006	11.362
5	17.353	0.0122	17.145	0.0001	17.196	0.0031	17.144	0.00001	17.157	0.0008	17.144
6	19.442	0.0027	19.390	0.0000	19.403	0.0007	19.390	0.00000	19.394	0.0002	19.390
7	23.950	0.0153	23.591	0.0001	23.684	0.0040	23.590	0.00001	23.615	0.0010	23.590
8	24.518	0.0024	24.459	0.0000	24.473	0.0006	24.459	0.00000	24.463	0.0001	24.459
9	26.226	0.0056	26.080	0.0000	26.115	0.0014	26.079	0.00000	26.089	0.0004	26.079
10	29.134	0.0153	28.696	0.0001	28.811	0.0040	28.695	0.00000	28.726	0.0011	28.695
11	30.986	0.0042	30.858	0.0000	30.895	0.0012	30.857	0.00000	30.867	0.0003	30.857
12	32.240	0.0163	31.726	0.0001	31.850	0.0040	31.723	0.00001	31.756	0.0010	31.723
13	35.674	0.0227	34.887	0.0001	35.098	0.0062	34.883	0.00001	34.941	0.0017	34.883
14	37.028	0.0089	36.703	0.0000	36.776	0.0020	36.702	0.00000	36.721	0.0005	36.702
15	39.825	0.0183	39.112	0.0001	39.300	0.0049	39.108	0.00001	39.160	0.0013	39.108
16	40.850	0.0140	40.292	0.0001	40.446	0.0040	40.288	0.00001	40.331	0.0011	40.287
17	42.291	0.0174	41.575	0.0002	41.828	0.0062	41.569	0.00001	41.640	0.0017	41.569
18	42.885	0.0226	41.940	0.0001	42.088	0.0036	41.938	0.00000	41.974	0.0009	41.938
19	45.169	0.0103	44.713	0.0001	44.850	0.0031	44.710	0.00000	44.749	0.0009	44.710
20	46.698	0.0135	46.083	0.0001	46.250	0.0037	46.078	0.00001	46.126	0.0011	46.078

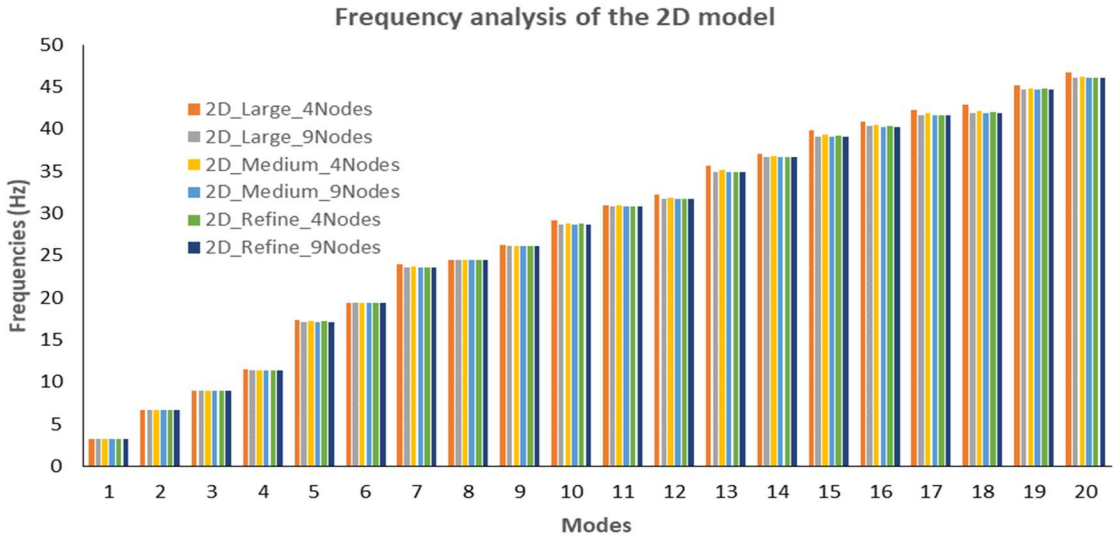

Table C.2 First twenty natural frequencies of the 3D model with different refinements

3D model											
Modes	Large				Medium size				Refined		
	8Nodes	Error	20Nodes	Error	8Nodes	Error	20Nodes	Error	8Nodes	Error	20Nodes
1	3.242	0.0031	3.233	0.0000	3.235	0.0008	3.232	0.00001	3.233	0.0002	3.232
2	6.675	0.0088	6.617	0.0001	6.631	0.0021	6.617	0.00002	6.620	0.0005	6.617
3	8.918	0.0009	8.910	0.0000	8.912	0.0003	8.910	0.00000	8.910	0.0001	8.910
4	11.476	0.0101	11.363	0.0001	11.390	0.0025	11.362	0.00002	11.369	0.0006	11.362
5	17.353	0.0122	17.145	0.0001	17.196	0.0030	17.144	0.00001	17.157	0.0008	17.144
6	19.442	0.0027	19.391	0.0000	19.403	0.0007	19.390	0.00001	19.394	0.0002	19.390
7	23.950	0.0153	23.592	0.0001	23.684	0.0040	23.590	0.00001	23.615	0.0010	23.590
8	24.518	0.0024	24.459	0.0000	24.473	0.0006	24.459	0.00000	24.463	0.0001	24.459
9	26.226	0.0056	26.081	0.0001	26.115	0.0014	26.079	0.00001	26.089	0.0004	26.079
10	29.134	0.0153	28.697	0.0001	28.811	0.0040	28.695	0.00001	28.726	0.0011	28.695
11	30.986	0.0042	30.858	0.0000	30.895	0.0012	30.857	0.00000	30.867	0.0003	30.857
12	32.240	0.0163	31.727	0.0001	31.850	0.0040	31.723	0.00002	31.756	0.0010	31.723
13	35.674	0.0227	34.887	0.0001	35.098	0.0062	34.883	0.00001	34.941	0.0017	34.883
14	37.028	0.0089	36.704	0.0000	36.776	0.0020	36.702	0.00001	36.721	0.0005	36.702
15	39.825	0.0183	39.114	0.0001	39.300	0.0049	39.109	0.00001	39.160	0.0013	39.108
16	40.850	0.0140	40.292	0.0001	40.446	0.0040	40.288	0.00001	40.331	0.0011	40.287
17	42.291	0.0174	41.576	0.0002	41.828	0.0062	41.569	0.00001	41.640	0.0017	41.569
18	42.885	0.0226	41.941	0.0001	42.088	0.0036	41.938	0.00001	41.974	0.0009	41.938
19	43.549	0.0198	42.705	0.0000	43.230	0.0123	42.703	0.00001	43.170	0.0109	42.703
20	45.169	0.0103	44.713	0.0001	44.850	0.0031	44.710	0.00000	44.749	0.0009	44.710

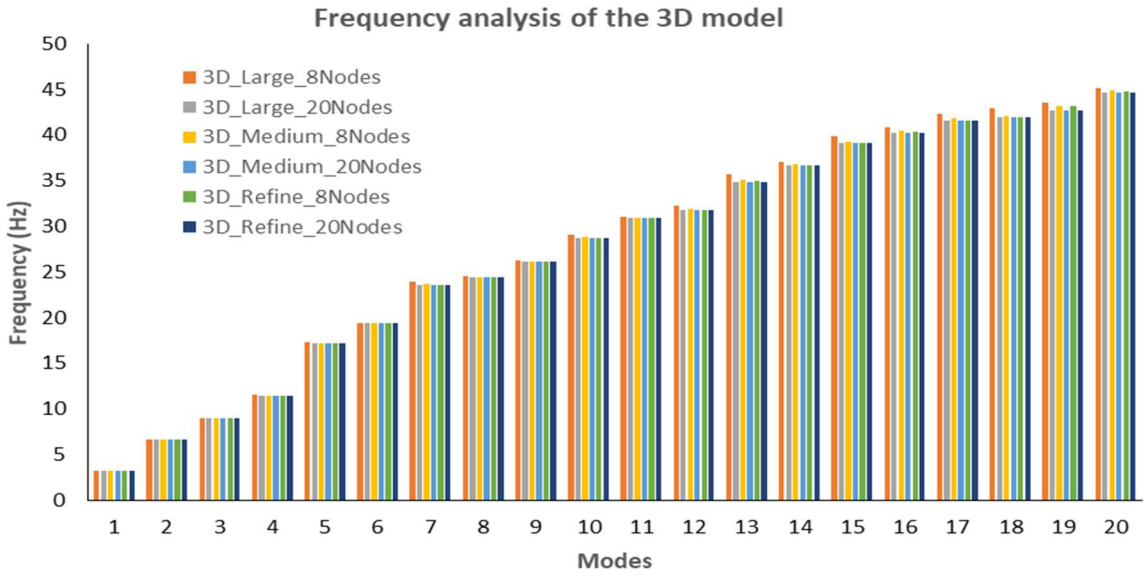

The results for the accumulative effective mass in the first twenty modes of the 3D refined model with 20-node elements for all three directions are presented in Table C.3. Since the dams is fixed on both sides for x-translation the values in this direction is obviously zero. For the first mode of vibration, the effective mass participation in Y direction is about 34% while it is 1.6% in Z direction. This accumulation masses reach 90% of total mass at the 12th mode in Y direction, although in Z direction it does not still attain for the 20th mode.

Table C.3: Accumulative modal participation factor

MODE	FREQUENCY (Hz)	MASS(X) %	MASS(Y) %	MASS(Z) %
1	3.232	0	34.198	1.626
2	6.617	0	58.620	2.081
3	8.910	0	65.153	57.606
4	11.362	0	76.684	64.089
5	17.144	0	84.062	64.091
6	19.390	0	84.132	77.266
7	23.590	0	87.175	78.221
8	24.459	0	87.222	78.245
9	26.079	0	88.124	79.881
10	28.695	0	88.522	80.248
11	30.857	0	88.755	84.800
12	31.723	0	90.575	85.005
13	34.883	0	90.872	85.311
14	36.702	0	90.880	85.387
15	39.108	0	91.948	85.388
16	40.287	0	92.081	85.529
17	41.569	0	92.109	86.822
18	41.938	0	92.472	88.133
19	42.703	0.00018	92.472	88.133
20	44.710	0.00018	92.689	88.480

Figure C.3 shows the deformed shape of the structure in its first mode of vibration for both the 2D and 3D models. As it is shown, the deformation of the structure is almost completely dominant by Y direction (horizontal direction), which corresponds to the numbers in the table above for the 3D model. Deformation in both directions is illustrated as well for the 20th mode, which shows the deformation in both Y and Z directions, although it's likely never happens.

Using the medium size of described meshing for both 2D and 3D model, a frequency analysis is done for all cases from dam-only to the complete system, considering the first six modes of each

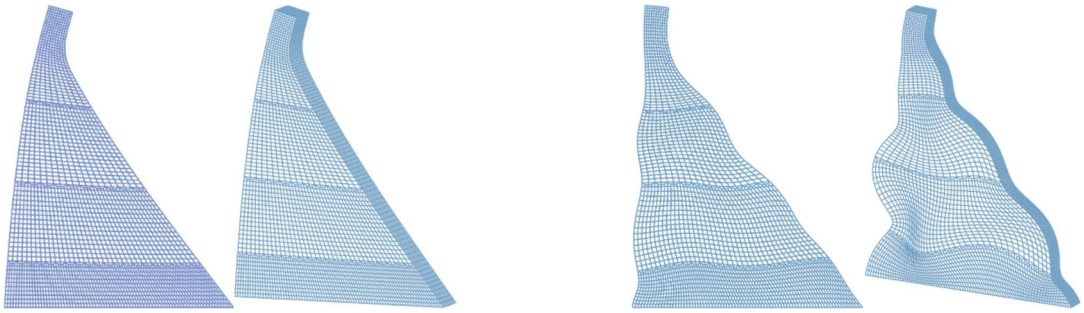

(a) (b)

Figure C.3 Vibrational Mode of the 2D and 3D model of the dam monolith: (a) first mode of vibration; (b) 20th mode of vibration

model. Figure C.4 illustrates the results related to 2D and 3D models respectively. Table C.4 shows the values of the frequencies related to each model.

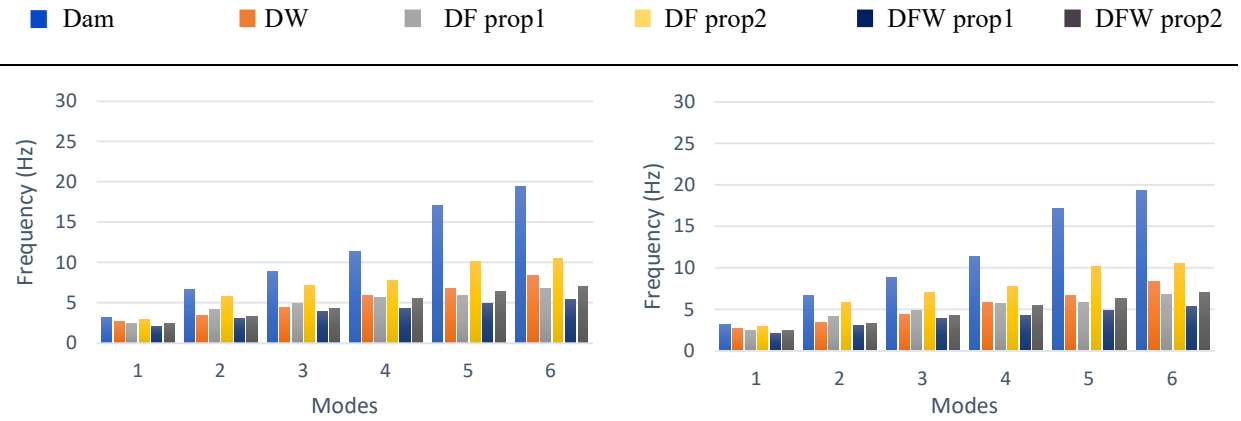

Figure C.4 Natural frequencies of the six first modes for the 2D (left) and 3D (right) Pine Flat model

Table C.4 Natural frequency values of the six first modes for the 2D and 3D PineFlat model

	2D models					
Modes	**Dam**	**DW**	**DF Prop1**	**DF Prop2**	**DFW Prop1**	**DFW Prop2**
1	3.2320	2.6535	2.492	2.9801	2.0737	2.4458
2	6.6170	3.4570	4.202	5.8323	3.1008	3.3635
3	8.9100	4.4155	4.861	7.1128	3.8861	4.3049
4	11.362	5.8761	5.678	7.8002	4.3176	5.4900
5	17.144	6.7155	5.915	10.1751	4.8844	6.3718
6	19.390	8.3414	6.746	10.5477	5.3822	7.0777

	3D models					
Modes	**Dam**	**DW**	**DF Prop1**	**DF Prop2**	**DFW Prop1**	**DFW Prop2**
1	3.2320	2.6536	2.492	2.9802	2.0741	2.4459
2	6.6170	3.4570	4.202	5.8325	3.1008	3.3635
3	8.9100	4.4155	4.861	7.1129	3.8861	4.3049
4	11.362	5.8761	5.678	7.8002	4.3176	5.4901
5	17.144	6.7155	5.915	10.1752	4.8847	6.3718
6	19.390	8.3414	6.747	10.5480	5.3825	7.0778

APPENDIX D DECONVOLUTION COMPARISON USING RESPONSE SPECTRUM

In this appendix, a comparison is made between the horizontal and vertical target ground motions and their corresponded convolved signals obtained from phase-amplitude modification method and the amplitude adjustment technique described in Chapter 4. The response spectrum is used to demonstrate the similarity or differences between the results for each model.

Figure D.1 illustrate comparison of response spectra for the foundation model with 1H depth. The results obtained using phase-amplitude adjustment technique. As it is shown in Figure D.1 (a) and (b), corresponding to the foundation only model excluding the self-weight, a perfect match is achieved between the response spectra of the free-field ground motions and the convolved signals at the top of the flat box respectively for the horizontal and vertical components, for all the models. Figure D.1 subplot (c) related to the foundation only model including its self-weight illustrate an excellent match for the horizontal convolved components. Comparing vertical spectral accelerations in subplot (d), the difference between target and convolved signal are quite noticeable for the model with sliders. Fig. D.1 (e) and (f) show the comparison between the signals including the effects of the dam. as illustrated, the inaccuracy is higher for the vertical convolved signal of the model with sliding lateral boundary condition. However, a very good agreement is achieved for all the models in terms of horizontal convolved signals. By joining the reservoir, subplots (g) and (h), same trend is exhibited for the horizontal and vertical convolved signals.

Figure D.2 compares the results obtained by phase-amplitude technique for the models having foundation with 3H depth. As the depth increases, the precision of the results for the fixed model decreases. Plots in Figure D.2 (a) and (b) show a perfect match between horizontal and vertical target motions and related convolved signals for the sliding and absorbing boundary conditions. For the model with fixed lateral boundary condition, horizontal convolved signal loses its accuracy, while the vertical convolved signal illustrate a perfect match. The same results in terms of accuracy is obtained by including the weight of the foundation as it is illustrated in Figure D.2 (c) and (d). By joining the dam to the model, Figure D.2(e) and (f), the horizontal convolve signal for the model with fixed lateral boundary condition significantly looses its accuracy. Results for the sliding and absorbing models still show a very good agreement for both horizontal and vertical components. Same trend is observed in Figure D.2 (g) and (h) by including the reservoir to the system.

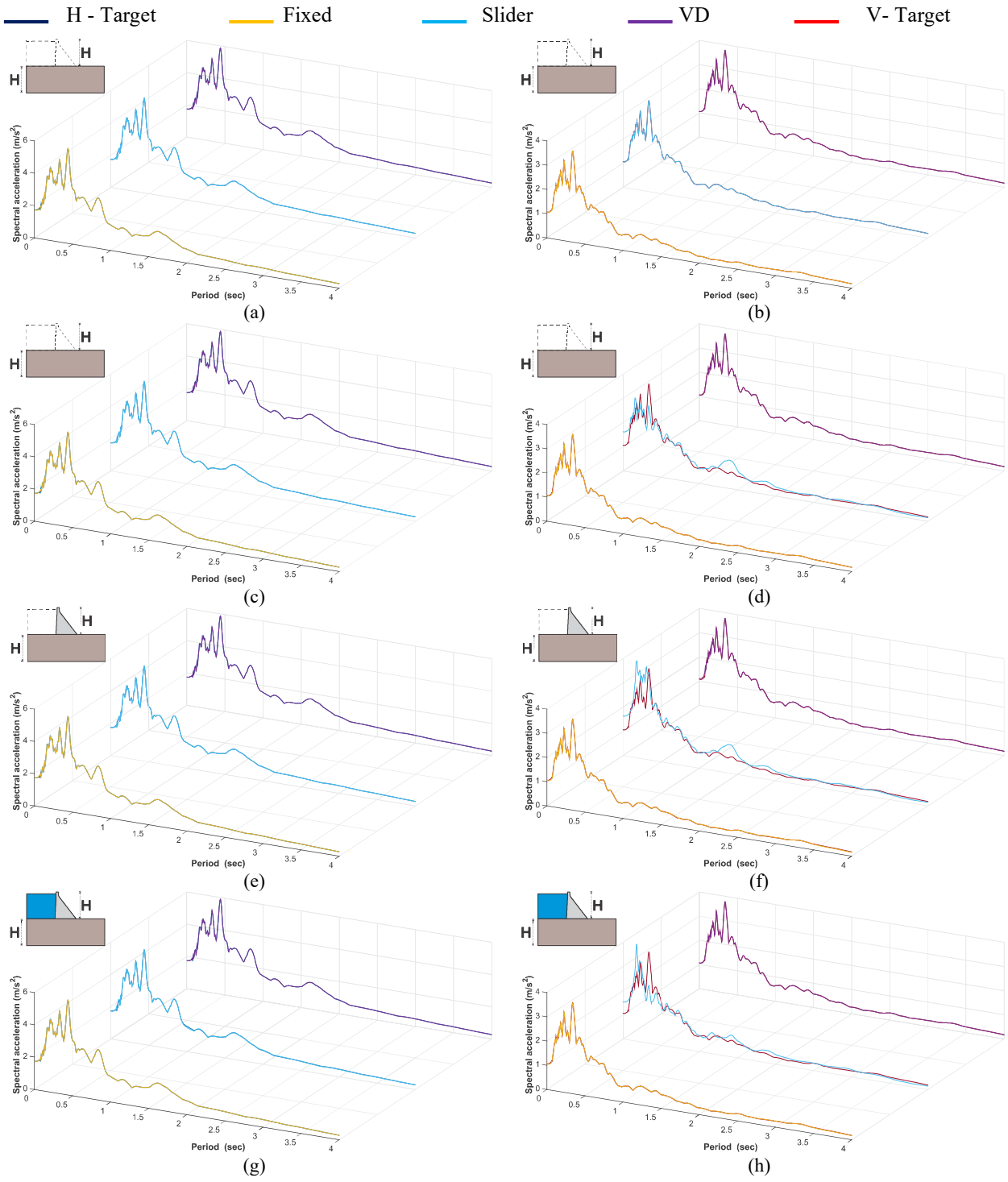

Figure D.1 Comparing spectral acceleration of horizontal (left) and vertical (right) components of free-field vs convolved signals for the model with 1H depth including fixed, sliding and absorbing later B.C

(a) and (b) Foundation only excluding its self-weight; (c) and (d) Foundation only including self-weight; (e) and (f) dam-foundation including static weight; (g) and (h) dam-reservoir-foundation including static weight

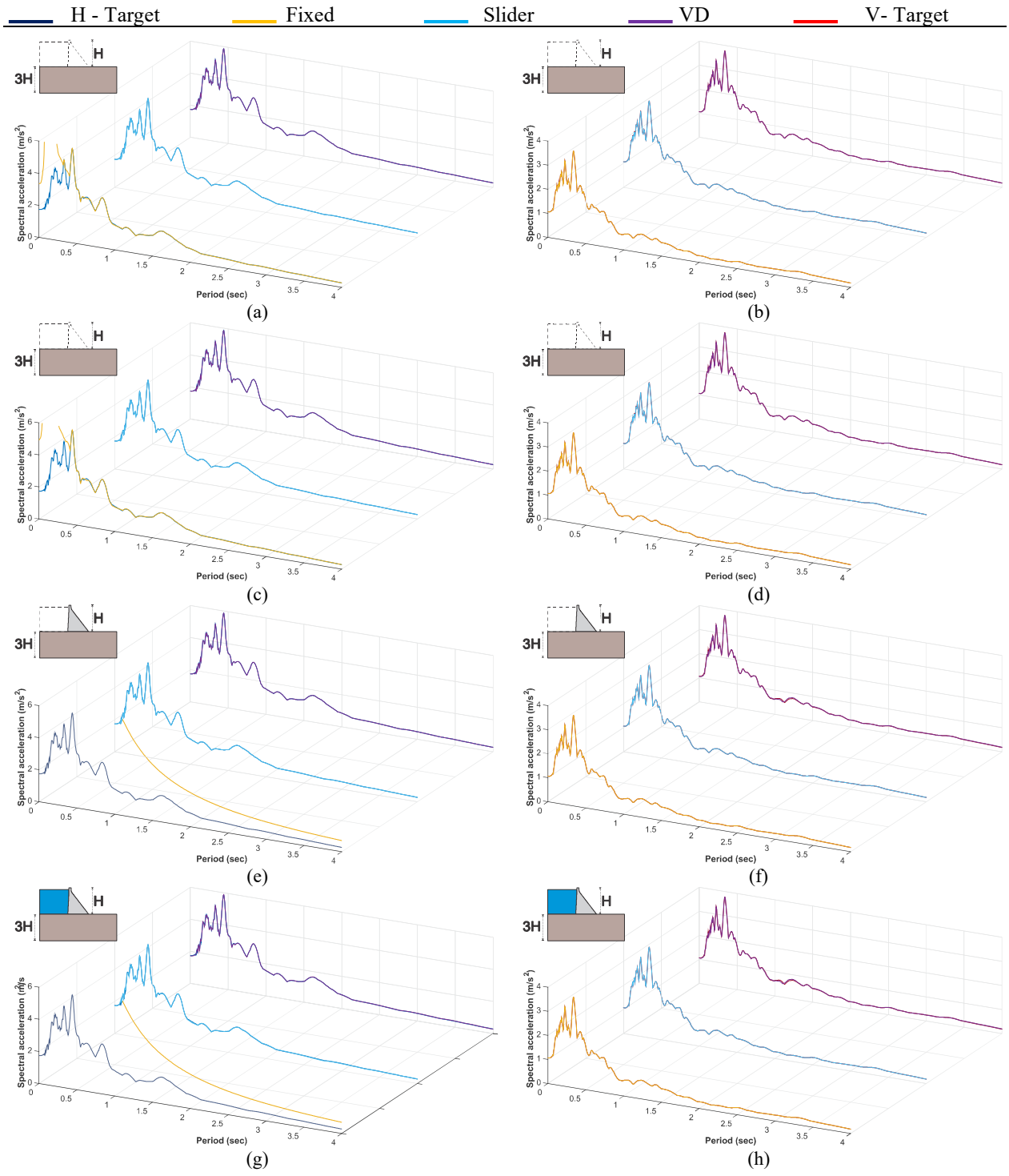

Figure D.2 Comparing spectral acceleration of horizontal (left) and vertical (right) components of free-field vs convolved signals for the model with 3H depth including fixed, sliding and absorbing later B.C.

(a) and (b) Foundation only excluding its self-weight; (c) and (d) Foundation only including self-weight; (e) and (f) dam-foundation including static weight; (g) and (h) dam-reservoir-foundation including static weight

Comparison of the horizontal and the vertical convolved signals for the flat box model with 3H depth having a very small value of modulus of elasticity is illustrated in figure D.3. The results are obtained using phase-amplitude adjustment technique.

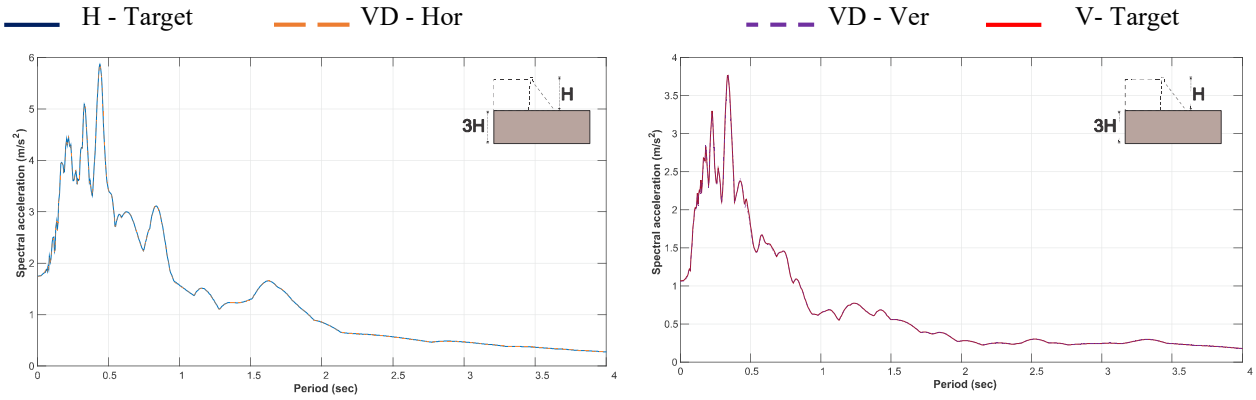

(a) (b)

Figure D.3 Comparing response specta of the free-field ground motion accelerations versus convoled signals obtained by phase-amplitude technique for the foundation-only model with 3H depth with a very small value of Young's modulus

(a) Horizontal components; (b) Vertical components

Figure D.4 shows the spectral accelerations obtained from the amplitude approach. A good agreement is obtained for the horizontal component of the model with lateral absorbing boundary condition.

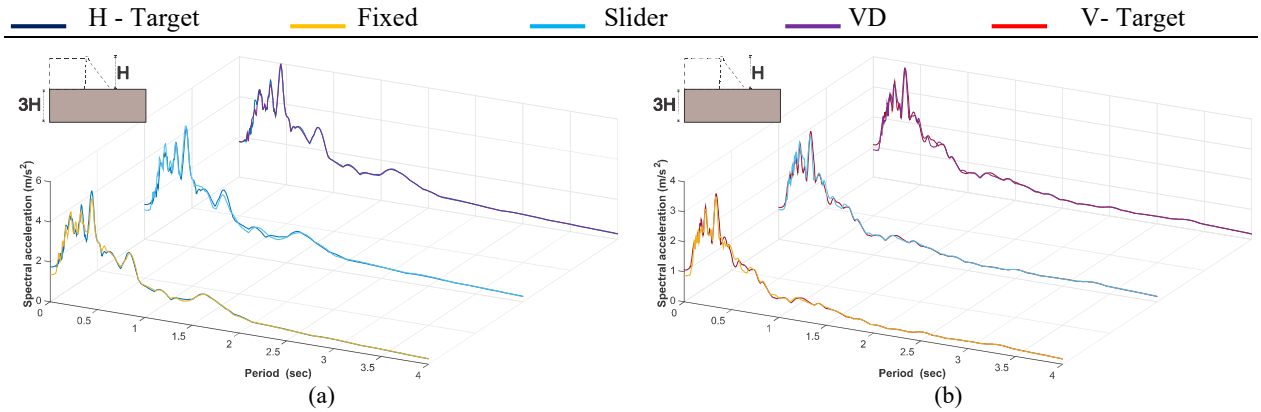

(a) (b)

Figure D.4 Comparing response spectra of the free-field ground motion acceleration versus convolved signals obtained by amplitude modification techique for the foundation only model with 3H depth:

(a) horizontal components; (b) Vertical components